6. IN-DRIFT PHYSICAL AND CHEMICAL ENVIRONMENT

6.1 INTRODUCTION

Drip shield and waste package degradation (see Section 7) depends on the environmental conditions to which these components are exposed: the in-drift physical and chemical environment. Drift degradation and consequent rockfall have the potential to affect drip shield integrity and the thermal-hydrologic, chemical (THC) environment in drifts. After a waste package is breached, the transport of radionuclides released from the waste form (see Section 10) also depends on the environment in the emplacement drifts. A descriptive conceptualization of the in-drift processes and parameters that can affect the environment is given in *Physical and Chemical Environmental Abstraction Model* (CRWMS M&O 2000 [DIRS 151563]) and in the *Total System Performance Assessment for the Site Recommendation* (TSPA-SR) (CRWMS M&O 2000 [DIRS 153246], Sections 3.3 and 3.6). More recent models and analyses are summarized in Table 6-1.

Important in-drift processes that can affect the physical and chemical environment include evaporation and condensation of water, formation of salts by precipitation, dissolution of salts, microbial activity, reaction of gas phase constituents with aqueous solutions and solids, corrosion, and mass transport, including initiation and changes in transport paths such as those caused by drip shield and waste package degradation (see Section 10).

Principal in-drift parameters that can affect those processes are influx rates of seepage water (see Section 4) and advection or diffusion rates of incoming gas from the host rock, other advective and diffusive mass transport rates (see Section 10), evaporation rate (see Section 5), relative humidity (see Section 5), temperature (see Section 5), gas phase composition, aqueous solution composition, compositions of solid phases within and around the drift, and the effects of rockfall due to host rock degradation.

The treatment of these processes and parameters in the TSPA-SR (CRWMS M&O 2000 [DIRS 153246]), including uncertainties, is reviewed in Section 6.2.

Scientific bases for the total system performance uncertainty analyses in Volume 2 (McNeish 2001 [DIRS 155023]) and results of supplemental subsystem performance uncertainty analyses are introduced and presented in Section 6.3 under the following subheadings.

Composition of Liquid and Gas Entering Drift (Thermal-Hydrologic-Chemical) (Section 6.3.1)–Includes the composition of seepage water and gas and the rates at which water and gas enter the drift. An introduction to THC seepage models is provided in Section 6.3.1.1. Goals of modeling are provided in Section 6.3.1.2. Sections 6.3.1.3 and 6.3.1.4 describe the original model work and later updates. Results of new simulations that further evaluate the uncertainty of predicted water and gas compositions due to variations in thermal operating mode are presented in Section 6.3.1.5. The remainder of Section 6.3.1 abstracts the currently available data for use in the total system performance assessment (TSPA) effort and summarizes remaining model uncertainties and the implications for predicted compositions of fluids that could enter the drift.

Table 6-1. Summary of Supplemental Models and Analyses

Key Attributes of System	Process Model (Section of S&ER)	Topic of Supplemental Scientific Model or Analysis	Reason For Supplemental Scientific Model or Analysis			Section of Volume 1	Performance Assessment Treatment of Supplemental Scientific Model or Analysis[a]	
			Unquantified Uncertainty Analysis	Update in Scientific Information	Lower-Temperature Operating Mode Analysis		TSPA Sensitivity Analysis	Included in Supplemental TSPA Model
Long-Lived Waste Package and Drip Shield	Water Diversion Performance of EBS (4.2.3)	Composition of liquid and gas entering drift	X		X	6.3.1	X	X
		Evolution of in-drift chemical environment	X		X	6.3.3	X	X
		Thermo-Hydro-Chemical model comparison to plug-flow reactor and fracture plugging experiment		X		6.3.1		
		Rockfall		X		6.3.4		

NOTE: S&ER = *Yucca Mountain Science and Engineering Report* ([DOE 2001 [DIRS 153849]).

[a] Performance assessment treatment of supplemental scientific model or analysis discussed in SSPA Volume 2 (McNeish 2001 [DIRS 155023]).

Effects of Engineered Materials on the Chemical Environment (Section 6.3.2)–Includes engineered materials, such as steel and cement, but not the contents of the waste packages (see Section 9). A brief introduction and modeling goals are provided in Sections 6.3.2.1 and 6.3.2.2. Section 6.3.2.3 describes current work and previously unquantified uncertainties in the modeling of steel corrosion, alloy corrosion, and cement grout degradation. Section 6.3.2.6 summarizes remaining uncertainties.

Evolution of In-Drift Chemical Environment (Section 6.3.3)–Includes evaporation and condensation of water, formation of salts by precipitation, dissolution of salts, microbial activity, reaction of gas phase constituents with aqueous solutions, and resulting changes in aqueous solution composition. This section discusses three submodels within the engineered barrier system (EBS). Section 6.3.3.3 discusses initial results and previously unquantified uncertainties. Section 6.3.3.4 discusses developments since the initial release of the analysis model reports (AMRs). Section 6.3.3.5 contains analysis results, which are abstracted in Section 6.3.3.6. Remaining uncertainties are listed in Section 6.3.3.7, and a final summary of the information is provided in Section 6.3.3.8.

Rockfall (Section 6.3.4)–Includes sensitivity studies for model predictions of size ranges and quantities of rock that may fall into drifts. Section 6.3.4.1 introduces key processes and modeling software. A discussion of past efforts, unquantified uncertainties, and uncertainties selected for quantification is found in Section 6.3.4.3. Analysis results are detailed in Section 6.3.4.5. Multiple lines of evidence are provided in Section 6.3.4.7. Remaining uncertainties are listed in Section 6.3.4.8, and a summary and conclusion are provided in Section 6.3.4.9.

Section 6.4 presents, a summary and discussion of parameters and information provided to the TSPA for the uncertainty analyses in Volume 2 (McNeish 2001 [DIRS 155023]), including model uncertainties and input data uncertainties.

6.2 REVIEW OF TOTAL SYSTEM PERFORMANCE ASSESSMENT-SITE RECOMMENDATION TREATMENT

6.2.1 Composition of Liquid and Gas Entering the Drifts (Thermal-Hydrologic-Chemical)

The model for compositions of liquid and gas entering the drifts is the THC seepage model (CRWMS M&O 2000 [DIRS 142022]). This model predicts, at the drift scale, the composition of seepage and the associated gas-phase chemistry for 100,000 years, including the effects of heating. Uncertainties are discussed in more detail in Sections 6.3.1.1 and 6.3.1.3.

Work documented in *Drift-Scale Coupled Processes (DST and THC Seepage) Models* (CRWMS M&O 2000 [DIRS 142022]) included one THC seepage model with a drift located in the middle nonlithophysal unit of the Topopah Spring tuff (Tptpmn). The simulated design included backfill, an initial mean linear heat load of 1.54 kW/m, and a 50-year preclosure period with 70 percent heat removal. This thermal load was predicted to yield temperatures above the boiling point of water (near 96°C at Yucca Mountain) in the rocks in the vicinity of the emplacement drifts for hundreds of years. THC seepage simulations were also performed for an

ambient temperature case (no heat load) to serve as a baseline for evaluations of model results under thermal loading conditions. Uncertainties in this THC seepage model were not explicitly quantified in the TSPA-SR (CRWMS M&O 2000 [DIRS 153246]) treatment.

The initial THC seepage model (CRWMS M&O 2000 [DIRS 142022]) is based on information obtained, in part, from thermal testing in the Tptpmn unit, which may exhibit somewhat different thermal-hydrologic (TH) behavior or mineralogy than the lower lithophysal unit (Tptpll), in which most of the repository emplacement drifts will be located. Although this could change the system response, the bulk chemistry is similar for all of the welded host rock units.

Two geochemical systems were considered in this model. The first was an extended case system that included aluminum silicates (e.g., clays, zeolites, feldspars, and sepiolite), silica phases (e.g., quartz, amorphous silica, tridymite, and glass), gypsum, calcite, fluorite and iron minerals (e.g., hematite, and goethite), and a suite of aqueous species, including calcium, magnesium, sodium, potassium, silica, chloride, aqueous carbonate species, sulfate, fluoride, aluminum, and iron. The second was a base case system that excluded aluminum silicate minerals and iron minerals, thus excluding such aqueous species as aluminum, magnesium, potassium, and iron, which are found in these minerals.

The inclusion or exclusion of aluminum silicate minerals in the system provided a first crude approach for evaluating the model sensitivity to the effective reaction rates of these minerals: either reacting at rates determined from published kinetic and thermodynamic data and estimated reactive surface areas, or reacting so slowly that the reactions could be neglected.

The initial THC seepage model (CRWMS M&O 2000 [DIRS 142022]) is useful to evaluate, in a semiquantitative sense, the model sensitivity to the reaction rates of aluminum silicate minerals and to a range of infiltration rates, including future climates wetter than the present day. However, under the high infiltration rate conditions most favorable to in-drift seepage, uncertainties in these parameters are likely to be overshadowed by the assumed composition of fluids infiltrating at the top model boundary. Therefore, while the initial THC seepage model (CRWMS M&O 2000 [DIRS 142022]) simulations provide some quantitative assessment of uncertainties related to mineral reaction rates and infiltration rates, the effect of infiltration composition remains to be quantified. None of the uncertainties discussed here were included in the TSPA-SR model (CRWMS M&O 2000 [DIRS 153246]). The complete data set for the abstraction detailed in Section 6.3.1.6 can be found in Jolley (2001 [DIRS 154762]).

6.2.2 Effects of Engineered Materials on the Chemical Environment

An evaluation of corrosion products on the aqueous concentrations of metal ions in solution in an oxidizing environment was conducted and found to have a minimal impact on the concentrations of major ions in solution, as reported in the *In Drift Corrosion Products* report (CRWMS M&O 1999 [DIRS 125130], Section 7.2). That conclusion was based on a generalized set of Eh-pH diagrams for the major elements in a three- or four-chemical component system and a general search of available scientific literature.

Uncertainties in the models about the effects of engineered materials on the chemical environment were not explicitly quantified in the TSPA-SR model (CRWMS M&O 2000

[DIRS 153246]). The uncertainties are in three general areas: corrosion of steel and alloys, cement grout reactions, and colloids. The first two areas are specifically discussed in Section 6.3.2.3; the third area is discussed in Section 10.3.5. An evaluation of the effects of corrosion products on the aqueous concentrations of metal ions in solution in an oxidizing environment was conducted. Two conclusions were that only minor impacts are expected to occur in the bulk in-drift chemical environment and that any impacts will occur during active corrosion of the metals and alloys in an oxidizing environment, as reported in the *In Drift Corrosion Products* report (CRWMS M&O 1999 [DIRS 125130], Section 7.2). It was also concluded that effects of cementitious materials would be negligible (CRWMS M&O 2000 [DIRS 153246], Section 3.3.4.5.4).

6.2.3 Evolution of In-Drift Chemistry

The model of the evolution of the in-drift chemical environment uses inputs from three models: the precipitates and salts model, the invert water mixing model, and the microbial communities model.

The precipitates and salts model is based on literature data that describe the minerals and salts produced by evaporative concentration and the relations between solution composition and relative humidity. This model was developed and validated in *In-Drift Precipitates/Salts Analysis* (CRWMS M&O 2001 [DIRS 153265]). It is composed of two submodels that predict pH, chloride concentration, and ionic strength as a function of relative humidity, carbon dioxide fugacity, temperature, seepage water composition, and relative rates of evaporation and seepage. When the relative humidity is above 85 percent, the EQ3/6 Pitzer submodel (often referred to as the high relative humidity salts submodel) is used. Below 85 percent relative humidity, the low relative humidity salts submodel is used. Lookup tables produced for the TSPA-SR (CRWMS M&O 2000 [DIRS 143665]) are documented in *Precipitates/Salts Model Results for THC Abstraction* (CRWMS M&O 2001 [DIRS 153995]). The complete data set for the inputs, outputs, and lookup tables detailed in Section 6.3.3.5.1 can be found in Jolley (2001 [DIRS 154762]).

Uncertainties about mixing in the invert of seepage waters, concentrated brines, waters containing corrosion products, and waters containing waste degradation products were not explicitly quantified in the TSPA-SR (CRWMS M&O 2000 [DIRS 153246]). Instead, ranges of solution compositions were evaluated for properties such as solubility under an in-drift carbon dioxide gas fugacity for a given time period. There was also no explicit unified water chemistry that was internally consistent for all areas of the drift.

The microbial communities model is not intended to quantify localized microbial activity or its consequences, but bounds overall microbial growth and activity in the EBS. The *In-Drift Microbial Communities* report (CRWMS M&O 2000 [DIRS 151561]) provides bounding estimates of the numbers of microbes that could grow in the repository drift as a function of time. This time-dependent set of calculations includes the evaluation of several sets of uncertain parameters, such as the effects of drift temperature and relative humidity, changes in water chemistry and gas entering the drift, and variability in percolation flux through time. The calculations also incorporate the material masses and compositions used in the repository and waste package designs and variable corrosion rates for those materials. Uncertainties directly

associated with the TSPA-SR model (CRWMS M&O 2000 [DIRS 153246]) include: the composition (including the key microbial nutrients nitrate and phosphate) and rate of flux for gas and water entering the drift, the composition of EBS components and their degradation products, and the chemical interactions of EBS components with one another. The in-drift microbial communities model has been validated by testing against laboratory data, natural system observations, and other modeling efforts. Uncertainties in the models of evolution of the in-drift chemical environment were not explicitly quantified in the TSPA-SR model (CRWMS M&O 2000 [DIRS 153246]).

6.2.4 Environment on the Surfaces of the Drip Shield and Waste Package

Uncertainties in corrosion rates due to uncertainties in the chemical environment on the surfaces of the drip shield and waste package were quantified in the TSPA-SR model (CRWMS M&O 2000 [DIRS 153246]) by sampling over a wide range of corrosion rates. The range also encompasses the range of corrosion rates expected because of the predicted range of chemical conditions on the drip shield and waste package. However, explicit uncertainties in the chemical environment on the drip shield and waste package were not quantified in this section. These issues are discussed in Section 7.

6.2.5 Rockfall

The deterioration of the rock mass surrounding the potential repository emplacement drifts was predicted using a probabilistic key-block analysis. Key blocks are formed in the rock mass surrounding an excavation by the intersection of three or more planes of structural discontinuities. *Drift Degradation Analysis* (CRWMS M&O 2000 [DIRS 151635]) provides an assessment of the possible formation of key blocks within the potential repository horizon based on the orientations of discontinuities in the Exploratory Studies Facility (ESF) main loop and in the Enhanced Characterization of the Repository Block (ECRB) Cross Drift. Block failure due to seismic and thermal effects has also been analyzed.

Uncertainty in the rockfall model is affected by how well the data inputs describe actual fracture conditions. The natural variability of fractures within a rock mass always represents uncertainty in the design of structures in rock. The extensive fracture data collected at Yucca Mountain provide a good representation of fracturing at the emplacement drift horizon. Fracture data have been represented in the discrete region key block analysis model by simulating joint radii, spacings, and positioning with beta distributions based on field mapping data (CRWMS M&O 2000 [DIRS 151635], Section 6.3.2). Individual joints within each joint set are represented as circular discs in three-dimensional space with radii drawn from a distribution estimated on the assumption that the radius is equal to twice the mapped trace length (CRWMS M&O 2000 [DIRS 151635], Section 5.1). All joint spacing data have been corrected for "true" spacing (i.e., the spacing measured normal to the plane of the joint sets) (CRWMS M&O 2000 [DIRS 152286], Section 6.4.2.1). This correction for true spacing is referred to as a Terzaghi correction. The range of fracture variability from tunnel mapping has been captured in the rockfall model through multiple Monte Carlo simulations of the rock mass. To account for uncertainties associated with seismic, thermal, and time-dependent effects on rockfall, a conservative reduction of joint strength parameters has been included in the approach.

It was concluded in the TSPA-SR (CRWMS M&O 2000 [DIRS 153246], Section 3.3.1.4) that the effect of rockfall on thermal hydrology and other in-drift conditions is likely to be negligible because the calculated volume of fallen rock is small (about 0.1 percent) compared with the unoccupied drift volume of 16,650 m^3/km in the emplacement drifts (i.e., drift volume outside the drip shield and above the invert).

Uncertainties in the model for rockfall were not explicitly quantified for TSPA activities.

6.3 UNCERTAINTY ANALYSES AND NEW MODELS

6.3.1 Composition of Liquid and Gas Entering the Drifts

This section discusses results and uncertainties of THC simulations (THC seepage models) that have been performed to predict the chemical evolution of pore water and gases that could enter emplacement drifts. Most of these simulations, as well as the validation of modeled processes and evaluations of model uncertainty, are presented in detail in *Drift-Scale Coupled Processes (DST and THC Seepage) Models* (CRWMS M&O 2000 [DIRS 142022]; BSC 2001 [DIRS 154677]). Work presented in the initial issue of that report (CRWMS M&O 2000 [DIRS 142022], Section 6.3) is reviewed in Section 6.3.1.3. This earlier work evaluated model uncertainties with respect to infiltration rates and mineral reaction rates, but was otherwise of limited scope in terms of addressing other model uncertainties. A substantial amount of new work was presented in a revision of that report (BSC 2001 [DIRS 154677], Sections 6.4 through 6.6), which examined model sensitivity to various factors such as thermodynamic and kinetic input data, repository host rock unit, and drift design parameters, with the goal of assessing (at least qualitatively) some of the important model uncertainties. This work is discussed in Section 6.3.1.4. New simulations were performed to further evaluate the uncertainty of predicted water and gas compositions around drifts with respect to design heat load (temperature), boundary carbon dioxide concentrations, and initial water compositions (Bodvarsson 2001 [DIRS 154669], Attachment 5, pp. 10 to 59). Results of these new simulations are presented in Section 6.3.1.5.

Results of the initial THC seepage simulations (CRWMS M&O 2000 [DIRS 142022]) were abstracted for the TSPA-SR (CRWMS M&O 2000 [DIRS 153246]), but model uncertainties were not explicitly quantified. Abstraction of recent THC seepage simulations and other work is discussed in Section 6.3.1.6. A summary of remaining model uncertainties and implications on the predicted composition of fluids that could enter drifts is presented in Sections 6.3.1.8 and 6.3.1.9.

6.3.1.1 Introduction

The THC seepage models provide an analysis of the effects of THC processes in the near-field host rock around the potential emplacement drifts on the seepage water chemistry and gas-phase composition. This analysis includes a comprehensive description of the pertinent mineral-water-gas interaction processes in the host rock and their effect on the near-field environment. The THC seepage models take into account the effects of mineral dissolution and precipitation, the effects of carbon dioxide exsolution and transport in the region surrounding emplacement drifts, and the resulting changes to porosity, permeability, seepage, and chemical

composition of seeping waters. As such, these models are subject to the uncertainty of a large number of input parameters, as well as to the uncertainties in the methods implemented to simulate these complex coupled processes and assumptions regarding the physical setup of the model. Uncertainties in model input data that could affect calculated water and gas compositions include:

- Thermodynamic data (equilibrium constants for mineral-water reactions and aqueous species dissociation)
- Kinetic data (rate constants, reactive surface areas, and activation energies)
- Initial compositions of pore water and gas (carbon dioxide)
- Initial composition of infiltration water and gas (carbon dioxide)
- Infiltration rates
- Transport parameters (diffusion coefficients of aqueous species and gases, tortuosity)
- Initial rock mineralogy (model location and stratigraphy)
- Number of geochemical constituents included in simulations
- Number and types of potential secondary mineral phases
- Rock thermal, physical, and hydrologic properties (including input data for water-saturated and unsaturated rock).

Process model uncertainties may also affect calculated water and gas compositions. These include:

- Formulation of models to simulate fluid flow in dual-permeability media (e.g., fracture-matrix interactions, relative permeability and saturation-capillary pressure models)
- Activity coefficient models
- Kinetic mineral precipitation and dissolution models
- Inclusion or exclusion of certain specific THC processes (e.g., active fracture model, vapor pressure lowering, mineral solid solutions, and redox reactions).

Uncertainties in the setup of the model could also affect the results of THC seepage models. These include:

- Physical model representation (stratigraphic/geologic extrapolations)
- Representation of the fracture and matrix continua in the model mesh

- Model discretization (in space and time)
- Boundary conditions (e.g., drift open versus closed to fluid flow).

These uncertainties illustrate that, given the large number of input parameters and the complexity of the modeled THC processes, a rigorous quantification of model uncertainty is not achievable. For this reason, the THC modeling work has concentrated on limiting and qualitatively assessing uncertainty, rather than attempting statistical quantification.

Generally, reducing the uncertainty of THC seepage models was achieved by validating simulated THC processes against field and experimental data. TH process models have been extensively tested against field data and experiments conducted in the ESF, as well as in the laboratory, providing a basis to assess and reduce the uncertainty in TH process models and their input parameters (see Sections 3.3.5, 3.3.6, 4.3.6, 4.3.7, and 5.3.1). Simulated THC processes have been validated against water and gas compositions measured during thermal tests (i.e., the Drift Scale Test and Single Heater Test) and a plug flow reactor laboratory experiment. Uncertainty was also reduced by calibrating some of the model input data against observed hydrologic and geochemical data, as well as performing various sensitivity studies on the effect of fracture permeability heterogeneity, mineral reaction rates, host rock mineralogy, and the geochemical systems considered. The validation of THC simulations against experimental data is ongoing (e.g., Section 4.3.6.7), and the possibility of further validation of THC seepage models against natural analogues is being pursued.

From these efforts it would appear that uncertainties related to parameters directly affecting water-rock-gas chemical reactions, besides TH conditions (e.g., equilibrium constants, reaction rates, and input rock, water, and gas compositions) have a large effect on computed water and gas compositions. Therefore, limiting the uncertainty of these parameters is critical for increasing the confidence in THC seepage models. Uncertainties in reaction-related parameters are compounded by uncertainties in hydrologic parameters. It may not always be clear whether uncertainties in chemical reaction parameters have a greater effect on computed water and gas compositions than uncertainties in hydrologic parameters. However, in cases studied here, it would appear that small variations in fundamental thermodynamic properties of reacting minerals and aqueous species, for example, can cause large changes in effective reaction rates, which may affect computed water and gas compositions more significantly than hydrologic property changes of similar proportions.

Temperature is also a critical parameter, because it directly affects equilibrium constants and reaction rates, the degree of water evaporation and boiling, and the amount of carbon dioxide volatilization from pore water, with direct implications on computed water and gas chemistries. In this case, however, uncertainties in rock properties affecting computed temperatures (i.e., rock conductivity and heat capacity) are overshadowed by the direct effect of design heat load (e.g., high temperature versus low temperature). For this reason, the effect of design heat load is also evaluated by simulating two different predetermined design heat load covering a range largely encompassing potential uncertainties affecting the heat load values themselves. Thermal and hydrologic effects at the edge of the repository can also affect temperature significantly, and therefore affect computed gas and water compositions at these locations. These edge effects are evaluated with mountain-scale THC simulations presented in Section 3.3.6.

6.3.1.2 Goal of Model

The THC seepage models consist of two-dimensional, half-drift (symmetric) chimney models extending vertically from near the ground surface down to the water table and horizontally from drift center to the midpoint between drifts (Figure 6.3.1.2-1). The goal of these models is to analyze the effect of THC processes in the rock around emplacement drifts, including predicting the composition of waters and gases that could enter the drift (addressed in this section) and evaluating the effect of THC processes on seepage (addressed in Section 4.3.6).

Given the large number of input data and their uncertainties, the THC seepage models cannot be expected to predict exact water and gas compositions, especially over the long simulated time periods required to evaluate repository performance. The THC seepage models are still useful in evaluating general chemical trends around the drift with time (over a 100,000-year time period) and the variations of these trends with variations in model input data, drift design parameters, heat loads, locations, and boundary conditions.

The goal of the THC seepage models is not to simulate actual seepage into the drift. The range of simulated infiltration rates (which includes rates for future climate conditions of high infiltration, up to 47 mm/yr) remains well below the theoretical seepage threshold for the rock properties assumed around the drift (see Section 4.3.1). Therefore, the models are used to compute the compositions of pore water and gas in rock fractures around the drifts, and these fluids are assumed to be representative of fluids that could enter the drift. Pore water compositions in the rock matrix are also computed by the THC seepage models, but are not discussed here because the rock permeability is many orders of magnitude smaller in the matrix than in fractures, so any water entering drifts would enter from fractures instead of the rock matrix.

Finally, the THC seepage models did not consider advective fluid movement across the drift wall. Because the seepage threshold is never exceeded, this has no direct effect on the percolation of water towards the drift crown. The THC seepage models were not intended to model water-rock interactions in the drift, such as in the invert (or in the backfill material that was considered in earlier repository designs). Therefore, the effect of pore water potentially reacting with the invert is neglected. Another consequence of closing the drift wall to advective fluid flow is the exclusion, from modeled processes, of the effects of any imposed pressure and relative humidity boundary conditions within the drift. These conditions are likely to differ from conditions within the rock during preclosure ventilation, and could remain so for some time after closure. One of the main consequences is that the effect of water removal (evaporation) at the drift wall due to ventilation is not considered in the THC seepage model simulations. The effects of water imbibition in the invert and of seepage evaporation in the drift are, however, evaluated by the acid neutralizing capacity/pH mixing model and the precipitates and salts model discussed in Section 6.3.3.

6.3.1.3 Discussion of Results and Identification of Previously Unquantified Uncertainties

The initial work documented in *Drift-Scale Coupled Processes (DST and THC Seepage) Models* (CRWMS M&O 2000 [DIRS 142022], Section 6.3) included one THC seepage model with a

drift located in the Tptpmn. The simulated design included backfill, an initial mean linear heat load of 1.54 kW/m, and a 50-year preclosure period with 70 percent heat removal. This thermal load was predicted to yield temperatures above the boiling point of water (near 96°C at Yucca Mountain) in the rocks in the vicinity of the emplacement drifts for hundreds of years. THC seepage simulations were also performed for an ambient temperature case (no heat load) to serve as a baseline for evaluations of model results under thermal loading conditions. Uncertainties in this THC seepage model were not explicitly quantified in the TSPA-SR (CRWMS M&O 2000 [DIRS 153246]).

The initial THC seepage model (CRWMS M&O 2000 [DIRS 142022]) is based on information obtained, in part, from thermal testing in the Tptpmn unit, which may exhibit somewhat different TH behavior or mineralogy than lower lithophysal units, in which most of the repository emplacement drifts will be located. Although this could change the system response, the bulk chemistry is similar for all welded host rock units.

Two geochemical systems were considered in this model. The first was, an extended case system that included aluminum silicates (e.g., clays, zeolites, feldspars, and sepiolite), silica phases (e.g., quartz, amorphous silica, tridymite, and glass), gypsum, calcite, fluorite, iron minerals (e.g., hematite and goethite), and a suite of aqueous species (including calcium, magnesium, sodium, potassium, silica, chloride, aqueous carbonate species, sulfate, fluoride, aluminum, and iron). The second was, a base case system was considered that excluded aluminum silicate minerals and iron minerals, thus excluding aqueous species such as aluminum, magnesium, potassium, and iron, which are found in these minerals.

The inclusion or exclusion of aluminum silicate minerals in the system provided a first crude approach to evaluate the model sensitivity to the effective reaction rates of these minerals: either reacting at rates determined from published kinetic and thermodynamic data and estimated reactive surface areas, or reacting so slowly that the reactions could be neglected.

The initial THC seepage model (CRWMS M&O 2000 [DIRS 142022]) predicted large variations in carbon dioxide concentrations and water compositions at ambient temperatures (no heat load) around the drift when using the extended case geochemical system, and much less with the base case system. Predicted ambient trends showed fairly large pH increases, calcium depletion, and sodium enrichment resulting from the dissolution of feldspars to form calcium zeolites (stellerite) and clays (illite and smectites). Fairly steady ambient water compositions could not be achieved unless aluminosilicate minerals were excluded from the modeled geochemical system. This was observed even though rate constants and effective mineral surface areas were already significantly reduced to yield low effective reaction rates accounting for processes such as mineral armoring. The apparently overestimated dissolution of feldspars to form clays and zeolites was in large part attributed to poorly constrained thermodynamic data for these minerals. A revision of these data (see Section 6.3.1.4) yielded much steadier concentration trends under ambient conditions. In this respect, the initial THC seepage simulations (CRWMS M&O 2000 [DIRS 142022]), as compared to revised THC model results (BSC 2001 [DIRS 154677]), are useful to illustrate the large effect that thermodynamic and kinetic data impose on computed water and gas compositions. For example, small changes in the Gibbs free energies of zeolites and clay minerals (on the order of 0.5 percent) affected predicted concentrations of carbon

dioxide gas and reactive aqueous species such as calcium, magnesium, and sodium by several orders of magnitude (see Section 6.3.1.4).

The initial THC seepage model (CRWMS M&O 2000 [DIRS 142022]) was also useful to evaluate the effect of infiltration on computed water and gas compositions around drifts because a wider range of infiltration rates was considered than in subsequent work (BSC 2001 [DIRS 154677]). Three infiltration rate scenarios were considered, each with varying infiltration over time to simulate future wetter conditions: a mean case (rates between 6 and 25 mm/yr), an upper-bound case (rates between 15 and 47 mm/yr), and a lower-bound case (rates between 0.6 and 6 mm/yr). A fixed ambient mean infiltration rate near 1 mm/yr was also considered for ambient THC simulations.

The different infiltration cases did not significantly affect predicted trends of temperature at the wall of the modeled drift, with no more than an approximately 15 percent temperature variation (under thermal load) between the lower-bound and upper-bound infiltration cases. A similar conclusion was reached for the *Multiscale Thermohydrologic Model* (CRWMS M&O 2000 [DIRS 149862], Sections 6.11.1.4, 6.11.2, 6.11.3.2, and 6.11.4.2), and the *Water Distribution and Removal Model* (CRWMS M&O 2001 [DIRS 152016], Sections 6.3.3.1 and 6.3.3.2).

During the cooling phase, significant fluid composition differences were predicted around the drift between the lower-bound and the mean infiltration cases (up to 1.5 pH units and nearly two orders of magnitude carbon dioxide concentration). Such large differences were not observed between the mean and upper-bound infiltration cases (mostly within half an order of magnitude). As previously, these simulations were affected by overly reactive aluminosilicate minerals, which likely exacerbated the predicted concentration differences between the lower-bound and mean infiltration cases. As infiltration rates increase, advective rates (i.e., seepage velocity) increase relative to reaction rates, such that calculated concentrations become more dependent on advective rates than on reaction rates (and less sensitive to the latter).

The probability of seepage into drifts increases with increasing infiltration rates. However, as infiltration rates increase, the effect of mineral reactions on water composition decreases (at least for minerals with slow reaction rates such as aluminosilicate minerals), and the assumed composition of infiltration waters and gases becomes important in determining the composition of fluids that may enter drifts. Therefore, in this respect, uncertainties on the assumed composition of infiltrating water should largely dominate the effect of uncertain infiltration rates. In addition, if uncertainties in reaction rates can be minimized through a justifiable calibration of thermodynamic and kinetic data to the initial (measured) water composition, as was done for the revised THC simulations (BSC 2001 [DIRS 154677]) (see Section 6.3.1.4), the assumed composition of initial pore water and infiltration water input into the model (and associated carbon dioxide partial pressures) become among the main model uncertainties regarding predicted water compositions.

To summarize, the initial THC seepage model (CRWMS M&O 2000 [DIRS 142022]) is useful to semiquantitatively evaluate the model sensitivity to the reaction rates of aluminum silicate minerals and to a range of infiltration rates including future climates wetter than the present day. However, under high infiltration rate conditions most favorable to in-drift seepage, uncertainties in these parameters are likely to be overshadowed by the assumed composition of fluids

infiltrating at the top model boundary. Therefore, while the initial THC simulations provide some quantitative assessment of uncertainties related to mineral reaction rates and infiltration rates, the effect of infiltration composition remains to be quantified. None of these uncertainties were included in the TSPA-SR (CRWMS M&O 2000 [DIRS 153246]).

6.3.1.4 Revised Model Developments and Results

Unquantified uncertainties identified since the TSPA-SR (CRWMS M&O 2000 [DIRS 153246]) include those related to the rates of fast-reacting minerals (such as calcite and amorphous silica), differences in repository host rock geologic units (effects of mineralogy and rock TH properties), drift design parameters, drift wall boundary conditions, and initial pore-water compositions. Several of these uncertainties were addressed in the revised THC drift-scale modeling studies (BSC 2001 [DIRS 154677]), while others required additional work (see Section 6.3.1.5). Similar uncertainties apply to alternative thermal operating modes. However, some of these uncertainties (e.g., reaction rates) affect predicted fluid compositions more strongly at high temperatures than at low temperatures. The effect of a lower thermal load on model uncertainty is evaluated in Section 6.3.1.5.

The revised *Drift-Scale Coupled Processes (DST and THC Seepage) Models* (BSC 2001 [DIRS 154677]) included a THC seepage model with a drift located in the Tptpll, consideration of heterogeneous permeability distributions, more extensive validation of modeled THC processes, and an evaluation of the model sensitivity to various input parameters. The seepage models were simulated with a higher-temperature operating mode, with a slightly lower (but otherwise similar) thermal load compared to the initial THC simulations (CRWMS M&O 2000 [DIRS 142022]), and with a more recent drift design that excluded backfill.

6.3.1.4.1 Thermal-Hydrologic-Chemical Seepage Model Developments

Three new THC seepage models were presented in the revised *Drift-Scale Coupled Processes (DST and THC Seepage) Models* (BSC 2001 [DIRS 154677]).

Tptpmn Thermal-Hydrologic-Chemical No-Backfill Model–This model considers a heat load in the Tptpmn (BSC 2001 [DIRS 154677], Section 6.4). This model is essentially the same as the THC seepage model presented in the initial THC simulations (CRWMS M&O 2000 [DIRS 142022]) (see Section 6.3.1.3), but with the following important differences:

- No backfill is in the drift
- Slightly lower heat load (1.45 kW/m)
- Revised drift thermal conductivities (invert, inner, and outer zones)
- Stronger coupling of permeability to porosity changes
- A revised activity-coefficient model for aqueous species, revised thermodynamic and kinetic data, and treatment of clay minerals (smectites) as an ideal solid solution phase rather than individual phases

- Calcite reacts at equilibrium with an allowed supersaturation gap that results in effectively larger reaction rates

- Increased effective fracture mineral reactive surface areas (over 50 percent higher)

- Increased initial precipitation rate of secondary minerals under kinetic constraints (by at least one order of magnitude)

- Increased carbon dioxide diffusion coefficient (by a factor of approximately 30).

Tptpmn Thermal-Hydrologic-Chemical Heterogeneous Model–This model is identical to the Tptpmn no-backfill model, except that it considers initial heterogeneous fracture permeability variations of about four orders of magnitude (BSC 2001 [DIRS 154677], Section 6.5). The purpose of this model is to address the effects of fracture permeability heterogeneity at the drift scale on water and gas chemistry, hydrologic properties, and the potential for enhanced or reduced seepage owing to THC processes (see Section 4.3.6).

Tptpll Thermal-Hydrologic-Chemical Model–This model considers a heat load in the Tptpll without backfill (BSC 2001 [DIRS 154677], Section 6.6). The main differences between the Tptpll THC model and the Tptpmn seepage models described above are:

- Different repository host rock unit

- Increased invert thickness (from 0.6 to 0.8 m)

- Updated hydrologic properties calculations, including fracture permeabilities for most units of the Topopah Spring tuff, capillary properties of the Tptpll, and fracture porosities of all units (except Tptpmn)

- Updated rock mineralogy, volume fractions, and mineral surface areas calculations for all units, with the addition of an opal phase in the geochemical systems considered.

For these new THC seepage models, sensitivity studies involving systematically changing input parameters over a wide range of values were not conducted. Variations in input parameters were mostly related to model improvements and changes in drift design parameters and drift location, but nonetheless allowed some qualitative or semiquantitative assessment of the model sensitivity to various input data and design parameters.

These new models considered only the mean infiltration scenario modeled in the initial THC simulations (CRWMS M&O 2000 [DIRS 142022]): initial 6 mm/yr, changing to 16 mm/yr at 600 years, then 25 mm/yr after 2,000 years. For each model, two geochemical systems were considered (as in the previous study): a base case without feldspars, clays, zeolites, or iron minerals and an extended case including these minerals. Some minor changes were also made to the type of minerals considered compared to the initial THC simulations.

Compared to the initial THC simulations, the revised THC seepage models (BSC 2001 [DIRS 154677]) produced a fairly steady hydrochemical system under ambient conditions (no thermal load), yielding water compositions close to the initial (observed) water composition.

This was achieved primarily by calibrating the equilibrium constants of smectites (clays) and zeolites to the initial (measured) pore-water composition. This exercise corresponded to a change of 0.5 percent or less of the Gibbs free energies of these minerals, which is largely within the original error margin of these values. These small changes significantly affected reaction trends and rates, such that the large fluctuations in calculated ambient water compositions in the initial THC simulations were not observed (Figures 6.3.1.4-1 and 6.3.1.4-2).

The steadiness of water and gas concentrations calculated under ambient conditions over long periods of time was improved by allowing calcite to remain supersaturated (by the same amount as in the initial water) before precipitating, and by significantly decreasing the surface area of anorthite (three orders of magnitude). The mineral sepiolite was removed from the modeled system to improve calculated ambient magnesium concentrations. In addition, the revised THC seepage models (BSC 2001 [DIRS 154677]) included a top boundary water with a lower pH (pH = 7.75 versus 8.32) and higher partial pressure of carbon dioxide (approximately 3,700 versus 900 ppmv) than was considered in the initial THC simulations, as this seemed to improve the results of simulations under ambient conditions.

Changes in the revised THC simulations (BSC 2001 [DIRS 154677]) in thermodynamic and other input data described above can be regarded as a model calibration against the initial (ambient) water composition. These changes were necessary and justifiable (i.e., the model should be able to reproduce observed ambient conditions before an attempt is made to simulate thermal loading), as well as defensible (i.e., changes were carried out within the range of the uncertainty of the affected data). As a result, the revised THC simulations can be viewed as better constrained than the initial THC simulations. Another effect of these changes was that in the revised THC simulations, fewer differences were observed between water compositions calculated using the base case and extended case geochemical systems than were observed in the initial THC simulations.

6.3.1.4.2 Sensitivity to General Model Improvements (Tptpmn Models)

Most differences in computed water and gas chemistries (at the drift wall) between the initial (CRWMS M&O 2000 [DIRS 142022]) and revised THC seepage models (BSC 2001 [DIRS 154677]) are not related to differences in drift design (backfill versus no backfill), differences in host rock unit (Tptpmn versus Tptpll), or improvements in implemented process models. These differences, with exceptions discussed below, are primarily attributed to the changes, previously mentioned, made to thermodynamic and other input data to better reproduce ambient water compositions.

The general predicted trends of carbon dioxide concentrations around the drift are similar to those predicted in the initial THC simulations (CRWMS M&O 2000 [DIRS 142022]), with a large decrease during dryout followed by a steep increase during the initial cooling and rewetting stage (Figure 6.3.1.4-1). Predicted concentrations during dryout are below ambient values and are generally smaller in the initial THC simulations than in the revised THC simulations (by up to three orders of magnitude when using the base case geochemical system, not shown here) because the carbon dioxide diffusion coefficient in the initial THC simulations is smaller (by a factor of 30) than in revised THC simulations (diffusive fluxes into the drift are most significant

during this time period). During other simulated time periods, the increased diffusion coefficient does not appear to have a significant effect.

Modeled concentration trends of aqueous species in the revised THC simulations (BSC 2001 [DIRS 154677]) are less variable than in the initial THC simulations, with concentrations returning to ambient values within the simulated time period (Figures 6.3.1.4-1 and 6.3.1.4-2). At the drift wall, predicted pH values range from pH = 7.1 to 8.6, and the total aqueous carbonate concentrations remain less than 250 mg/L over the 100,000-year simulated time interval (range defined by the revised THC simulations using the extended case and base case geochemical systems). With time, calcium and sodium concentrations do not show marked decreases and increases, respectively, as was predicted in the initial THC simulations. Chloride and fluoride concentrations show trends similar to those previously modeled in the initial THC simulations for similar infiltration rates.

The only significant qualitative differences between the water compositions predicted in the revised Tptpmn THC model (BSC 2001 [DIRS 154677]) and the initial model results are that the large variations in pH and the concentrations of carbon dioxide, aqueous carbonate, calcium, magnesium, and sodium during the cooling stage are no longer predicted. In this respect, the predicted water composition in fractures around the drift in the revised THC simulations fall within a narrower range than in the initial THC seepage model (CRWMS M&O 2000 [DIRS 142022]). This is largely the result of the better-constrained thermodynamic data for clays and zeolites, also with other changes noted earlier. Comparison between the initial and revised results provides some qualitative analysis of the model sensitivity to the choice of minerals included in simulations, their stability, and reaction rates. Because ambient simulations in the revised THC simulations predict water compositions more consistent with the initial (measured) water composition, it is expected that the overall uncertainty of the revised THC seepage models (BSC 2001 [DIRS 154677]) has been reduced (at least to a range within the uncertainty of input pore water and infiltration water compositions).

6.3.1.4.3 Sensitivity to Host Rock Unit (Tptpll versus Tptpmn)

Differences in mineralogy and mineral surface areas between the Tptpmn and Tptpll hydrogeologic units are small and, therefore, have only a small effect on modeled water compositions around drifts within the 100,000-year time period investigated. The same can be said for differences in hydrologic properties between both units. Under ambient and thermal loading conditions, overall concentration trends predicted for fractures (at the drift wall) for the considered chemical species differ little between the Tptpmn and the Tptpll models. During the cooling phase, the difference in predicted concentrations around the modeled drift between both models remains mostly within 50 percent, except for fluoride, as discussed below.

Predicted fluoride concentrations in the Tptpll model under ambient and thermal loading conditions are higher (by up to an order of magnitude) than in the Tptpmn model because of CaF_2 dissolution (Figure 6.3.1.4-3). This mineral is observed in fractures and lithophysae of the TSw geologic units (Carlos et al. 1995 [DIRS 101326], Appendix I) and was included as a fracture mineral in the Tptpll model (TSw geologic units). However, it was not included as a primary mineral in the Tptpmn model (secondary mineral only). In the Tptpll model, predicted ambient fluoride concentrations tend toward equilibrium with fluorite (5 to 6 mg/L for the

modeled ambient geochemical conditions) because the reaction rate of this mineral is fast. However, less than 1 mg/L is reported in the initial pore water. Predicted fluoride concentrations are therefore sensitive to the presence of fluorite in the modeled rock units. Including this as a primary mineral is likely to provide an upper bound for predicted fluoride concentrations.

6.3.1.4.4 Sensitivity to Heterogeneous Permeability Distribution

Comparisons of predicted water chemistry data around the modeled drift between initially homogenous and heterogeneous models show little difference (Figures 4.3.6-6 and 4.3.6-7 in Section 4.3.6.4.3). Spatial differences in water chemistry are not affected significantly by permeability heterogeneities for these simulations, so it is expected that heterogeneities in fracture permeability (within the range observed in the Tptpmn unit) would not significantly affect the overall composition of fluids that could enter the drifts.

6.3.1.4.5 Increasing Confidence through Additional Model Validation and Sensitivity Studies

In addition to the new THC seepage models, the revised *Drift-Scale Coupled Processes (DST and THC Seepage) Models* (BSC 2001 [DIRS 154677]) presents a systematic evaluation of mineral reaction rate uncertainty using data collected during the Drift Scale Test. Although these sensitivity analyses cover a relatively short time (two to three years) compared to the simulated length of the THC seepage models (100,000 years), these relate to the same process models as those implemented in the THC seepage models. These analyses also use the same revised thermodynamic data for clays and zeolites and assumed calcite supersaturation gap as in the THC seepage models (BSC 2001 [DIRS 154677]), and, therefore, relate directly to the validity and uncertainty of these models.

These analyses were conducted by comparing the compositions of waters and gases collected during the Drift Scale Test with compositions predicted using THC simulations of this thermal test and assuming various reaction rates and sets of reacting minerals. The simulations conditions included a base case geochemical system without aluminum silicate minerals (see Section 6.3.1.3) or an extended case system that includes these minerals, included calcite reacting at equilibrium or under kinetic constraints (with a supersaturation gap), and included anorthite reacting with surface areas differing by three orders of magnitude.

Results are shown in Figures 4.3.6-2 and 4.3.6-3, with further details presented in Section 4.3.6.4.1, as well as in *Drift-Scale Coupled Processes (DST and THC Seepage) Models* (BSC 2001 [DIRS 154677], Section 6.2.8). These figures do not show large differences in predicted concentrations for the various cases investigated, and have generally similar predicted concentration trends and concentrations mostly remaining within the same order of magnitude as measured values.

The initial analyses also included THC simulations of a plug-flow reactor tuff dissolution experiment (BSC 2001 [DIRS 154677], Section 6.7). These simulations are discussed in Section 4.3.6.7. In general, using the same thermodynamic and kinetic data, as well as the same rock mineralogy and geochemical components as those used in the THC seepage models (BSC 2001 [DIRS 154677]), these simulations yield relatively good agreement between

measured and predicted water compositions. While these THC simulations were useful to demonstrate the validity of modeled processes, the length of the modeled experiment (two months) is likely too short to fully assess the uncertainty of the THC seepage model over thousands of years. Nevertheless, this work improved the confidence in the THC seepage models (BSC 2001 [DIRS 154677]) and their input thermodynamic and kinetic data.

6.3.1.5 Recent Work

Additional THC simulations were conducted to further evaluate the uncertainties associated with the THC seepage models (Bodvarsson 2001 [DIRS 154669], Attachment 5, pp. 10 to 59). The conditions for these simulations are summarized in Table 6.3.1.5-1. The goal of these simulations was to evaluate previously unquantified uncertainties that may significantly affect the predicted compositions of fluids that could enter drifts. From the list of potential uncertainties discussed in Section 6.3.1.1 and the uncertainty analyses presented in Sections 6.3.1.3 and 6.3.1.4, three uncertainties were selected for further analysis: the effects of operating temperature, the effects of different carbon dioxide partial pressures at the top model boundary, and the effects of different initial pore water (and infiltration) compositions.

For these analyses, a set of consistent (thus directly comparable) THC seepage model simulations were developed, with each model using identical model grid and setup parameters, including identical pressure and temperature boundaries, identical rock thermal and hydrologic properties, and identical drift design (no backfill). These simulations also made use of identical input thermodynamic and kinetic data, initial rock compositions, mineral surface areas, and geochemical systems. These simulations were performed using the updated Tptpll THC seepage model (BSC 2001 [DIRS 154677], Section 6.6). Slight changes were made in the drift configuration, thermal properties of in-drift systems, and thermal properties of the Tptpll unit to reflect more recent revisions. Also, smaller time steps were used for the first simulated 2,000 years. Two heat loads were considered.

The first case used an initial heat load of 1.45 kW/m and a 50-year forced ventilation period, during which 70 percent of the heat is assumed to be removed. These are the same conditions as in the revised THC models (BSC 2001 [DIRS 154677]), giving rise to above-boiling temperatures in rocks around the drift for hundreds of years (referred to the higher-temperature case). The second case used, an initial heat load of 1.13 kW/m and a 300-year forced ventilation period, during which 80 percent of the heat is assumed to be removed. These conditions give rise to temperatures staying below boiling in rocks around the drift, with temperatures at the surface of the waste package remaining below 85°C (referred to as the lower-temperature case).

The results of the higher-temperature case are similar to those documented in the Tptpll THC seepage model (BSC 2001 [DIRS 154677]; (see also Section 6.3.1.4). This is because of the small differences between the simulation conditions. The update of the Tptpll thermal properties from values used in BSC (2001 [DIRS 154677]) caused less than a 10 percent change in calculated drift wall temperatures. Predicted carbon dioxide and aqueous concentrations at the drift crown, after rewetting, mostly remained within 10 percent as well (DTN: LB0011DSTTHCR1.001 [DIRS 154759], Table 6.3.1.5-1).

For both operating temperature modes, two conditions of carbon dioxide partial pressures at the top model boundary were considered:

- A partial pressure of $10^{-2.5}$ bars (approximately 3,700 ppmv at the top boundary atmospheric pressure). This is the same partial pressure as in the THC seepage models (BSC 2001 [DIRS 154677]) (referred to as the high-CO_2 case)

- A partial pressure corresponding to the saturation pressure of carbon dioxide in the initial pore water (at an approximate boundary temperature of 17°C). This pressure is calculated to be $10^{-3.2}$ bars (near 750 ppmv at the top boundary atmospheric pressure) (referred to as the low-CO_2 case).

For all of these simulations, as in the initial THC simulations (BSC 2001 [DIRS 154677]), the carbon dioxide partial pressure in the drift was assumed to be unaffected by ventilation and dictated primarily by the pore water composition at the drift wall. Preliminary simulations for another lower-temperature, high-CO_2 case, using input data similar to (but revised since) those described above, also investigated the effect of fixing the carbon dioxide partial pressure at atmospheric pressure (near 400 ppmv) in the drift during 300 years of ventilation (DTN: LB0102DSTHLTD.001 [DIRS 154868]). The effect on water composition (pH) at the drift wall was small (less than 0.5 pH units) and short-lived, with little effect after 300 years and essentially no effect after 1,000 years. For this reason, this case was not pursued further.

There is a large degree of uncertainty regarding the pore water composition in the potential repository host units. No full characterization of pore waters from the Tptpll is available. At the time of the start of the initial work (BSC 2001 [DIRS 154677]), the only nearly complete pore water analyses for samples collected from a rock unit near the potential repository footprint were analyses of three samples ultra centrifuged from core obtained from the Tptpmn geologic unit in Alcove 5 near the Drift Scale Test. These analyses are shown in Table 6.3.1.5-2 (samples labeled HD-PERM-1, HD-PERM-2, HD-PERM-3), together with other water compositions discussed later. An average of the two Alcove 5 water analyses with the closest pH and concentrations (HD-PERM2 and HD-PERM3) was used as the initial pore water composition in the initial and revised THC seepage models, as described in *Drift-Scale Coupled Processes (DST and THC Seepage) Models* (BSC 2001 [DIRS 154677], Section 4.1). This water composition, computationally re-equilibrated at the temperature and carbon dioxide concentration at the top model boundary, was also used for infiltration water in the previous models. To evaluate the model sensitivity to the use of other initial waters, additional simulations were conducted using different water compositions (i.e., UZ-14 perched water and infiltration water).

UZ-14 perched water was used as the initial pore water (Table 6.3.1.5-2). This water is calculated to be at saturation with calcite at 25°C, charge balanced, and is not subject to the uncertainties regarding extraction procedures of pore waters from welded tuffs. The pH of this water is lower (pH = 7.8) than that of the Alcoves Tptpmn pore water (pH = 8.3), and its calculated carbon dioxide partial pressure at 25°C (corresponding to approximately 2,500 ppmv at the drift atmospheric pressure) is greater than in the water used previously (near 1,000 ppmv at the drift atmospheric pressure). This water is representative of sodium-bicarbonate waters (such as groundwater from Well J-13) that yield an alkaline brine upon evaporative concentration.

Infiltration water consisted of the same UZ-14 perched water as described above, but re-equilibrated with calcite at the approximate boundary temperature of 17°C and the same carbon dioxide partial pressure as in the high-CO_2 case ($10^{-2.5}$ bars, for consistency of all high-CO_2 cases).

The higher- and lower-temperature cases were investigated using the UZ-14 perched-water composition. It is emphasized, however, that this water exhibits a carbon dioxide partial pressure that is not consistent with measurements in the ESF and borehole UZ-1, as discussed below. Therefore, the use of UZ-14 water as initial pore water in the THC seepage models should only be viewed as a sensitivity exercise. For this reason, as well as time constraints, analyses using the UZ-14 water were not abstracted for TSPA (see Section 6.3.1.6).

6.3.1.5.1 Higher-Temperature and Lower-Temperature Operating Mode Comparison (Alcove 5 Pore Water)

This section discusses differences between the two operating temperature modes, as simulated with the THC seepage models (BSC 2001 [DIRS 154677]), with respect to predicted water and gas compositions around drifts. Differences in TH behavior between the two operating temperature modes are also discussed in Sections 4.3.5, 5.4.1 and 5.4.2 for TH simulations considering input TH parameters and heat loads similar to those used in the THC seepage models.

The higher-temperature case causes temperatures above boiling in rocks around the drift. The drift wall is predicted to dry out for approximately 1,600 years, after which time the drift crown starts to rewet. The extent of predicted rock dryout around the drift varies depending on the infiltration rate and host rock thermal properties. The THC seepage models predict dryout from approximately 6 to 12 feet at the crown in fractures. However, these models may predict a larger dryout zone than other TH simulations (e.g., Sections 4.3.5, 5.4.1, 5.4.2) because lowering of the water vapor pressure, which is caused by the capillary pressure in the rock matrix, is not considered in THC simulations. This may affect the predicted composition of water around the drift. Neglecting vapor pressure lowering could result in overestimating concentrations of aqueous species, as a result of overestimated evaporative concentration. In this respect, the higher-temperature case may be viewed as providing an upper bound on the effect of evaporative concentration. In contrast, in the lower-temperature case, rocks around the drift are not predicted to dry out, significantly reducing the effect of evaporative concentration at the drift wall. This is one of the two main differences between the two operating temperature modes being investigated.

The second important difference between the higher- and lower-temperature cases, with respect to the composition of fluids that may enter drifts, results from the large temperature effect on mineral reaction rates and stability. Temperature also increases the partial pressure of gases (e.g., carbon dioxide) dissolved in the pore water. Most rock-forming minerals are less stable and dissolve faster at high temperatures. One exception is calcite, which has a decreasing solubility with increasing temperature.

Figures 6.3.1.5-1 through 6.3.1.5-3 compare predicted concentrations of carbon dioxide and aqueous species in fractures at the drift crown for the higher-temperature, lower-temperature, and

ambient (no heat load) cases, using Alcove 5 pore water as the initial and infiltrating water composition. In the higher-temperature case, the drift wall is dry from approximately 50 to 1,600 years, so no aqueous species concentrations are shown.

For the cases considered here, the most visible effect of increasing temperature on water chemistry is the volatilization of carbon dioxide from the pore water (there are a large number of naturally dissolved carbonate species in the pore water). This is a common phenomenon observed in many geothermal areas around the world. In the TSw geologic units, the porosity and liquid saturation are significantly larger in the rock matrix than in fractures (DTN: LB990861233129.001 [DIRS 110226]; DTN: GS980808312242.014 [DIRS 106748]). Therefore, the bulk of the water (moisture) present in the rock is contained in the matrix, not in fractures. When heated, carbon dioxide exsolved from matrix water is transported into fractures. This can cause the carbon dioxide partial pressure to rise above ambient values in fractures, and also cause a pH decrease in fracture water when steam condenses. However, during the dryout period in the higher-temperature case, carbon dioxide concentrations at the drift wall fall largely below ambient values (i.e., decrease up to four order of magnitude) as the result of boiling and displacement by steam. During early rewetting of fractures at the drift crown, the carbon dioxide partial pressure in the higher-temperature case is still depressed relative to the lower-temperature case, causing predicted pH values approximately 0.4 units higher than in the lower-temperature case. The volatilization of carbon dioxide causes total aqueous carbonate concentrations at the drift wall to decrease below ambient values in fractures (by a factor of approximately two in the lower-temperature case and approximately four in the higher-temperature case).

For most major cations and anions, except aqueous carbonate species, initial concentrations predicted in fractures at the drift crown at the time of rewetting (near 1,600 years) in the higher-temperature case are considerably larger (one or more orders of magnitude) than concentrations predicted in the lower-temperature case. This is primarily because of the larger evaporative concentration. Accordingly, the higher concentrations correspond to significantly smaller water saturation in fractures, which results in lower percolation fluxes. In this case, the predicted water saturation in fractures at the time of rewetting is too small for any significant water movement to occur. These effects of evaporative concentration, together with the depletion of aqueous carbonate species (Figures 6.3.1.5-1 to 6.3.1.5-3), appear to be more significant than the effect of mineral reactions (at least with respect to the composition of fluids at the drift wall), as very little mineral precipitation or dissolution is predicted to occur (see Section 4.3.6.4).

The general character of predicted water chemistry at the drift crown is examined later in terms of temperature and initial water composition. Predicted water compositions are more affected at high than at low temperatures, although in both cases water and gas compositions return to ambient values along with temperatures. This would indicate no long-lasting (greater than 100,000 years) effects from the thermal perturbations on predicted fluid compositions around the drift. In other words, the long-term composition of fluids around the drift seems to be largely dominated by the composition of infiltrating water (assumed, in the present case, to be similar to the initial pore water), regardless of the thermal operating mode of the repository.

6.3.1.5.2 High-CO_2 Compared with Low-CO_2 (Alcove 5 Pore Water)

The effect of the different carbon dioxide partial pressures at the top model boundary (reflected by the composition of infiltration water) is not seen until approximately 800 to 1,000 years. During this initial period of time, predicted fluid compositions at the drift wall are similar for the high-CO_2 and low-CO_2 cases in both operating modes. After that time, the effect is limited, resulting in an increased pH (by 0.2 to 0.4 units) for the low-CO_2 case compared to the high-CO_2 case in both operating modes and under ambient conditions (Figures 6.3.1.5-4 and 6.3.1.5-5). The carbon dioxide partial pressure differences affect predicted concentrations of reactive aqueous species to a negligible extent, with concentration reductions (at the drift wall) in the 10 percent range for calcium, sodium, and silica, and concentration increases of similar proportions for fluoride. For the water compositions used, the THC seepage model results were therefore not very sensitive to the range of investigated carbon dioxide partial pressures.

6.3.1.5.3 Uncertainty in Initial and Infiltration Water Compositions

The water analyses used to determine initial pore water and infiltration compositions in the THC seepage models were from the Tptpmn unit in Alcove 5 (HD-PERM samples in Table 6.3.1.5-2). As mentioned earlier, these were the only available nearly full suites of analyses from a repository host unit. The scarcity of such data is due to the fact that these units contain little water and the rock matrix has a low permeability, such that water extraction from the rock samples is difficult. Analyses are uncertain because the volumes of extracted samples are small and the impact of the extraction process (ultracentrifuge) on the water quality is largely unknown. For these reasons, these analyses were compared to water compositions of a few other samples (Table 6.3.1.5-2). These additional samples were selected because they could be good candidates for input into the THC seepage models. The source of each analysis in Table 6.3.1.5-2 is described below. Some of these analyses were incomplete and/or out of charge balance, and it was necessary to recalculate some of the analytical parameters.

Analyses labeled HD-PERM-1, HD-PERM-2, HD-PERM-3 are for three water samples ultracentrifuged from core obtained from the Tptpmn geologic unit in Alcove 5 (Table 6.3.1.5-2). Bicarbonate was not determined and it was recalculated from charge balance. The average of HD-PERM-2 and HD-PERM-3 (nearly identical analyses) was used as the initial pore water composition in the THC seepage models, as well as in the other THC seepage simulations discussed so far.

Sample DXD042 (Table 6.3.1.5-2) was ultracentrifuged from a core sample collected in the ECRB Cross Drift (CS2150), in the Tptpll unit. The pH and total aqueous carbonate content of this sample were not available, and were computed assuming calcite saturation. The resulting calculated carbon dioxide partial pressure of this sample was atmospheric (at 25°C). The sample was therefore re-equilibrated with calcite at a carbon dioxide value (10^{-3} bars) consistent with measured values in the ESF. Another sample ultracentrifuged from core collected in Niche 2 in the Tptpmn unit approximately one kilometer away revealed an essentially identical composition. The potassium concentration was below the detection limit. A potassium concentration was calculated from the illite-microcline equilibrium boundary for this water.

The analysis labeled SD-6 (Table 6.3.1.5-2) is for water extracted from core collected in borehole SD-6, interval 443.5 to 443.8 ft, in the upper part of the PTn hydrogeologic unit above the potential repository. This borehole is located (in plan view) near the center of the potential repository footprint. The original water analysis was not in charge balance. The bicarbonate concentration was adjusted for charge balance and at the same time, the pH was recalculated assuming calcite saturation (at 25°C).

The TSw-Avg composition (Table 6.3.1.5-2) was used in some of the early THC modeling work related to the thermal tests at Yucca Mountain (Tsang et al. 1999 [DIRS 148905]). This composition was determined by averaging the analyses of waters extracted from core samples taken directly above and below the potential repository units (in drill holes UZ-16, SD-9, and SD-12) and reported in Yang et al. (1996 [DIRS 100194]), and by balancing charge on bicarbonate. The potassium concentration was an assumed value at the time.

The analysis labeled UZ-14-Pore (Table 6.3.1.5-2) is for water extracted from core collected in borehole UZ-14 at interval 1258.5 to 1258.8 (ft), at the same depth where perched water was collected. The pH of the sample was not reported. It was computed assuming calcite saturation (at 25°C) and adjusting charge balance on bicarbonate. The potassium concentration was not determined, and the value shown was calculated from the illite-microcline equilibrium boundary for this water.

The analysis labeled UZ-14-Perch (Table 6.3.1.5-2) is for perched water collected from borehole UZ-14 in 1993. This analysis is charge balanced and yields almost exact calcite saturation (at 25°C). It has not been corrected.

The mean J-13 analysis (Table 6.3.1.5-2) is for groundwater samples collected in well J-13. Bicarbonate was adjusted for charge balance (from input alkalinity). The water from J-13 has been extensively studied and serves as a benchmark for many studies involving Yucca Mountain waters. This water also has been used extensively as a proxy for the pore water in the host rock when modeling chemical processes in the near-field environment.

These water compositions (using corrected concentrations) were plotted on a Piper diagram to evaluate the character and variability of these data (Figure 6.3.1.5-6). These compositions show significant scatter, with Alcove 5 samples at the calcium-sulfate-chloride end of the composition range and the J-13 sample at the sodium-bicarbonate end. These analyses are useful in illustrating the range of uncertainty regarding initial pore water and infiltration water compositions input into the THC seepage models. As noted earlier, the composition of infiltrating water is anticipated to dictate the long-term compositions of waters that could enter drifts.

One piece of available information that can be used to narrow the range of potential pore water compositions in the TSw units is the carbon dioxide concentrations measured in pore gas samples collected in the potential repository host rock. The gas analyses are not subject to the uncertainties regarding sample volume and extraction that affect pore water samples. Ambient carbon dioxide concentrations were measured in pore gas samples from potential repository units in drill hole UZ-1 over a 3-year period (DTN: GS930408312271.014 [DIRS 145533]) and in boreholes drilled in the ESF (DTN: LB991215123142.001 [DIRS 128157]). These

concentrations range from approximately atmospheric (400 ppmv) to 1,300 ppmv. These values are significantly lower than concentrations calculated for the UZ-14, SD-6, and J-13 water samples (between approximately 2,700 and 5,800 ppmv). Because of their comparatively elevated carbon dioxide partial pressures, the UZ-14, SD-6, and J-13 samples are uncertain representatives of pore waters from potential repository units, even though analyses of two of these samples are the most reliable because the samples did not need extraction.

Results of THC seepage simulations with UZ-14 perched water were plotted on Piper diagrams with results of the same simulations conducted with Alcove-5 water. These plots can be directly compared to the Piper plot of potential initial water compositions (Figure 6.3.1.5-6). The predicted evolution of the Alcove 5 and UZ-14 waters is shown for fractures at the drift crown: under ambient conditions (Figure 6.3.1.5-7), for the lower-temperature case (Figure 6.3.1.5-8), and for the higher-temperature case (Figure 6.3.1.5-9). Points are shown for given times and corresponding temperatures, and cover the 100,000-year simulated time period.

When heated, both waters generally exhibit a similar behavior, with a larger response (scatter) in the higher-temperature case than in the lower-temperature case, as would be expected. The effect of carbon dioxide volatilization due to the temperature increase, discussed earlier, is clearly shown by the progressive decarbonation of the waters as they undergo heating (lower right triangle on these plots), then return to ambient values as the temperature decreases. Under ambient conditions, both water compositions are predicted to evolve with time from a somewhat more calcium-dominant nature to a somewhat more sodium-dominant character. This trend is typically observed in natural systems over long periods of time. For the simulated UZ-14 water, this trend under ambient conditions is predicted to yield a composition of the same nature as J-13 water. After the thermal perturbation, the composition of both waters returns to ambient values within the simulated time period. Except for the large depletion of aqueous carbonates during the heating period, the scatter in predicted compositions for the two waters falls largely within the variability of potential initial water compositions (Figure 6.3.1.5-6).

The initial pH of the UZ-14 perched water is lower by approximately 0.5 units than the average (HD-PERM-2 and HD-PERM-3) Alcove 5 pore water used in previous simulations (Table 6.3.1.5-2). Under ambient conditions, the pH of UZ-14 perched water in fractures is predicted to increase, from an initial value of 7.8 to approximately 8.1 after 100,000 years. A smaller increase, from 8.3 to 8.4, is predicted with Alcove 5 fracture pore water for the same time period. Upon heating, at the crown of the drift, the pH in the UZ-14 case remains within the range defined by ambient conditions. However, at the base of the drift where evaporation is strongest, pH increases to a maximum near 9.4 for the higher-temperature case and 8.6 for the lower-temperature case. This is not observed with simulations using the Alcove 5 pore water, which predict pH to remain below the range of ambient pH values as long as temperatures exceed ambient values (Figure 6.3.1.5-5). This difference in pH trends is consistent with experimental data (Rosenberg et al. 2001 [DIRS 154862]).

6.3.1.6 Abstraction for Total System Performance Assessment

The abstraction of the above THC calculations follow arguments similar to those as reported in the *Abstraction of Drift-Scale Coupled Processes* (CRWMS M&O 2000 [DIRS 123916]). However, the abstraction includes more variability and an expanded set of time periods, uses

only the results from the extended case models, and includes an ambient period that uses the results from the extended mineral case ambient modeling runs. The decision to base the abstraction solely on the extended mineral case results was made to ensure conservation of charge balance and to ensure consistency between THC model results and abstraction results. The abstracted results presented below carry with them the assumptions, caveats, and limitations of the THC model calculations presented in the preceding sections.

6.3.1.6.1 Use of Abstraction

This abstraction is intended to simplify the THC results presented in Section 6.3.1.5 so that other modeling efforts, such as those found in Section 6.3.3 below and previously documented in the *In-Drift Precipitates/Salts Analysis* model (CRWMS M&O 2001 [DIRS 153265]), can produce a set of appropriate in-drift chemistry lookup tables for TSPA model calculations. The simplifications include a number of time histories of aqueous species (e.g., anion and cation concentrations) that are at or near charge balance and gas phase components (e.g., partial pressure of carbon dioxide, PCO_2) at a representative location in the near-field host rock adjacent to the emplacement drift wall. The abstraction will also produce lookup tables that set the initial results for other abstracted geochemical processes occurring within the repository drift (e.g., in drift gas values will be used to indicate which PCO_2 value to use for the waste form solubility abstractions).

There are three primary uses of the abstraction tables presented below (see Sections 6.3.1.6.3.1 and 6.3.1.6.3.2). First, the abstraction tables are used as input for initial water and gas chemistries, as used in the *In-Drift Precipitates/Salts Analysis* (CRWMS M&O 2001 [DIRS 153265]), to determine the compositions of the brine and precipitates that react with the surfaces of the drip shield, waste package, and invert (see Section 6.3.3). Second, the tables are used to set the PCO_2 in the drift for the given time period. This parameter is used as a governing parameter on several lookup tables that determine the pH and compositional information of fluids interacting with waste package materials and mixing of fluids in the invert (see Section 6.3.3). The PCO_2 values also determine one of the parameters necessary for selecting the solubility of the various radionuclides from their respective functions or lookup tables (see Section 6.4.1). Third, the tables are used as a source of variability and uncertainty in the chemical regime that is imposed on the in-drift environment. The chemistries reported in the tables below represent waters that have interacted with the Tptpll in the following ways: different spatial locations around the drift wall (crown and base of invert); different imposed PCO_2 starting conditions in the soil horizon (high PCO_2 and low PCO_2); different thermal operating modes (higher-temperature versus lower-temperature); and differences between waters primarily derived from fracture seepage (fracture water at crown of drift) and invert imbibition (matrix water at base of invert). These different conditions represent much of the uncertainty and/or variability that is presently incorporated into the chemical system being modeled above.

One specific uncertainty that has been evaluated in the THC calculations in Section 6.3.1.5, but for which results were not abstracted for incorporation into downstream calculations, is the use of a different starting water chemistry (perched water sampled in well UZ-14).

6.3.1.6.2 Conceptual Approach for Abstraction

Two specific criteria are inherent in this abstraction. The first is the need to simplify the THC results reported above for use in the TSPA model. The second is the need to generally reproduce the obvious changes in gas and ion concentrations entering the drift that occur through time as they have potential to influence performance of EBS materials, chemical conditions, and radionuclide transport characteristics.

Two sets of tables have been prepared for use in EBS calculations. The first represent the chemical composition of the seepage flux through the crown of the drift (see Section 6.3.1.6.3.1). The assumption applied to these tables is that any seepage coming into the drift from above would be water that would flow through fractures into the drift. This is a reasonable assumption based on *Abstraction of Drift-Scale Coupled Processes* (CRWMS M&O 2000 [DIRS 123916], Section 5.1.1). The results from *Thermal Hydrology EBS Design Sensitivity Analysis* (BSC 2001 [DIRS 154855]; DTN: MO0008SPATHS03.001 [DIRS 151812]) indicate that seepage into the invert is controlled by matrix flow over the regulatory period and that fracture flow into the invert dominates after the repository cools. As the abstracted water chemistries do not drastically differ between fractures and the matrix, it is assumed that the tables representing the waters being imbibed or wicked into the invert will be those associated with water found in the matrix at the base of the invert (see Section 6.3.1.6.3.2). This is a reasonable assumption based on the principles of matrix imbibition in unsaturated porous media (Jury et al. 1991 [DIRS 102010], pp. 87 to 110) and the similarities in water chemistries.

A discussion in *Abstraction of Drift-Scale Coupled Processes* (CRWMS M&O 2000 [DIRS 123916], pp. 18 to 19) explains the general difficulty of applying a specific statistical methodology to the abstraction. Therefore, the following approach was used to determine the number and duration of the periods. The same reason leads to the approach devised in selecting a specific THC result for that given period, as discussed below.

The establishment of the abstraction periods was based on determining a few appropriate inflection points, then using those points to visually inspect the given THC calculation files produced, as discussed in Section 6.3.1.5 (Table 6.3.1.5-1). After initial inspection of the results, several inflection points were selected: length of the preclosure period (50 or 300 years), length of the boiling period (for higher-temperature cases only), obvious pH changes (about 0.2 units) with a secondary discriminator of noticeable change (generally an order of magnitude) in PCO_2 concentrations, and the reimposition of ambient conditions (post-100,000 year results). These criteria were sufficient to limit the number of abstraction periods to six for the high-temperature abstraction and five for the lower-temperature abstraction (Table 6.3.1.6-1). The six time periods for the higher-temperature abstraction are a preclosure period from 0 to 50 years, a boiling period from 51 to 1500 years, a cooldown period from 1,501 to 4,000 years, an extended cooldown period ranging between 4,001 and 25,000 years, a transition to ambient period from 25,001 to 100,000 years, and an ambient period that goes from 100,001 to 1 million years. The five periods for the lower-temperature abstraction are a preclosure period from 0 to 300 years, a postclosure hot period from 301 to 10,000 years, a cooldown period ranging between 10,001 and 30,000 years, a transition to ambient period between 30,001 and 100,000 years, and an ambient period that goes from 100,001 to 1 million years.

The specific ion concentration, pH, and PCO_2 were determined in a somewhat different way or the ambient period (post-100,000 year) than the other periods discussed below. To determine the ambient period chemistry, the associated ambient temperature case THC calculation (e.g., Run ID thc6_ambL; Table 6.3.1.5-1) was abstracted by taking the results from year 2,000 to year 100,000 and averaging them. The basis for this is two-fold: first, the pH, PCO_2, and ion concentrations do not differ significantly over this period. Second, the infiltration rate is assumed to change at year 2,000 to a rate associated with that of a glacial climate and would be more representative of the boundary conditions for the post-100,000 year period.

For all other periods, the methodology for selecting the specific THC run time is as follows. The time-dependent sets of results (pH, PCO_2, and the reported ions) for the given period abstraction are averaged. The averaged values for pH, PCO_2, and the ions are compared to each individual time-dependent result value. The value nearest to the average is flagged (i.e., all pH values in each of the reported times are looked at and the pH value nearest the average is marked). After all the ions, the pH, and the PCO_2 are sequentially evaluated and flagged, the individual time-dependent chemistry that was most representative of the averaged values for pH, PCO_2, and the reported ions was selected for use during the abstracted period. If there was a tie (e.g., four flags each for time x and time y), the complete chemistries of those that tied were reevaluated for the next closest set of values nearest the average until a determination could be made.

This selection approach has the effect of maintaining consistency with the THC results, since the abstracted chemistry is actually a specific time-dependent result from the THC model and the abstracted chemistry is as close to an averaged chemistry over that period as can be obtained without actually using the averages for the period. This approach also maintains charge balance (sum of cations vs. sum of anions), an important factor in minimizing the potential error to some ions of importance (speciation calculations are often charge balanced by adjusting ions such as Na^+ or Cl^-), as discussed in Section 6.3.3 below, where adding Na^+ or Cl^- could change the ultimate compositional character of the brines interacting on the waste package. This abstraction can also be directly validated, since the values used are actual results from the THC model.

For the boiling period, a decision was made to use the results from the THC calculations for the higher-temperature operating mode directly rather than the compositions from the condensate zone above the drift as previously abstracted (CRWMS M&O 2000 [DIRS 123916], p. 19). This decision is intended to be a somewhat conservative assumption, as the cations and anions are more concentrated in these potential fluids than in those of the condensate water. The rationale for this assumption is that the higher concentrations would tend to form more concentrated brines on the surfaces of the waste package and drip shield. A conceptual basis for this assumption is that the composition of fluids that could flow into the drift would not be too unlike the compositions reported at the drift wall as the calculations in the THC model neared a saturation of 0.0001 because any salts deposited in the fractures from complete evaporation due to boiling and dryout would be rapidly redissolved by condensate water as it flowed down a fracture into the drift.

6.3.1.6.3 Abstracted Results

The results presented below have two main discriminators: the temperature (thermal operating mode) that the drift is allowed to obtain and the imposed soil gas PCO_2 conditions. For use in

TSPA calculations, the tie-in to different thermal operating modes is evident. However, implementing the imposed soil gas PCO_2 condition tables is not. Therefore, for each realization in the TSPA model, either the high soil gas PCO_2 condition or the low soil gas PCO_2 condition will be selected. Once a soil gas mode is selected, it must remain the same throughout the realization. This can be achieved by creating a stochastic switch where, at the beginning of each realization, a uniform distribution from 0 to 1 is sampled, with the low soil gas PCO_2 tables being used over the range of 0 to 0.49 and the high soil gas PCO_2 tables being used over the range from 0.50 to 1. There are separate sets of tables for seepage at the crown (or sides) of the drift and for water imbibed into the invert.

When setting the PCO_2 concentrations for in-drift gas in the TSPA model, the value of PCO_2 for the node at the crown of the drift differs from the value for the node at the base of the invert during any given period (compare Tables 6.3.1.6-1 and 6.3.1.6-5). However, within the drift the value of PCO_2 should be constant throughout. Therefore, when selecting the appropriate PCO_2 value for use within the drift for a given time period, values from the tables associated with the chemistries at the crown of the drift should be used because as advective flow into the drift from the fractures should dominate the fraction that might diffuse through the invert into the drift. Once a given PCO_2 is selected for a period, it should be the only concentration of CO_2 that is used in the drift, including conditions in the invert and breached waste packages. Therefore, this value should be the concentration of PCO_2 for any radionuclide solubility calculation or invert mixing calculation (see Section 6.3.3 for further discussion).

Also presented on each table below are the actual THC model run time for the selected chemistry and the temperature at the drift wall for that given run time. These values may not necessarily apply to TSPA modeling, as the TSPA model will use TH results from a different source. They are given here to maintain the traceability of the abstraction to the process model results. All electronic input and output files for this abstraction are documented in Jolley (2001 [DIRS 154762]).

6.3.1.6.3.1 Tables for the Chemical Composition of Seepage at Crown of Drift

Tables 6.3.1.6-1 through 6.3.1.6-4 list the chemical composition of seepage entering the crown and sides of the drift via advection through fractures. The tables also set the PCO_2 level within the drift. The PCO_2 values for water imbibing into the drift (Tables 6.3.1.6-5 through 6.3.1.6-8) should not be used to set the PCO_2 concentrations within the drift. Using two different PCO_2 values for the same volume of gas is physically incorrect. Based on the assumptions and boundary conditions of the process model (BSC 2001 [DIRS 154677]), gas compositions in the drift would be set by advection through the fractures, not diffusion through the rock matrix.

Higher-Temperature Operating Mode–Tables 6.3.1.6-1 and 6.3.1.6-2 show the composition of seepage entering the crown (or sides) of the drift via advection through fractures when evaluating the higher-temperature operating mode. Table 6.3.1.6-1 is for use during low soil gas PCO_2 realizations in TSPA modeling. Table 6.3.1.6-2 is for use during high soil gas PCO_2 realizations in the TSPA.

Lower-Temperature Operating Mode–Tables 6.3.1.6-3 and 6.3.1.6-4 show the composition of seepage entering the crown (or sides) of the drift via advection through fractures when evaluating the lower-temperature operating mode. Table 6.3.1.6-3 is for use during low soil gas PCO_2 realizations in TSPA modeling. Table 6.3.1.6-4 is for use during high soil gas PCO_2 realizations in the TSPA.

6.3.1.6.3.2 Tables for the Chemical Composition of Water Imbibed into the Invert

Tables 6.3.1.6-5 through 6.3.1.6-8 show the chemical composition of water entering the invert via matrix imbibition from the host rock. These four tables do not show the PCO_2 of the gas in the drift.

Higher-Temperature Operating Mode–Tables 6.3.1.6-5 and 6.3.1.6-6 show the composition of water entering the invert via matrix imbibition from the host rock when evaluating the higher-temperature operating mode. Table 6.3.1.6-5 is for use during low soil gas PCO_2 realizations in TSPA modeling. Table 6.3.1.6-6 is for use during high soil gas PCO_2 realizations in the TSPA.

Lower-Temperature Operating Mode–Tables 6.3.1.6-7 and 6.3.1.6-8 show the composition of water entering the invert via matrix imbibition from the host rock when evaluating the lower-temperature operating mode. Table 6.3.1.6-7 is for use during low soil gas PCO_2 realizations in TSPA modeling. Table 6.3.1.6-8 is for use during high soil gas PCO_2 realizations in the TSPA.

6.3.1.7 Multiple Lines of Evidence

See Section 3.3.6.5 for details of the physical and chemical processes that apply to these calculations.

6.3.1.8 Summary of Remaining Uncertainties

6.3.1.8.1 Thermal-Hydrologic-Chemical Seepage Models

Except for the analyses reported in Section 6.3.1.5, sensitivity studies of the THC seepage models did not involve systematically changing input parameters over a range of values. Variations in input data were mostly related to model improvements and changes in drift design parameters and drift location, which then enabled assessment of model sensitivity to various input parameters. Investigated ranges of input parameters were typically within the bounds of values reasonably applicable to the Yucca Mountain thermal, hydrologic, and geochemical environments.

Table 6.3.1.8-1 summarizes the uncertainties regarding the predicted composition of fluids that may enter emplacement drifts and lists how these uncertainties were treated and their potential effect on model results. This table complements uncertainties summarized in a similar fashion in Table 4.3.6-2, relating to seepage and general seepage chemistry. Although many uncertainties are listed on these tables, only a few appear to dominate the overall uncertainty of the predicted water compositions and thus the uncertainty of further analyses which rely on these results. These include, in order of importance:

- Kinetic and thermodynamic data
- Input initial and infiltration water compositions
- Secondary mineral phases included in simulations
- Trace primary mineral phases (and related aqueous species) included in simulations.

If calibration of the most uncertain kinetic and thermodynamic data can be achieved, such that the model reproduces observed water composition trends (as done in recent analyses), the current uncertainty in water composition input into the model (initial and infiltration) may become the dominant model uncertainty.

6.3.1.8.2 Abstraction

All the uncertainties discussed above regarding the THC seepage model results are propagated in the abstraction of these results (discussed in Section 6.3.1.6). Some of these uncertainties have been assessed by the THC seepage models, but have not been incorporated in the abstractions for the TSPA. These include the variability imposed by the location of the repository (since the majority of the repository is located in the Tptpll but some portions of it may be constructed in the Tptpmn or other units. THC seepage simulations using the Tptpmn lithology around the drift were not conducted because results indicated that the model is not very sensitive to changes in repository host rock unit. The only significant difference between results of the Tptpmn and Tptpll THC seepage models was that higher fluoride concentrations were predicted because small amounts of CaF^2 were included as primary minerals in the TSw units of the Tptpll model (see Section 6.3.1.4). The same mineralogy (including fluorite) was used in the Tptpll model (see Section 6.3.1.5). Therefore, water compositions abstracted from this model are more conservative, in terms of the fluoride concentrations, than in earlier abstractions (CRWMS M&O 2000 [DIRS 123916], p. 9). These earlier abstractions were for a Tptpmn host rock unit. However, the main differences between these earlier abstractions and those from the updated studies are not a result of host rock mineralogy (except for fluoride), but the result of apparently overestimated effective-reaction rates of aluminum silicate minerals in the initial abstraction, as discussed in Sections 6.3.1.3 and 6.3.1.4.

Climate change and increased water availability during glacial times were previously evaluated and found to impact the abstraction tables used in TSPA modeling by a factor of two to five (CRWMS M&O 2000 [DIRS 123916], p. 25). These effects have not been carried forward into this set of abstractions, are therefore an unqualified uncertainty in this work. Another climate-change issue concerns the possible variations through time of soil-zone carbon dioxide partial pressure caused by climate change, which might change the precipitation of calcite, the availability of bicarbonate ion, and the pH. This is demonstrated by Jolley (1997 [DIRS 154535]), who predicted soil-gas carbon dioxide partial-pressure fluctuations between

present-day 1,000 ppmv to 4,700 ppmv during wetter and cooler climates. The THC seepage modeling studies presented in Section 6.3.1.5 indicate that fixed carbon dioxide partial pressures (750 and 3,700 ppmv) at the top model boundary have little effect relative to other model uncertainties (notably those regarding input water compositions in the model).

The THC seepage models do not evaluate locations close to the edge of the repository, where increased infiltration and lower temperatures resulting from edge-effects may affect predicted concentrations of fluid around drifts.

An evaluation of the composition of the initial water used in the THC seepage models is presented in Section 6.3.1.5. A number of possible input water compositions exists for these models, with large uncertainties caused primarily by the difficulty of extracting and analyzing pore water from the low-permeability repository host units (e.g., Higgins et al. 1997 [DIRS 101246]). To address the issue of initial water uncertainty, THC seepage simulations have been initiated using perched water from well UZ-14 (see Section 6.3.1.5). The carbon dioxide partial pressure of this water (and therefore its pH) is not consistent with reliable analyses of carbon dioxide concentrations in pore gas samples from the potential repository host units (see Section 6.3.1.5). Therefore, this water was used only for sensitivity analyses. The results of these evaluations have not been incorporated into a TSPA.

Other specific issues related to the THC seepage model uncertainties discussed earlier that could have a direct bearing on results of the TSPA through the abstracted data include:

- $[Ca_5(PO_4)_3(OH, F, Cl)$ could be added as a primary mineral in the model. If phosphates are included in the simulations, this mineral may affect the predicted phosphate geochemistry. It could also provide a lower bound of predicted fluoride concentrations (under ambient conditions) in geologic units where CaF_2 is either absent or not fully reacting. For the results abstracted here, fluorite equilibrium sets an upper limit in predicted fluoride concentrations (under ambient conditions).

- Lithophysae in the rock properties of the Tptpll could be included, which can add calcite to the mineral inventory and change the porosity of portions of the Tptpll, affecting abstracted water compositions from the THC seepage model.

- An evaluation could be done to determine how the spatial distribution of modeling gas advection versus diffusion out in the host rock might control gas fugacities at localized portions of the drift wall (i.e., advection in highly fractured areas could mask the effect of diffusion in less fractured areas even after the repository is sealed). In conjunction, sensitivity studies on the THC model boundary condition imposed at the drift wall (no advection) could add more understanding of drift wall processes.

- The effect of unrepresentative chemical thermodynamic or kinetic data, or of an incompletely defined geochemical system, on predicted concentrations of key species such as calcium and magnesium could influence model uncertainty.

An example of this last effect is the differences between the predicted calcium, sodium, and magnesium concentrations between the initial (CRWMS M&O 2000 [DIRS 142022]) and

revised THC model simulations (BSC 2001 [DIRS 154677]) (see Section 6.3.1.4). Small changes in equilibrium constants for clays (calcium, sodium, and magnesium smectites) and zeolites, within the original uncertainty of these values, together with other changes discussed in Section 6.3.1.4, caused differences of several orders of magnitude in predicted concentrations for these species. Consequently, a comparison of the abstracted data for both cases (CRWMS M&O 2000 [DIRS 123916], Table 3 with Tables 6.3.1.6-1 and 6.3.1.6-2 show similar large differences. The small change in thermal-chemical (TC) data significantly affects the results of other models that rely on output data from the updated THC seepage models. This change also determines the likelihood of success for such models to predict the accumulation of magnesium and calcium chloride salts on waste packages during the boiling periods (see Section 6.3.3). However, the changes in kinetic and thermodynamic data between the initial (CRWMS M&O 2000 [DIRS 142022]) and updated THC seepage models (BSC 2001 [DIRS 154677]; see also Section 6.3.1.4) were made to calibrate these models such that ambient pore water compositions could be reproduced. Therefore, in this case, the uncertainty lies more strongly in the pore water composition than in the model adjustments that were necessary to reproduce these data. This further emphasizes the potential large effect of initial water composition uncertainty on TSPA results, as noted earlier.

6.3.1.9 Summary and Conclusions

6.3.1.9.1 Thermal-Hydrologic-Chemical Seepage Models

THC seepage models were used to predict the composition of fluids (water and gas) that could enter potential emplacement drifts. Because of the large number and variability of input parameters, as well as the complexity of modeled THC processes, a rigorous quantification (in a statistical sense) of the uncertainty of the THC seepage predictions is not achievable. For this reason, the uncertainty of THC seepage models can only be evaluated in a deterministic, semiquantitative or qualitative manner, with a focus on narrowing rather than quantifying uncertainty. Limiting the uncertainty of the THC seepage models relies strongly on model validation against field and experimental data. While most of these data cover a short time range compared to the long simulated periods of time (thousands of years) in the THC seepage models, successful validation efforts using the same model input data as for the THC seepage models boost confidence in the model results.

Uncertainties affecting the predicted composition of fluids that could enter drifts were identified (Section 6.3.1.1). Some of these uncertainties were evaluated in a semiquantitative manner from modeling work presented in *Drift-Scale Coupled Processes (DST and THC Seepage) Models* (BSC 2001 [DIRS 154677]; see also Sections 6.3.1.3 and 6.3.1.4). Others were addressed by more recent work see Section 6.3.1.5). These evaluations related primarily to infiltration rates, thermodynamic and kinetic data, pore water and infiltration water compositions, boundary carbon dioxide partial pressures, potential repository operating temperature modes, and potential repository host rock units. Other uncertainties more directly related to TH parameters and flow and transport process models were discussed in Section 4.3.6. These uncertainties, treatments, and potential effects on the predicted composition of fluids that may enter drifts are summarized in Tables 4.3.6-2 and 6.3.1.8-1.

The model input thermodynamic and kinetic data, are among the main uncertainties affecting predicted compositions of fluids at the drift wall directly affecting predicted mineral reaction rates. An attempt was made to improve the confidence in model results by adjusting the most uncertain kinetic and thermodynamic data (within their uncertainties) in such a way that observed ambient water compositions would be reproduced fairly well. Once such calibration was achieved, uncertainties in the model results appeared to become more a function of the uncertainty over input initial and infiltration water compositions. At high infiltration rates, predicted concentrations are more a function of transport than reaction. Thus, the model result uncertainty becomes more directly related to infiltration and initial water composition and less dependent on reaction or infiltration rates. At low infiltration rates, the effect of uncertainties in reaction and infiltration rates becomes large, but the likelihood of seepage into the drift is minimal. Therefore, with respect to predicting the composition of fluids that may enter drifts, the uncertainty in the composition of initial infiltration water input into the THC seepage models may largely overwhelm other uncertainties.

Among the various cases evaluated, THC simulations were performed using two significantly different input water chemistries (UZ-14 perched water and Alcove-5 pore water) with significant differences in initial pH and carbon dioxide partial pressures. Using both waters under a higher- and a lower-temperature operating mode, the scatter defined by the predicted water compositions at the drift crown over time fell largely (but not entirely) within the variability of water compositions that could be used for input into the model. For the cases considered, the largest effect of thermal loading on predicted water compositions, relative to ambient water compositions, was decarbonation through volatilization of carbon dioxide. This is a common heating effect observed in natural geothermal systems. Higher temperatures increase the variability of predicted concentrations at the drift wall relative to lower temperatures. However, this effect is predicted to be relatively short-lived. The general nature of predicted water compositions returns largely to within the range defined by observed ambient compositions within 10,000 years. As temperatures decrease and return to ambient values (within 100,000 years), the predicted water compositions at the drift crown return to ambient values for all temperature and water composition cases considered.

6.3.1.9.2 Abstraction

As discussed in Section 6.3.1.6.1, the abstraction tables provide input into downstream models (see Section 6.3.3) and to TSPA modeling. Look up tables, provided in Sections 6.3.1.6.3.1 and 6.3.1.6.3.2, are designed to represent the process model results reported in Section 6.3.1.5 above. They include evaluation or implementation of several uncertain parameters. Depending on the thermal operating mode, the chemistries have been abstracted into five or six periods that represent changes in temperature (122° to 23°C), pH (7.23 to 8.57), and PCO_2 (1.06×10^{-3} to 8.91×10^{-6}), along with the following ions: calcium, magnesium, sodium, chloride, SiO_2, HCO_3, SO_4K, AlO_2F, and FeOOH. These tables are representative of the chemistries that would enter the drift through time for the conditions specified in the process model reported in Section 6.3.1.5.

6.3.2 Effects of Engineered Materials on the Chemical Environment

6.3.2.1 Introduction

Corrosion of steel and other alloys, chemical reactions of cementitious grout in conjunction with rock bolts, and formation of colloids from engineered materials have the potential to affect the in-drift chemical environment as it relates to the performance of the potential repository system.

6.3.2.2 Goal of Model

The models for corrosion, reactions of cementitious materials, and colloid formation are intended to evaluate the significance of these processes and quantify their effects where necessary.

6.3.2.3 Discussion of Total System Performance Assessment-Site Recommendation Result, and Identification of Previously Unquantified Uncertainties

Uncertainties in the models of the effects of engineered materials on the chemical environment were not explicitly quantified in the TSPA-SR (CRWMS M&O 2000 [DIRS 153246]) in three general areas, each of which is specifically discussed below. Except for the effects of boiling, uncertainties associated with alternative thermal operating modes are generally the same as those for the higher-temperature mode in the TSPA-SR. For example, the ability to model the effects of temperature on in-drift aqueous geochemistry will still be necessary at temperatures below 96°C.

6.3.2.3.1 Corrosion of Steel and Alloys

An evaluation of corrosion products on aqueous concentrations of metal ions in solution in an oxidizing environment was conducted, and the corrosion products were found to have a minimal impact on the concentrations of major ions in solution (CRWMS M&O 1999 [DIRS 125130], Section 7.2). The discussion in the *In Drift Corrosion Products* report (CRWMS M&O 1999 [DIRS 125130]) was based on a generalized set of Eh-pH diagrams for the major elements in a three-or four-chemical component system (generally, oxygen, hydrogen, and sometimes carbon dioxide) and a search of available scientific literature. The conceptual evaluation predicts the composition of the corrosion product and gives some understanding of the remaining chemical species in solution. This general prediction indicates that as the steels corrode nearly all of the corrosion products from the steels and alloys will form oxides and oxyhydroxide minerals, and it indicates that the aqueous concentrations of any aqueous species formed during the corrosion of these materials will also be small.

However, two important uncertainties were identified. First, the composition of steels, alloys, and their associated corrosion products can have an impact on the aqueous concentrations of trace metals in solution that may interact with either the waste package surface or the waste form. The compositions of steels and alloys used in geochemical modeling are based on values reported in the American Society for Testing and Materials standard for the given steel or alloy design (BSC 2001 [DIRS 154441], Section 6), and they do not include concentrations of trace metals that could dissolve into fluids that come in contact with the materials or their associated corrosion products.

The second important uncertainty deals with the ability of iron hydroxides and oxyhydroxides (by far the largest mass of corrosion products resulting from engineered materials) to sorb radionuclides and trace metals. If sorption is included in the performance calculations, a significant reduction in any of the dissolved concentrations of trace metals can be achieved. In previous EBS and TSPA-SR (CRWMS M&O 2000 [DIRS 153246]) modeling efforts, the sorptive ability of the corrosion products was conceptually acknowledged but conservatively ignored. However, these unquantified effects are being looked at in some detail, as discussed in Section 10. Because the model in Section 10 is based on a K_d approach, it is not fully linked with the effects of the aqueous chemistry modeled in Section 6.3.3. In addition, a K_d model will not operate outside the bounds in which the K_d data were collected, whereas a surface complexation model will. However, before a surface complexation model for sorption onto corrosion products is developed, the evaluation of sorption by the simpler K_d approach is needed to assess the potential consequences on radionuclide release from the EBS (i.e., its significance to performance). The results from implementing the K_d model discussed in Section 10 will define the need to develop a more detailed surface complexation approach that will be valid for the range of aqueous chemistries that may be imposed on the corrosion products produced from the degradation of the engineered materials placed in a repository drift. With the implementation of a surface complexation model, the uncertainty of having competitive uptake of the various radionuclides and trace metals can be modeled in a coupled manner.

An analysis of in-drift gas flux and compositions (CRWMS M&O 2000 [DIRS 129278], Section 6.2.2) using a simple mass balance approach indicates that oxygen gas depletion in the drift from the corrosion of steels and alloys will be about 14 percent. When this depletion is integrated over the expected material lifetimes, it does not drive the repository into sub-oxic or anoxic conditions. However, this analysis is based on TH models developed for the TSPA for the viability assessment (VA) (CRWMS M&O 1998 [DIRS 100358], Section 4.4.2.1), and it is only a simplified mass balance analysis. Some uncertainties exist with this analysis, which could further limit the amount of O_2 available for reaction. These include differences in thermal design, exclusion of the waste form as a sink of O_2, uncertain corrosion rates, and differences in gas transport (diffusion dominated vs. advection dominated). These processes if adequately evaluated in process models could result in further depletion of oxygen that could cause a decrease in corrosion rates. Ideally, the process models would capture all of these unquantified effects. Fortunately, the impact of not having quantified these uncertainties is small. Quantifying these uncertainties gives the increased potential for reducing corrosion and solubility, which would have a beneficial impact on the lifetime of the engineered materials and the rate at which the radionuclides would be released into solution. The potential for sub-oxic conditions is at its greatest during the boiling period. In a cooler design, this effect would be minimized. Modeling documented in the *Engineered Barrier System: Physical and Chemical Environment Model* (CRWMS M&O 2000 [DIRS 151951]), tends to corroborate this; on a detailed scale, the opportunity to drive the oxygen levels down into a regime that may be sub-oxic only exists for short periods of time. These periods are associated with boiling periods, when gas and water fluxes into the drift will be limited. These same general results were also reported in the total system performance assessment for the viability assessment (TSPA-VA) (CRWMS M&O 1998 [DIRS 100358], Section 4.4.2.1). Overall, no impacts to TSPA-SR (CRWMS M&O 2000 [DIRS 153246] would occur because the effects of including these unquantified uncertainties have been conservatively bounded by the TSPA-SR and are thought to

reduce waste package corrosion and the potential solubility of radionuclides (CRWMS M&O 1999 [DIRS 125130], Section 6.5.3.1).

In addition to the uncertainties with oxygen gas, there are uncertainties in other gas components, such as carbon dioxide and nitrogen. Several uncertainties concerning carbon dioxide are addressed in other sections (e.g., Section 6.3.1). Nitrogen is generally so abundant (80 percent of air) that the uncertainties associated with it are not important to EBS models for the reasons discussed above (i.e., the boiling periods will reduce the gas flux, otherwise nitrogen will be sufficiently abundant).

6.3.2.3.2 Cement Grout

An evaluation of the role of carbonation of cement grout as a controlling factor on whether the grout used in rock bolt emplacement could produce alkaline waters (pH greater than 9) is found in *Seepage/Cement Interactions* (CRWMS M&O 2000 [DIRS 129281], Section 7). This analysis indicates that the pH of seepage water is impacted by cement grout longevity. The duration of the impact to EBS chemistry is currently bounded at 40 years. However, due to uncertain parameters, the effects could last on the order of 40,000 years, based on rapid diffusion of carbon dioxide gas in the host rock, or to about 300,000 years for aqueous-phase advection or diffusion reactions with emplaced grout. With this large uncertainty range, cement grout could influence chemistry in those portions of the repository where rock bolts are used for at least several thousand years. Some of the uncertainties associated with the carbonation of the cement grout are discussed in the *Seepage/Cement Interactions* report.

Carbonation is thought to be the major driver in the evolution of the composition of cement leachate. The unknown parameters are the uncertainties in diffusion coefficient and the mass of calcium available for reaction. The effects of these uncertainties will be minor if sensitivity analyses demonstrate that impacts to performance from cement leachate-influenced seepage water are minor.

A new cementitious materials model that predicts the composition of seepage water that interacts with cement has been provided in *Engineered Barrier System: Physical and Chemical Environment Model* (CRWMS M&O 2000 [DIRS 151951], Table 6.3-3). This model reports three potential leachate compositions available through time (CRWMS M&O 2000 [DIRS 123916]) that could be used as inputs to the *In-Drift Precipitates/Salts Analysis* model (CRWMS M&O 2001 [DIRS 153265], Section 4) to predict the effects of cement leachate on precipitation and subsequent chemistries. This model is adapted from simplifying assumptions and studies of concrete reported in the literature. These compositions provide a broader range of chemistries than previously available. The results of the cementitious materials model will allow, if appropriate, an investigation of water chemistries that have not been carried forward from current EBS and TSPA models into subsequent modeling for consequence. The sensitivity of the precipitates salts model to grout-influenced leachate on seepage is discussed in Section 6.3.3.5.1.1. The sensitivity study in Section 6.3.3.5.1.1 evaluates several different starting water compositions (including cement leachate) to determine whether a specific reaction pathway (or chemical divide) will occur during evaporation and cause an unexpected aqueous composition to develop. The results of the study indicate that after the cement leachate waters were evaporated, they reflected the chemical composition of the original input waters that were

used to model the leaching reaction with cement. Thus, the chemical divide did not develop a water composition different than the abstracted waters used in the TSPA-SR (CRWMS M&O 2000 [DIRS 153246]). However, this analysis did not include other water chemistries that may have the potential to leach the cement grout, such as those abstracted in Section 6.3.1.6.3.

The study of additional uncertainties in the cementitious materials model pertaining to confirmatory testing of rock bolt longevity, carbonation of the grout, microbial attack of organic superplasticizers, and other aspects of grouted rock bolt performance have not been performed. The final design of ground support in the emplacement drifts is under development, and the analysis of ground support function is preliminary. Accordingly, the longevity of grouted rock bolts in response to thermal loading and environmental conditions remains uncertain. Rock mass deformation could lead to failure of the rock bolts (not necessarily associated with failure of the drift openings). It should be noted that most of these uncertainties are of minor consequence to the TSPA-SR (CRWMS M&O 2000 [DIRS 153246]) because the sensitivity analyses demonstrate that the impact to performance from cement leachate-influenced seepage water is minor.

6.3.2.3.3 Colloids

The uncertainties related to the chemical effects of colloids generated from corrosion products are discussed in Section 10.3.5.

6.3.2.4 Model Development

With the exception of the development of the sorption and colloids models discussed in Section 10, the inclusion of cement leachate water as a sensitivity study is discussed in Section 6.3.3.5.1.1.

6.3.2.5 Multiple Lines of Evidence

It is generally known that steels and alloys corrode over time (see Section 6.3.2.3.1), that cement can carbonate and degrade over time (see Section 6.3.2.2), and that colloids can be generated from corrosion products (Section 10.3.5). Some additional evidence for these processes is discussed in Sections 7 and 10.

6.3.2.6 Summary of Remaining Uncertainties

One uncertainty not discussed directly above is the effect of variations in the amounts and compositions of materials introduced into the drift (e.g., Alloy 22 used in the waste package design) that might differ in the final design from those assumed at this stage of design. These types of uncertainty will not have any significant impact on TSPA-SR results (CRWMS M&O 2000 [DIRS 153246]). *Committed Materials in Repository Drifts* (BSC 2001 [DIRS 154441]) mitigated much of the previous design uncertainty by providing masses and material compositions for the in-drift ground support design. However, this type of information is not reported for access or perimeter drifts or any other lined access tunnels. In addition, only compositional information as provided in American Society for Testing Materials standards or other design assumptions is reported. This information is not sufficient to evaluate the impacts of trace elements that may be present. However, some issues concerning impacts due to trace

elements are discussed in Section 7.3.1. Additionally, many trace elements will behave the same way that radionuclides will in the EBS. Many, for example, would be expected to sorb and form solid solutions. Although there are uncertainties, impacts on TSPA-SR results should be minimal, as these types of physical processes (such as sorption) were conservatively ignored.

As an example, one item of particular importance pertaining to uncertainty with an unfinalized subsurface design is the potential effects to the chemical environment from using large quantities of cementitious materials in the construction of main drifts and ventilation shafts. Locally, these volumes of cement would be far larger than the reported quantities planned for use in grouting rock bolts. Perhaps on a local scale, this quantity could be on the order of magnitude of the cement use in the VA design (CRWMS M&O 1998 [DIRS 100358], Section 4.3), in which the emplacement drifts were lined with concrete. This uncertainty would have an effect on water chemistries if alkaline plumes generated from unsaturated zone (UZ) waters that are equilibrating with concrete used in lining ventilation shafts and access drifts (some shafts or drifts could potentially be located above the repository horizon) flow into an emplacement drift. Coupled with this uncertainty is a potential for an alkaline plume generated from the same type of source that might flow and react with a contaminant plume containing radionuclides that may have left the drift and could be moving in the UZ.

6.3.2.7 Conclusions

Most of the uncertainty not previously investigated in models is discussed or incorporated above. Table 6.3.2-1 summarizes the key uncertainties and model improvements discussed above. Additional work on these uncertainties is needed for a more comprehensive understanding of the processes being modeled. However, the uncertainties addressed above should not impact the validity of the TSPA-SR results (CRWMS M&O 2000 [DIRS 153246]). This is due to conservative TSPA modeling assumptions (e.g., no credit was taken for sorption onto corrosion products including it would only improve performance).

6.3.3 Evolution of the In-Drift Chemical Environment

6.3.3.1 Introduction

The model of the evolution of the in-drift chemical environment uses input from three submodels: the precipitates/salts model, the microbial communities model, and the seepage/invert interactions model.

6.3.3.2 Goal of Model

The submodels discussed below are used to determine in-drift geochemical conditions that may influence materials corrosion and to estimate the composition of waters and gas that can affect dissolution and transport of radionuclides from the EBS. These submodels are influenced by coupled thermal-hydrologic-chemical-mechanical processes that will occur over thousands to millions of years. Some of the main inputs considered are the effects of temperature, relative humidity, introduced material compositions, material lifetimes, and compositions of gas and water fluxing into the drift. These inputs influence the timing and duration of many of the chemical-dependent processes that could occur, and thus, have great ability to impact radionuclide release from the EBS. Therefore, these submodels are used to determine the

chemical conditions over time that are used for the calculation of radionuclide release from the EBS.

6.3.3.3 Discussion of Results and Identification of Previously Unquantified Uncertainties

6.3.3.3.1 Precipitates/Salts Model

The precipitates/salts model was developed and validated for the TSPA-SR (CRWMS M&O 2000 [DIRS 153246]) in the *In-Drift Precipitates/Salts Analysis* (CRWMS M&O 2001 [DIRS 153265]). This model is composed of two submodels that predict pH, chloride concentration, and ionic strength as a function of relative humidity, carbon dioxide fugacity, temperature, seepage water composition, and relative rates of evaporation and seepage. When the relative humidity is above 85 percent, the EQ3/6 Pitzer submodel (often referred to as the high relative humidity model) is used. Below 85 percent relative humidity, the low relative humidity salts submodel is used. Lookup tables produced for the TSPA-SR (which provide pH, chloride concentration, and ionic strength as a function of abstraction period, relative humidity, relative evaporation rate, and temperature) are documented in *Precipitates/Salts Model Results for THC Abstraction* (CRWMS M&O 2001 [DIRS 153995]). This modeling approach is based on literature data that describe the minerals and salts produced by evaporative concentration and the relations between solution composition and relative humidity.

Precipitates/Salts Model Unquantified Uncertainties–The accuracy of the high relative humidity salts model was tested using three sets of independently collected laboratory data for the evolution of solids and water composition during evaporation (CRWMS M&O 2001 [DIRS 153265], Section 6.5.1). Two sets of data were derived from evaporation of synthetic J-13 well water (one prepared at a concentration factor of approximately 100), and a third set was derived from evaporation of synthetic Topopah Spring tuff pore water. For each measurement, the pH changes were predicted within a pH unit or less, the chloride concentrations were predicted within 20 percent, and the ionic strength was predicted within a factor of 2. In addition, handbook solubilities for ten simple salts having solubilities greater than 1 molal were easily predicted within a factor of 10 and almost always within a factor of 2. Model results also compare favorably with the results obtained using the qualified project thermodynamic database (DTN: MO0009THRMODYN.001 [DIRS 152576]) over its validated ionic strength range.

Data are not available to directly evaluate the accuracy of the low relative humidity salts model. However, this model does produce reasonable trends for changes in chloride and ionic strength as relative humidity decreases for the waters modeled. It also produces results consistent with the high relative humidity model at 85 percent relative humidity.

A final method used to evaluate and account for uncertainty in the precipitates/salts analysis is the generation of a set of lookup tables intended to cover the range of possible combinations of input values (CRWMS M&O 2001 [DIRS 153995], Tables 2 through 4). The primary objective of the lookup tables is to summarize the effects of evaporation processes for a wide range of possible conditions so that evaporation effects and uncertainty can be easily incorporated into coupled analyses. These lookup tables are used in several ways. They are used to evaluate the

sensitivity of input variables on outputs; for example, the sensitivity of pH to the relative evaporation flux is evaluated by comparing the pH output for a range of values for the relative evaporation flux. Input variables that are not included in the tables are not sensitive inputs, except for the composition of the incoming seepage water, which was held constant in this analysis (the sensitivity of these outputs to water composition is evaluated in Section 6.3.3.5.). Similarly, an estimate of the approximate maximum range of possible values of a given output variable for a range of input conditions can be assessed from the lookup tables.

Model validation has demonstrated that, given accurate inputs for starting water and gas compositions, the precipitates/salts model will likely provide results that are within a factor of two for chloride concentrations and ionic strength and within a pH unit for pH predictions (CRWMS M&O 2001 [DIRS 153265], Section 6.5.1). These quantified ranges of uncertainty can be propagated into downstream models. These ranges reflect only the uncertainties involved in simple evaporation of a given starting water.

Application of the precipitates/salts model to the drift environment has additional uncertainties involving the conceptual model, model design, model implementation, and model assumptions (CRWMS M&O 2001 [DIRS 153265], Sections 6.2, 6.3, 6.4, and 6.5). These include:

- Physical model representation (a flow-through homogeneous mixing cell)
- Steady-state and equilibrium assumptions
- Chemical activity models
- Thermodynamic database constants
- Composition of seepage water for a given time period
- Temperature, relative humidity, and gas fugacity inputs
- Relative humidity threshold for dry conditions, and
- Mineral assemblage determination.

These uncertainties reflect each major type of uncertainty identified in Section 1.2.1.1. Given the complexity of the modeled processes and large number of input parameters for this model, a rigorous quantification of each of these uncertainties is not possible. Therefore, work in this area has concentrated on assessing uncertainties in the model introduced by conservatively chosen parameter values or assumptions, which is the primary motivation for the unquantified uncertainties analyses (Section 1.2.1.3), and on performing sensitivity analyses on input parameter uncertainties. The bounding assumption in the precipitates/salts model that may introduce the most important biased effect on TSPA calculations is the relative humidity threshold assumption, which is based on the properties of a nitrate brine. This assumption is investigated, as well as the sensitivity of the model to seepage water composition, carbon dioxide fugacity, and mineral suppressions.

Precipitates/Salts Model Assumptions–In some cases, simplifying assumptions were required to reduce the complexity of the precipitates/salts analysis and to avoid sophisticated approaches where data and preexisting models were lacking. The major assumption identified in the TSPA-SR (CRWMS M&O 2000 [DIRS 153246], Appendix F) and used in the precipitates/salts analysis is the threshold relative humidity of corrosion initiation. Currently, that threshold is assumed to be 50 percent. Below 50 percent, no brine is assumed to be stable within the drift; thus, no liquid water can occur that could cause corrosion. This threshold corresponds to the

approximate equilibrium relative humidity of a saturated aqueous solution of sodium nitrate at its boiling point of approximately 120°C (CRWMS M&O 2000 [DIRS 151568], Section 6.4.2). According to this assumption, sodium nitrate is the last salt to precipitate during evaporation of in-drift waters. This assumption is developed in *Environment on the Surfaces of the Drip Shield and Waste Package Outer Barrier* (CRWMS M&O 2000 [DIRS 151568], Section 6.4.2) and is based on the solubility of nitrate salts and experiments conducted on well J-13 water.

A relative humidity of 50 percent was assumed to be conservative for the TSPA-SR (CRWMS M&O 2000 [DIRS 153246] because a more soluble and hygroscopic salt, such as calcium chloride or magnesium chloride, was not likely to develop based on results and initial documentation of laboratory evaporation experiments. In addition, evaporation of the seepage provided by the THC model described in *Abstraction of Drift-Scale Coupled Processes* (CRWMS M&O 2000 [DIRS 123916]) and abstracted for in-drift calculations resulted in a sodium-dominated brine in which calcium and magnesium were depleted primarily by evaporative precipitation of anhydrite, calcite, and sepiolite (DTN: MO0001MWDEQ346.007 [DIRS 154636]). In these waters, the last salts expected to precipitate would be the nitrate salts.

To date, laboratory and field experiments (e.g., the Single Heater Test and Drift Scale Test) using waters based on observed Yucca Mountain waters have not documented production of a calcium or magnesium chloride brine. However, laboratory experiments are ongoing, and the possibility that a calcium/magnesium chloride brine could be produced from evaporation of waters similar to tuff matrix pore water has not been eliminated. It is possible that processes other than pure evaporation may give rise to a seepage composition that has a chloride:sodium molar ratio greater than one. In the THC calculations developed for preliminary performance analyses, mineral data were adjusted to enhance model calibration (Section 6.3.1.4). The results showed an increase in the chloride:sodium molar ratio from less than one to greater than one during the early cooldown period of the higher-temperature cases (Section 6.3.3.6). Simple evaporation of a chloride- sodium-calcium-magnesium water having a chloride:sodium molar ratio greater than one will cause depletion of sodium (due to halite precipitation) and production of a calcium and magnesium chloride brine (Section 6.3.3.5). At its elevated boiling temperature, such a brine would lower the relative humidity threshold below 30 percent (Weast and Astle 1981 [DIRS 100833], p. E-44; Dean 1992 [DIRS 100722], p. 11.6), further shortening the dry period. Because corrosion can occur in the presence of this type of brine, the possibility of such a brine forming is an important consideration. Further modeling efforts, lab experiments and field experiments could reduce the uncertainty in this area. For example, analysis of reflux water samples collected from the Drift Scale Test during cooldown to determine whether its evaporation would give rise to a calcium and magnesium chloride brine.

Studies of the alternative thermal operating modes indicate that higher temperatures give rise to higher chloride:sodium molar ratios. The lower-temperature results have a much smaller tendency to produce chloride:sodium ratios greater than one (Section 6.3.3.6), but the possibility of producing a calcium and magnesium chloride brine still exists in the lower-temperature mode.

6.3.3.3.2 Seepage/Invert Interactions Model

Seepage/Invert Interactions (CRWMS M&O 2000 [DIRS 129283]) contains no qualitative calculations or predictions. It was written to develop a logical conceptual model for physical and

chemical interactions between seepage and invert materials; to screen potential processes and reactions that may occur between seepage and the invert; and to outline how seepage/invert processes may be quantified. The conceptual model (CRWMS M&O 2000 [DIRS 129283], Figure 1) consists of three generalized inputs (sources of fluid flux) into the invert: the fluids that are diverted by the waste package and drip shield; the effluent leaving any failed waste package; and, any flux entering the invert from the host rock via wicking or imbibition. Also expected with these three sources are different volumes of water. These three volumetric sources of inputs to the invert will have traveled along different pathways, and therefore will be influenced chemically by the engineered materials along their individual pathways. Due to these differing pathways, predicting the bulk chemistry in the invert after mixing these fluids is the major uncertainty that needs to be quantified. Development of the quantitative model will increase the understanding of the physical processes involved during seepage/invert interactions. The processes that would need to be included include the effects of in-drift gas compositions and temperatures, precipitation and resultant fluid compositions that occur from mixing reactions, and changes to the physical properties of the invert (i.e., reduced porosity due to precipitation), among others.

Currently, sources exist for predicting the compositions and fluxes of the three conceptualized fluids. Compositions are generated in the precipitates/salts model, as discussed in Section 6.3.3.3.1, or in *In-Drift Precipitates/Salts Analysis* (CRWMS M&O 2001 [DIRS 153265], Section 7.2) and *In-Package Chemistry Abstraction* (CRWMS M&O 2000 [DIRS 129287], Section 6). However, in previous calculations, only the composition of waters evaporating in the invert from waters fluxing from the crown of the drift was used to set the chemical conditions within the invert (CRWMS M&O 2001 [DIRS 153265]). No mixing reactions were applied when fluids from other sources were thought to interact in the invert.

In summary, for *Seepage/Invert Interactions* (CRWMS M&O 2000 [DIRS 129283]), water chemistry and interactions in the invert fall in the area of EBS geochemical modeling, which has not been implemented past its conceptual framework. Therefore, the uncertainties are large. Since uncertainty has not been quantified, the appropriate chemistries that need to be applied to transport processes in the invert have not been determined. For cases such as those discussed in Sections 6.3.2 and 10.3.4, the invert chemistry will affect sorption. The chemistries will also affect the solubility and precipitation of radionuclides, and therefore could affect potential releases from the EBS.

6.3.3.3.3 Microbial Communities Model

The *In-Drift Microbial Communities* model (CRWMS M&O 2000 [DIRS 151561]) provides bounding estimates through time of the numbers of potential microbes that could grow in the repository drift. This time-dependent set of calculations includes the evaluation of several sets of uncertain parameters, including the affects of drift temperature and relative humidity, changes in water chemistry and gas entering the drift, and variability in percolation flux through time. The parameter that effects the modeling results the most is the material lifetimes (degradation rates) of the steels and alloys that are to be emplaced in the drift, because these rates affect the availability of nutrients and energy for biomass growth. Thus, the calculations also incorporate the material masses and compositions used in the repository and waste package designs and variable corrosion rates for those materials. Four unresolved issues (not all are classified as

uncertainties) directly associated with the *In-Drift Microbial Communities* model (CRWMS M&O 2000 [DIRS 151561]) include: the incorporation of gas fluxes and compositions associated with the TSPA-VA analysis (CRWMS M&O 1998 [DIRS 100358], Section 4.4.2.1), an unqualified thermodynamic database for the redox half reactions, an incomplete description of the design materials that might be used, and the use of an unqualified data source for augmenting the water chemistries (like those abstracted in Section 6.3.1.6 above) to add appropriate amounts of nitrate and phosphate (key nutrients required for microbial growth) to those chemistries, because they are not included in upstream modeling calculations. For these remaining issues, the uncertainty from the gas flux is small because the results are not very sensitive to this parameter. Any future changes in the thermodynamic database should not substantially change the results of the *In-Drift Microbial Comminutes* model (CRWMS M&O 2000 [DIRS 151561]) because the majority of the calculations are nutrient-limited instead of energy-limited. The other issues listed above are far less uncertain than the material degradation rates.

One uncertainty not yet incorporated into the model is the addition of uranium as a considered redox species. This has previously been ignored; however, results from the model show that the period of greatest microbial growth is after waste package failure, when the waste package internal components and the waste form are degrading (CRWMS M&O 2000 [DIRS 151561], Figures 11 and 14). Ignoring the uranium redox couple in this instance would mean that a substantial amount of potential redox energy is being neglected in the calculations, which could result in an even higher growth rate during the period when the waste form is degrading.

Included in the modeled results are bounding estimates for carbon dioxide gas production, colloid generation, and biofilm size and distribution (CRWMS M&O 2000 [DIRS 151561], Tables 73, 74, and 75). The impacts of these findings, along with other processes that were not addressed in the model, can have an impact throughout the EBS. Some of these impacts may affect waste package performance, transport of radionuclides, and dissolution of the waste form. Unmodeled processes that are discussed in the AMR include colloidal transport of radionuclides sorbed to microbes, impacts on dissolution of radionuclides due to increased carbon dioxide partial pressures in the drift, potential localized changes to aqueous geochemistry in and out of the waste packages due to the formation of siderophores and generation of polysaccharide based biofilms, and the impacts on waste package corrosion of biofilm processes.

Impacts from biofilms accumulating on surfaces such as the waste package could be substantial. This process is often termed microbially influenced corrosion (MIC). The same impacts could also affect waste form dissolution. Geochemical modeling in the EBS has not evaluated the impacts due to the addition of organic microbial exudates, such as siderophores and polysaccharides. Even the TC data set used for speciation and reaction path modeling does not include organic species (CRWMS M&O 2000 [DIRS 152575]). However, there is a brief discussion on how these byproducts of microbial growth and metabolism might affect radionuclide transport in *In-Drift Microbial Communities* (CRWMS M&O 2000 [DIRS 151561], Section 6.3.5).

Carbon dioxide gas generation from microbial respiration, especially during waste form degradation, could be significant, as shown by some of the bounding estimates for carbon dioxide concentrations from *In-Drift Microbial Communities* (CRWMS M&O 2000 [DIRS 151561], Table 75). These estimates would represent a substantial increase to the in-drift

P_{CO2} values used in initial models for waste package chemistry and waste form solubility. This substantial increase could significantly elevate reported radionuclide solubilities, alter the pH of in-drift waters due to the direct interaction of the elevated carbon dioxide with waters, resulting in carbonate buffering, and influence sorption properties of corrosion products due to carbonate complexation.

The *In-Drift Colloids and Concentration* model (CRWMS M&O 2000 [DIRS 129280], Table 2) did not evaluate microbes as a potential colloid, based on a bounding but unquantified modeling assumption that biological influences have been known to enhance colloid agglomeration. As an example of how abundant microbial colloids could become, the in-drift colloids model reports a range for U.S. Department of Energy high-level radioactive waste colloids between 6×10^{-8} and 1×10^{-11} mol/L (CRWMS M&O 2000 [DIRS 129280], Table 1). However, potential levels of colloid generation reported in CRWMS M&O (2000 [DIRS 151561], Table 73) and converted to mol/L is above the midpoint of that distribution (1.92×10^{-9}). This indicates that an equivalent number of microbes could exist as colloids within the EBS, and therefore, could become an additional source of colloids leaving the drift. The uncertainties associated with a new model for microbial transport are described in detail in Section 10.3.6. However, the numbers provided above are based on a bounding estimate (the largest biomass reported from the modeling run with the largest biomass produced) taken from a modeling case that rapidly corrodes the internals of a 44-BWR waste package. The levels of colloids released from the EBS produced over the time length of modeling runs reported in *In-Drift Microbial Communities* (CRWMS M&O 2000 [DIRS 151561]) will not be maintained at this bounding level. Refer to Section 10.3.6 for an expanded discussion of these topics.

6.3.3.4 Model Development since Revision 00 of the Analysis Model Reports

6.3.3.4.1 Precipitates/Salts Model

The precipitates/salts model has been modified in several ways since the revised *In-Drift Precipitates/Salts Analysis* report (CRWMS M&O 2001 [DIRS 153265]) was released. Each modification involved the high relative humidity submodel. The Pitzer database was improved by the addition of several minerals and thermodynamic data, and the amount of output data reported in lookup tables was increased. These changes are discussed in Mariner (2001 [DIRS 155041]).

To ensure that the Pitzer database modifications did not affect validation of the high relative humidity model, the J-13 and Topopah Spring tuff pore water evaporation experiments were resimulated. The predictions and experimental data are plotted in Figures 6.3.3-1, 6.3.3-2, and 6.3.3-3 for the qualified outputs prepared for the TSPA-SR (CRWMS M&O 2000 [DIRS 153246]) calculations. For the J-13 evaporation simulations, differences between the new and old predictions of pH, chloride concentration, and ionic strength are approximately 1 percent or less. In the tuff pore water evaporation simulation, pH predictions are lower but appear to improve by creating a smoother trend. The chloride concentration and ionic strength predictions were nearly unchanged. A more detailed account of the Pitzer database modifications and their implications is included in Mariner (2001 [DIRS 155041]).

Another modification since the initial calculations is that the lookup tables include additional outputs. Instead of providing only the predicted pH, chloride, and ionic strength approximation, concentrations of the full suite of elements and a select number of aqueous species potentially used to estimate alkalinity are provided (Section 6.3.3.6). Many of these outputs can be validated and therefore qualified by existing experimental data, but the rest may not. Those that can likely be validated are carbon, potassium, fluorine, nitrogen, sodium, sulfur, HCO_3^-, CO_3^{-2}, H^+, and OH^-. Those that may not be able to be validated are aluminum, calcium, iron, magnesium, silicon, $H_3SiO_4^-$, $H_2SiO_4^{-2}$, and $MgOH^+$.

An additional improvement to the lookup tables is that they now provide for the possibility of condensation. Previous TSPA analyses indicated that condensation instead of evaporation might occur at times. The precipitates/salts model was run to determine the outputs appropriate for seepage plus condensation. These results were added to the tables.

6.3.3.4.2 Seepage/Invert Interactions Model

6.3.3.4.2.1 Introduction to Acid Neutralizing Capacity/pH Mixing Model

Uncertainties in mixing of natural water and leaking radioactive waste-bearing solutions while in the in-drift environment were not explicitly quantified in the TSPA-SR (CRWMS M&O 2000 [DIRS 153246]) treatment. Instead, ranges of solution compositions were evaluated for properties, such as solubility, under an in-drift carbon dioxide gas fugacity for a given time period. There was also no explicit unified water chemistry that was internally consistent for all areas of the drift. The present in-drift mixing model attempts to establish a unified water chemistry model within the drift. This can be applied to prior TSPA model development by producing analogous output feeds of pH, ionic strength, and acid neutralizing capacity (ANC) for mixed solutions in the drift.

This section gives a theoretical approach to abstracting the various process models for calculating the following variables for in-drift mixed solutions: ionic strength, pH, and ANC (which is an indication of the resistance of a solution to pH changes). These in-drift solutions are mixtures of seepage fluxes from the crown above the drift, the water wicked through the rock and corroded metals in the invert, and the diffusion film or flux from a waste package after failure.

The new aspects of this ANC/pH in-drift mixing model integrate process model chemistry (CRWMS M&O 2001 [DIRS 153265]; CRWMS M&O 2000 [DIRS 129287]; CRWMS M&O 2000 [DIRS 129283]) to provide consistent solution chemistry for use in modeling radionuclide solubilities, colloidal properties and transport, radionuclide sorption, and carbon dioxide gas equilibria within and leaving the repository drift for the TSPA model. Additionally, ionic strength is evaluated as part of the combined water source mixtures in order to provide values to the TSPA model.

The integrated outputs of this model are designed to be the same TSPA model feeds as before: pH, ionic strength, plus ANC values in solutions which are mixed from three sources (crown seepage, invert wicking, and waste package leakage).

6.3.3.4.2.2 Acid Neutralizing Capacity Definitions–Theoretical and Operational

In this abstraction, the theoretical and operational definitions of ANC follow those suggested by Morel and Hering (1993 [DIRS 151052], pp. 166 to 167): the theoretical ANC "of a solution is the negative of the TOTH (Total Hydrogen Concentration in Solution) expression when the components are the principal components of the solution at the carbon dioxide equivalence point." The reason for defining the ANC in this way is that it is numerically equivalent to the operational laboratory measurement of ANC described below, and that it is possible to simulate the ANC of mixed waters theoretically using EQ3/6 V7.2b software or in simple laboratory ANC titration experiments. Another advantage is that this derivation follows directly the use of the Morel and Hering (1993 [DIRS 151052], pp. 9 to 31). Tableaux format of species and chemical components are the basis for setting up a chemical speciation calculation with EQ3/6 V7.2b software.

According to Morel and Hering (1993 [DIRS 151052], pp. 166 to 167), the ANC of a solution is its acid neutralizing capacity when the end point of the titration (with mineral acid) is the carbon dioxide equivalence point. The carbon dioxide equivalence point is the pH of a pure carbon dioxide solution, and is where the ANC goes to zero.

The geochemistry term "acid neutralizing capacity" to the carbon dioxide equivalence point is numerically equivalent to the analytical chemistry term "titration alkalinity" or the engineering term "alkalinity" as equivalent weight of $CaCO_3$ (Butler 1982 [DIRS 154647], p. 1-30; Stumm and Morgan 1981 [DIRS 100829], pp. 171 to 208.]). ANC is normally computed as equivalents per kg of water for high precision work (Stumm and Morgan 1981 [DIRS 100829], pp. 171 to 208). ANC is a conservative parameter when computed as equivalents per kg of water, which is invariant with changes in temperature, pressure, and carbon dioxide fugacity. This makes it ideally suited for chemical mixing models in systems like the drift, where carbon dioxide equilibria affect most chemical changes that can occur.

6.3.3.4.2.3 Theoretical Acid Neutralizing Capacity Abstraction Equations by Source Species Inputs

These abstraction equations were derived for each of the three sources of solution in the drift by consulting directly with geochemists who had been involved with the process. The three sources of in-drift ANC were the ANC_{WPL} (from waste package leaking), the ANC_{CS} (from crown seepage), and the ANC_{IW} (from invert wicking).

Crown Seepage

$$ANC_{CS} = [HCO_3^-] + 2[CO_3^{-2}] + [OH^-] - [H^+] + [MgOH^+] + [H_3SiO_4^-] + 2[H_2SiO_4^{-2}] \quad \text{(Eq. 6-1)}$$

Waste Package Leaking

$$ANC_{WPL} = [HCO_3^-] + 2[CO_3^{-2}] + 2[UO_2CO_3] + [OH^-] - [H^+] + [MoO_4^{-2}] \quad \text{(Eq. 6-2)}$$

Invert Wicking

$$ANC_{IW} = [HCO_3^-] + 2[CO_3^{-2}] + [OH^-] - [H^+] + [MgOH^+]$$
$$+ [H_3SiO_4^-] + 2[H_2SiO_4^{-2}] \quad \text{(Eq. 6-3)}$$

The criteria were to develop the top five or six contributing ANC species for each source, and then to abstract for the TSPA model the two or three species that provided at least 70 percent of the ANC for each source. The species that contributed to ANC were identified to isolate species from EQ3/6 runs (CRWMS M&O 2001 [DIRS 153265]; CRWMS M&O 2000 [DIRS 129287]) with a contribution to the total $[H^+]$ in the system, total hydrogen concentration in solution (Morel and Hering 1993 [DIRS 151052], pp. 161 to 191), at the carbon dioxide equivalence point.

The carbonate equilibria, with both aqueous species and carbon dioxide gas, are considered primary contributors for all three sources of ANC in the drift, as with most fresh waters and sea water (Stumm and Morgan 1981 [DIRS 100829], pp. 171 to 229). The silicate species are considered secondary ANC contributors for the crown seepage and invert wicking sources. One of the species in the molybdate equilibria, $[MoO_4^{-2}]$, is considered a secondary ANC contributor for the waste package leaking sources. Two species, $[MgOH^+]$ and $[UO_2CO_3^{-2}]$, are considered secondary or tertiary ANC contributors, but posed special problems in allowing an accurate abstraction for pH computations. For the current version of the ANC mixing model, $[MgOH^+]$ and $[UO_2CO_3]$ are considered negligible for calculations to second-order accuracy, but they will be added for completeness in later model revisions.

6.3.3.4.2.4 In-Drift Acid Neutralizing Capacity Mixing Model Equations

Waters from various sources are mixed in oceans, estuaries, lakes, the confluence of rivers, waste water disposal sites, and probably in potential repository drifts. As Morel and Hering (1993 [DIRS 151052], pp. 191 to 195) have shown, given detailed recipes for the waters and a description of the mixing process, one can predict the chemical characteristics of the mixture by mixing conservative properties of the waters, like the ANC. Although substantially more complicated in the details of the present case, this is the basic principle which guides the development of the in-drift ANC mixing model equations in this section. As Morel and Hering (1993 [DIRS 151052], pp. 191 to 195) explained, total concentrations can be divided by total masses to get an average concentration when solutions mix, but pH cannot be determined as a simple average of the pH values of the original 2 solutions. Like Morel and Hering (1993 [DIRS 151052], pp. 191 to 195), simple linear mixing models of ANC as weighted by the mass of solution for a given time step are used. However, the linear ANC mixing models are converted into the required non-linear pH mixing model in the following section.

$$ANC_{CS+IW} = \{(W_{CS} * ANC_{CS}) + (W_{IW} * ANC_{IW})\} / (W_{CS} + W_{IW}) \quad \text{(Eq. 6-4)}$$

where W_{CS}, W_{IW} are the masses of solution (kg) from the crown seepage and the invert wicking, respectively. This approach assumes complete mixing of the crown seepage and invert wicking solutions in every case. (There is an implied fractional mixing factor of 1.00 multiplied by both products in the numerator of Equation 6-4.)

For the case of solutions leaking from the waste package, it was assumed that this might often be through a diffusive film that would mix incompletely with waters in the drift. A representative mixing function was developed to abstract this behavior assuming one-half (from the tail at 1.1 percent mixing to the mean at 100 percent mixing) of a standard normal distribution (Evans et al. 1993 [DIRS 112115], pp. 114 to 118), with the relative frequencies scaled to 1.00 by dividing by a scaling factor ($F_{SCALING}$ = 0.398942). The mixing function assumes a symmetrical half of a normal distribution because it physically corresponds to a cross section of the symmetrical waste package in the symmetrical drift, consistent with the *Multiscale Thermohydrologic Model* (CRWMS M&O 2000 [DIRS 149862], pp. 89, 106, and 107). Operationally, slightly faster computations can be performed for one half of a symmetrical drift cross section. Although the possible mixing ranges from 1.1 percent at the tail to 100 percent mixing at the mean within the mixing function, there is a case that can provide 0 percent mixing of the waste package leaking. If the mass of solution coming from the waste package goes to zero, Equation 6-5 reduces to Equation 6-4, which shows 100 percent mixing of the crown and invert sources and no mixing from the waste package.

Two important characteristics of the envisioned diffusion and mixing process are abstracted with this function: some mixing always takes place if there is mass flux from the waste package (the minimum mixing is 1.1 percent), and the fractional mixing factor, F_{MIXING} (1.1 to 100 percent), is normally distributed. The x values from -3 through 0 may be pseudo-randomly generated in external stochastic algorithms (such as GoldSim in the TSPA model).

$$ANC_{MIXED} = ((F_{MIXING} * (ANC_{WPL} * W_{WPL})) + ((ANC_{CS+IW}) * (W_{CS} + W_{IW}))) / ((F_{MIXING} * W_{WPL}) + W_{CS} + W_{IW}) \quad \text{(Eq. 6-5)}$$

where

$$F_{MIXING} = (1/(\sigma * (2\pi)^{0.5}) \exp((-1/(2\sigma^2)) * (x - \mu)^2)) / F_{SCALING}$$

with x = -3 through 0, $F_{SCALING}$ = 0.398942, μ = 0, and σ = 1.

6.3.3.4.2.5 In-Drift pH from In-Drift Acid Neutralizing Capacity Mixing Equations

The calculations to compute pH from ANC measurements have to be abstracted as a series of successively more detailed approximations expressed in terms of $[H^+]$, equilibrium constants, species concentrations, ionization fractions, and carbon dioxide partial pressures. The initial pH values, calculated only from the log K value of water, are used to estimate the ionization fractions and species of the carbonate equilibria in the ANC mixing equations. The initial pH values computed from the carbonate equilibria allow ionization fractions and species concentrations for the in-drift ANC equations to be calculated, which cannot be solved without prior estimates of the solution pH. This is why a succession of improved estimates of pH is necessary. Estimates of pH are necessary to solve the nonlinear, in-drift ANC equation accurately for pH. The ultimate answer being calculated is the pH of the mixed solutions in the drift for use in the TSPA model.

First Iteration Set: Carbonate Equilibria–Present versions of the in-drift pH mixing equations ignore activity coefficient variations (all activity coefficients are assumed equal to one),

variations of log K for the appropriate equilibria as a function of temperature (all log K values are only abstracted for the 25°C case at present), variations of log K for the appropriate equilibria as a function of ionic strength (all log K values are only abstracted for the infinite dilution case at present), and precipitation of solids during the mixing process. These simplifications will be changed to more complex formulations that are more representative in any future revisions of the in-drift pH mixing model.

To begin the iterative process of calculating the in-drift pH for the mixed solutions, an initial approximation uses the input pH value from the source with the largest mass flux term for a given time step. This is substituted in the simple ANC equation for a pure carbonate system (Equation 6-6) given by Stumm and Morgan (1981 [DIRS 100829], p. 188, Equation 17) after the carbonate species are replaced by terms containing $[H^+]$, P_{CO2}, and the various carbonate equilibria (Stumm and Morgan 1981 [DIRS 100829], pp. 204 to 206).

$$ANC = [HCO_3^-] + 2[CO_3^{-2}] + [OH^-] - [H^+] \quad \text{(Eq. 6-6)}$$

which rearranges after substitution of Equations 6-7 through 6-9 into Equation 6-10.

$$[H_2CO_3^*] = (K_H * P_{CO2}) \quad \text{(Eq. 6-7)}$$

$$K_1 = \{H^+\}\ \{HCO_3^-\}/\ \{\ H_2CO_3^*\} = [H^+]\ [HCO_3^-]\ /\ [H_2CO_3^*] \quad \text{(Eq. 6-8)}$$

Since all activity coefficients are assumed to be one in this version, then species activities $\{\bullet\}$ are equal to concentrations $[\bullet]$.

$$K_2 = \{H^+\}\ \{CO_3^{-2}\}/\ \{HCO_3^-\} = [H^+]\ [CO_3^{-2}]\ /\ [HCO_3^-] \quad \text{(Eq. 6-9)}$$

Since all activity coefficients are assumed to be one in this version, then species activities $\{\bullet\}$ are equal to concentrations $[\bullet]$.

$$ANC = ((K_1 * K_H * P_{CO2}) / [H^+]) + ((2 * K_1 * K_2 * K_H * P_{CO2}) /$$

$$[H^+]^2) + [OH^-] - [H^+] \quad \text{(Eq. 6-10)}$$

where $K_H = 10^{-1.47}$, $K_1 = 10^{-6.352}$, $K_2 = 10^{-10.329}$, and P_{CO2} is the variable input partial pressure of carbon dioxide at atmospheric pressure. Near these total pressures, it is numerically equal to the fugacity of carbon dioxide (Stumm and Morgan 1981 [DIRS 100829], pp. 42, and 204 to 206).

Rearranging terms in Equation 6-11 to substitute for $[OH^-]$ in Equation 6-10 and making it equal to Equation 6-6 yields Equation 6-12:

$$[H^+] * [OH^-] = 10^{-14.00} = K_W \quad \text{(Eq. 6-11)}$$

$$[HCO_3^-]_{INPUT} + 2[CO_3^{-2}]_{INPUT} + [OH^-]_{INPUT} - [H^+]_{INPUT} =$$

$$((K_1 * K_H * P_{CO2}) / [H^+]) + ((2 * K_1 * K_2 * K_H * P_{CO2}) / [H^+]^2) +$$

$$(K_W / [H^+]) - [H^+] \quad \text{(Eq. 6-12)}$$

First Iteration Set: Inputs and Principles of Computation–Equation 6-12 is the basis for the first set of iterations to determine the in-drift mixed solution pH values. Two sets of pH calculations are performed for each time step: the pH from two-source mixing (crown seepage and invert wicking) and the pH from all three sources mixing (crown seepage, invert wicking, and waste package leaking). For most calculations, the three source terms will have the largest impact on dose after the period when waste packages begin leaking. However, in the later stages of waste form and waste package deterioration, radionuclides may be found in the invert solutions derived from two-horizontal wicking of contaminated invert waters after they have earlier mixed from the waste package to the drift floor.

Each species on the left side of Equation 6-12 is calculated from source input weighted either by Equation 6-4 or Equation 6-5, depending on whether there is an ANC contribution from waste package leakage.

Technically, the various carbonate, silicate, and molybdate species cannot be linearly mixed if they are only used separately as individual species. However, the mixed individual specs concentrations are used on the left side of Equations 6-12, 6-29, and 6-49 to sum to ANC_{MIXED}, which may be linearly mixed. On the right side of Equations 6-12, 6-29, and 6-49, individual species are replaced with terms composed of equilibrium constants, carbon dioxide fugacity, and hydrogen ion concentration which is iterated to solve for ANC_{MIXED}.

First Iteration Set: Convergence Criteria–The last stage for the left side is summing all 4 terms to compute a value for the weighted ANC from the sources. This ANC sum is then used to control the pH iteration computation through the convergence criterion that the right side computation is complete when the right side ANC is greater than the left side ANC.

Each term on the right side of Equation 6-12 is solved by substituting the carbonate equilibrium constants and the assigned variable P_{CO2} in the drift. Then, the only unknown variable is the $[H^+]$, which is solved by computer to optimize the right side ANC estimate. In order to begin the iterative process of computing the in-drift pH for the mixed solutions, an initial estimate starts at pH = 0.0 and goes to pH = 15.0 by 0.1 pH unit steps. With this approximation, all of the right side terms of Equation 6-12 are evaluated and the ANC sum is compared to check if it is larger than the left side ANC. If it is within the convergence criterion, the computation is sent to a high precision subroutine that computes $[H^+]$ within 0.01 pH unit. If it is not within the convergence criterion, the initial input $[H^+]$ is increased by 0.1 pH units. After this final $[H^+]$ is determined by the iteration process, it is used as an input estimate to the next iterative process discussed below.

Second Iteration Set: Silicate Equilibria–A more detailed abstraction of the acid neutralizing capacity of mixed solutions in the drift includes silicates from the crown seepage and invert wicking in Equation 6-13:

$$ANC = [HCO_3^-] + 2[CO_3^{-2}] + [H_3SiO_4^-] + 2[H_2SiO_4^{-2}] + [OH^-] - [H^+] \quad \text{(Eq. 6-13)}$$

which rearranges after substitution of Equations 6-12, and Equations 6-14 through 6-23 to Equation 6-24. Equations 6-16 through 6-23 are based on the diprotic acid dissociation equilibria and ionization fractions given by Stumm and Morgan (1981 [DIRS 100829], p. 174) for carbonate equilibria and are applied here for silicate equilibria.

$$K_{1Si} = \{H^+\}\ \{H_3SiO_4^-\}/\ \{H_4SiO_4\} = [H^+]\ [H_3SiO_4^-]\ /\ [H_4SiO_4] = 10^{-9.86} \quad \text{(Eq. 6-14)}$$

Because all activity coefficients are assumed to be one in this version, then species activities {•} are equal to concentrations [•] (Smith and Martell 1976 [DIRS 127382], p. 39)

$$K_{2Si} = \{H^+\}\ \{\ H_2SiO_4^{-2}\}/\ \{\ H_3SiO_4^-\} = [H^+]\ [H_2SiO_4^{-2}]\ /\ [H_3SiO_4^-] = 10^{-13.1} \quad \text{(Eq. 6-15)}$$

$$Si_{Total} = [H_4SiO_4] + [H_3SiO_4^-] + [H_2SiO_4^{-2}] \quad \text{(Eq. 6-16)}$$

$$[H_4SiO_4] = Si_{Total} * \alpha_{0Si} \quad \text{(Eq. 6-17)}$$

$$[H_3SiO_4^-] = Si_{Total} * \alpha_{1Si} \quad \text{(Eq. 6-18)}$$

$$[H_2SiO_4^{-2}] = Si_{Total} * \alpha_{2Si} \quad \text{(Eq. 6-19)}$$

$$\alpha_{0Si} = (1 + (K_{1Si} / [H^+]) + ((K_{1Si} * K_{2Si}) / [H^+]^2))^{-1} \quad \text{(Eq. 6-20)}$$

$$\alpha_{1Si} = (([H^+] / K_{1Si}) + 1 + (K_{2Si} / [H^+]))^{-1} \quad \text{(Eq. 6-21)}$$

$$\alpha_{2Si} = (([H^+]^2 / (K_{1Si} * K_{2Si})) + ([H^+] / K_{2Si}) + 1)^{-1} \quad \text{(Eq. 6-22)}$$

Substituting Equation 6-18 in Equation 6-16 yields Equation 6-23:

$$[H_4SiO_4] = ([H_3SiO_4^-]/\ \alpha_{1Si}) - [H_3SiO_4^-] - [H_2SiO_4^{-2}] \quad \text{(Eq. 6-23)}$$

Substituting Equation 6-21 in Equation 6-23 gives Equation 6-24:

$$[H_4SiO_4] = ([H_3SiO_4^-]/\ ((((([H^+] / K_{1Si}) + 1 + (K_{2Si} / [H^+]))^{-1}) - [H_3SiO_4^-]$$

$$- [H_2SiO_4^{-2}]) \quad \text{(Eq. 6-24)}$$

Rearranging Equation 6-14 yields Equation 6-25, and substitution of Equation 6-24 in Equation 6-25 yields Equation 6-26:

$$[H_3SiO_4^-] = K_{1Si} * [H_4SiO_4]) / [H^+] \quad \text{(Eq. 6-25)}$$

$$[H_3SiO_4^-] = K_{1Si} * ([H_3SiO_4^-]/\ ((((([H^+] / K_{1Si}) + 1 + (K_{2Si} / [H^+]))^{-1})$$

$$- [H_3SiO_4^-] - [H_2SiO_4^{-2}]) / [H^+] \quad \text{(Eq. 6-26)}$$

Rearranging Equation 6-15 yields Equation 6-27:

$$[H_2SiO_4^{-2}] = (K_{2Si} * [H_3SiO_4^-]) / [H^+] \quad \text{(Eq. 6-27)}$$

Substituting Equations 6-6, 6-10, 6-11, 6-24, and 6-27 in Equation 6-13 gives Equation 6-28:

$$ANC = ((K_1 * K_H * P_{CO2}) / [H^+]) + ((2 * K_1 * K_2 * K_H * P_{CO2}) / [H^+]^2)$$

$$+ (K_{1Si} * \{[H_3SiO_4^-]/ ((((([H^+] / K_{1Si}) + 1 + (K_{2Si} / [H^+]))^{-1}) - [H_3SiO_4^-] - [H_2SiO_4^{-2}])\} / [H^+])$$

$$+ (2 * K_{2Si} * [H_3SiO_4^-] / [H^+]) + (K_W / [H^+]) - [H^+] \quad \text{(Eq. 6-28)}$$

Equating Equations 6-28, and 6-13 yields Equation 6-29:

$$[HCO_3^-]_{INPUT} + 2[CO_3^{-2}]_{INPUT} + [H_3SiO_4^-]_{INPUT} + 2[H_2SiO_4^{-2}]$$

$$_{INPUT} + [OH^-]_{INPUT} - [H^+]_{INPUT} = ((K_1 * K_H * P_{CO2}) / [H^+]) + ((2 * K_1 * K_2 * K_H * P_{CO2})$$

$$/ [H^+]^2) + (K_{1Si} * \{[H_3SiO_4^-]/ ((((([H^+] / K_{1Si}) + 1 + (K_{2Si} / [H^+]))^{-1}) - [H_3SiO_4^-]$$

$$- [H_2SiO_4^{-2}])\} / [H^+]) + (2 * K_{2Si} * [H_3SiO_4^-] / [H^+]) +$$

$$(K_W / [H^+]) - [H^+] \quad \text{(Eq. 6-29)}$$

Equation 6-29 is the basis for iterating $[H^+]$ to estimate $ANC_{Right\ Hand\ Side}$ for the combined carbonate and silicate systems, just like Equation 6-12 was for the carbonate system alone. The convergence criteria are the same, and the iteration process is the same for solving Equation 6-29 as it was for Equation 6-12, so those procedures are not repeated here.

Third Iteration Set: Molybdate Equilibria–A more detailed abstraction of the acid neutralizing capacity of mixed solutions in the drift includes $[MoO_4^{-2}]$ from the waste package added to Equation 6-13 to yield:

$$ANC = [HCO_3^-] + 2[CO_3^{-2}] + [H_3SiO_4^-] + 2[H_2SiO_4^{-2}] +$$

$$[MoO_4^{-2}] + [OH^-] - [H^+] \quad \text{(Eq. 6-30)}$$

Equations 6-31 to 6-40 are based on the diprotic acid dissociation equilibria and ionization fractions given by Stumm and Morgan (1981 [DIRS 100829], p. 174) for carbonate equilibria and are applied here for molybdate equilibria.

$$K_{1Mo} = \{H^+\}\{MoO_4^{-2}\}/ \{HMoO_4^{-1}\} = [H^+][MoO_4^{-2}]/ [HMoO_4^{-1}] = 10^{-4.24} \quad \text{(Eq. 6-31)}$$

Because all activity coefficients are assumed to be one in this version, then species activities $\{\bullet\}$ are equal to concentrations $[\bullet]$.(Smith and Martell 1976 [DIRS 127382], p. 18)

$$K_{2'} = \{H^+\}^2 \{MoO_4^{-2}\}/ \{H_2MoO_4\} = [H^+]^2 [MoO_4^{-2}]/ [H_2MoO_4] = 10^{-8.24} \quad \text{(Eq. 6-32)}$$

Subtracting Equation 6-31 from Equation 6-32 yields:

$$K_{2Mo} = \{H^+\} \{HMoO_4^{-1}\}/ \{H_2MoO_4\} =$$

$$[H^+] [HMoO_4^{-1}] / [H_2MoO_4] = 10^{-4.00} \quad \text{(Eq.6-33)}$$

Because all activity coefficients are assumed to be one in this version, then species activities {•} are equal to concentrations [•].

$$Mo_{Total} = [H_2MoO_4] + [HMoO_4^{-1}] + [MoO_4^{-2}] \quad \text{(Eq. 6-34)}$$

$$[H_2MoO_4] = Mo_{Total} * \alpha_{0Mo} \quad \text{(Eq. 6-35)}$$

$$[HMoO_4^{-1}] = Mo_{Total} * \alpha_{1Mo} \quad \text{(Eq. 6-36)}$$

$$[MoO_4^{-2}] = Mo_{Total} * \alpha_{2Mo} \quad \text{(Eq. 6-37)}$$

$$\alpha_{0Mo} = (1 + (K_{1Mo} / [H^+]) + ((K_{1Mo} * K_{2Mo}) / [H^+]^2))^{-1} \quad \text{(Eq. 6-38)}$$

$$\alpha_{1Mo} = (([H^+] / K_{1Mo}) + 1 + (K_{2Mo} / [H^+]))^{-1} \quad \text{(Eq. 6-39)}$$

$$\alpha_{2Mo} = (([H^+]^2 / (K_{1Mo} * K_{2Mo})) + ([H^+] / K_{2Mo}) + 1)^{-1} \quad \text{(Eq. 6-40)}$$

Substituting Equation 6-36 in Equation 6-34 yields Equation 6-41:

$$[H_2MoO_4] = ([HMoO_4^{-1}]/ \alpha_{1Mo}) - [HMoO_4^{-1}] - [MoO_4^{-2}] \quad \text{(Eq. 6-41)}$$

Substituting Equation 6-39 in Equation 6-41 gives Equation 6-42:

$$[H_2MoO_4] = ([HMoO_4^{-1}]/(([H^+] / K_{1Mo}) + 1 + (K_{2Mo} / [H^+]))^{-1}) -$$

$$[HMoO_4^{-1}] - [MoO_4^{-2}]) \quad \text{(Eq. 6-42)}$$

Rearranging Equation 6-31 yields Equation 6-43, which then can be substituted in Equation 6-42, producing Equation 6-44, which allows the three molybdenum species to be described only in terms of equilibrium constants, $[MoO_4^{-2}]$, and $[H^+]$. Rearranging Equation 6-32 allows Equation 6-45 to be expressed in a form where Equations 6-43 and 6-45 do not have the same components. Then Equation 6-46 is computed by substituting Equation 6-44 in Equation 6-45. This allows an internal quality assurance check by using Equations 6-34 through 6-40 to check Equation 6-47.

$$[HMoO_4^{-1}] = ([H^+][MoO_4^{-2}]/ K_{1Mo}) \quad \text{(Eq. 6-43)}$$

$$[H_2MoO_4] = (([H^+][MoO_4^{-2}]/ K_{1Mo}) /(([H^+] / K_{1Mo}) + 1 + (K_{2Mo} / [H^+]))^{-1})$$

$$- ([H^+][MoO_4^{-2}]/ K_{1Mo}) - [MoO_4^{-2}]) \quad \text{(Eq. 6-44)}$$

$$[MoO_4^{-2}] = (K_{2'} * [H_2MoO_4]) / [H^+]^2 \quad \text{(Eq. 6-45)}$$

$$[MoO_4^{-2}] = (K_{2'} * \{(([H^+][MoO_4^{-2}]/ K_{1Mo}) /(([H^+] / K_{1Mo}) + 1 + (K_{2Mo} / [H^+]))^{-1})$$

$$- ([H^+][MoO_4^{-2}]/ K_{1Mo}) - [MoO_4^{-2}]\}) / [H^+]^2 \quad \text{(Eq. 6-46)}$$

$$\alpha_{0Mo} + \alpha_{1Mo} + \alpha_{2Mo} = 1 \quad \text{(Eq. 6-47)}$$

Substituting Equations 6-46 and 6-28 in Equation 6-30 gives:

$$ANC = ((K_1 * K_H * P_{CO2}) / [H^+]) + ((2 * K_1 * K_2 * K_H * P_{CO2}) / [H^+]^2)$$
$$+ (K_{1Si} * \{([H_3SiO_4^-]/ (([H^+] / K_{1Si}) + 1 + (K_{2Si} / [H^+]))^{-1}) - [H_3SiO_4^-] - [H_2SiO_4^{-2}]\} / [H^+])$$
$$+ \{(2 * K_{2Si} * [H_3SiO_4^-] / [H^+]) + (K_{2'} * \{(([H^+][MoO_4^{-2}]/ K_{1Mo}) /(([H^+] / K_{1Mo}) + 1$$
$$+ (K_{2Mo} / [H^+]))^{-1}) - ([H^+][MoO_4^{-2}]/ K_{1Mo}) - [MoO_4^{-2}]\}) / [H^+]^2\} +$$
$$(K_W / [H^+]) - [H^+] \qquad \text{(Eq. 6-48)}$$

Equating Equation 6-48 and Equation 6-30 yields Equation 6-49:

$$[HCO_3^-]_{INPUT} + 2[CO_3^{-2}]_{INPUT} + [H_3SiO_4^-]_{INPUT} + 2[H_2SiO_4^{-2}]_{INPUT}$$
$$+ [MoO_4^{-2}]_{INPUT} + [OH^-]_{INPUT} - [H^+]_{INPUT} = ((K_1 * K_H * P_{CO2}) / [H^+])$$
$$+ ((2 * K_1 * K_2 * K_H * P_{CO2}) / [H^+]^2) + (K_{1Si} * \{[H_3SiO_4^-]/ ((([H^+] / K_{1Si})$$
$$+ 1 + (K_{2Si} / [H^+]))^{-1}) - [H_3SiO_4^-] - [H_2SiO_4^{-2}])\} / [H^+]) + \{(2 * K_{2Si} *$$
$$[H_3SiO_4^-] / [H^+]) + (K_{2'} * \{(([H^+][MoO_4^{-2}]/ K_{1Mo}) /(([H^+] / K_{1Mo}) + 1$$
$$+ (K_{2Mo} / [H^+]))^{-1}) - ([H^+][MoO_4^{-2}]/ K_{1Mo}) - [MoO_4^{-2}]\}) / [H^+]^2\}$$
$$+ (K_W / [H^+]) - [H^+] \qquad \text{(Eq. 6-49)}$$

Equation 6-49 is the basis for iterating $[H^+]$ to estimate $ANC_{Right\ Hand\ Side}$ for the combined carbonate, silicate, and molybdate systems, just like Equation 6-29 was for the carbonate and silicate system. The convergence criteria are the same, and the iteration process is the same for solving Equation 6-49 as it was for Equations 6-29 and 6-12.

6.3.3.4.2.6 Ionic Strength Mixing Equations

Ionic strength is not a conservative parameter. Technically, it varies with temperature, pressure, and changing valence with changing species for a given element's total concentration in solution. In this computation, it is assumed to mix linearly within an order of magnitude of the true ionic strength, which is the same error criteria used for the ionic strengths that are fed to the model. These simplifications will be changed to more complex formulations that are more representative in future revisions of the in-drift ionic strength mixing model.

$$I_{CS+IW} = \{(W_{CS} * I_{CS}) + (W_{IW} * I_{IW})\} / (W_{CS} + W_{IW}) \qquad \text{(Eq. 6-50)}$$

where W_{CS} and W_{IW} are the masses of solution (kg) from the crown seepage and the invert wicking, respectively. This approach assumes complete mixing of the crown seepage and invert wicking solutions in every case. (There is an implied fractional mixing factor of 1.00 multiplied times both products in the numerator of Equation 6-50.)

For the case of solutions leaking from the waste package, it was assumed that this might often be through a diffusive film that would mix incompletely with all of the waters in the drift. A representative mixing function was developed to abstract this behavior assuming one half (from the tail at 1.1 percent mixing to the mean at 100 percent mixing) of a standard normal distribution (Evans et al. 1993 [DIRS 112115], pp. 114 to 118), with the relative frequencies scaled to 1.00 by dividing by a scaling factor, $F_{SCALING} = 0.398942$. The mixing function assumes a symmetrical half of a normal distribution because it physically corresponds to a cross section of the symmetrical waste package in the symmetrical drift, consistent with the *Multiscale Thermohydrologic Model* (CRWMS M&O 2000 [DIRS 149862], pp. 89, 106, and 107). Operationally, this allows slightly faster computations if they are performed for one half of a symmetrical drift cross section.

Two important characteristics of the envisioned diffusion and mixing process are abstracted with this function: some mixing always takes place if there is mass flux from the waste package (minimum mixing is 1.1 percent), and the fractional mixing factor, F_{MIXING} (1.1-100 percent), is normally distributed. The x values from -3 through 0 may be pseudo-randomly generated in external stochastic algorithms (such as GoldSim in the TSPA model):

$$I_{MIXED} = ((F_{MIXING} * (I_{WPL} * W_{WPL})) + ((I_{CS+IW}) * (W_{CS} + W_{IW}))) / ((F_{MIXING} * W_{WPL}) + W_{CS} + W_{IW}); \quad \text{(Eq. 6-51)}$$

The ionic strength produced as output for each time slice in the TSPA model is I_{MIXED}, which is the mixture of solutions from all three sources (crown, invert, and waste package). In general, the I_{MIXED} value will be the output ionic strength used in sorption, solubility, and colloidal transport computations in the TSPA model because its solution will contain the majority (or all) of the radionuclide species at a given location in the drift.

6.3.3.4.2.7 Output Feeds to Other Subroutines of the Total System Performance Assessment Model

The approach taken by the in-drift ANC and pH model for consistency with other previously developed TSPA subroutines is to compute of the previous output parameters (pH and ionic strength) for the mixed solutions from all three sources (crown seepage, invert wicking, and waste package leaking) producing pH_{MIXED}, and I_{MIXED}.

For most other subroutines (like sorption, solubility, colloids) the appropriate feeds will be the three source variables pH_{MIXED}, and I_{MIXED} produced from Equations 6-49, and 6-51, respectively. The mixing ANC parameter is an important one that may help describe chemistry in other subroutines when it is available. ANC_{MIXED} (computed from Equation 6-5) will also be output for feeds to other geochemical subroutines in the model.

6.3.3.4.3 Microbial Communities Model

Improvements to the microbial communities model dealing with microbial sorption and transport as colloids are described in Section 10.3.6.

6.3.3.5 Results of Analysis

6.3.3.5.1 Precipitates/Salts Model

6.3.3.5.1.1 Sensitivity of Starting Water Composition on Evaporative Chemical Evolution

An important uncertainty in the TSPA-SR (CRWMS M&O 2000 [DIRS 153246]) calculations is the sensitivity of the starting water composition on the evaporative chemical evolution of water in the drift. The TSPA-SR model makes the assumption that nitrate salts will set the lower limit on the relative humidity at which liquid water is stable within the drift (the relative humidity threshold discussed in Section 6.3.3.3.1). To address this uncertainty, a sensitivity analysis was performed. The results, documented in detail in Mariner (2001 [DIRS 155041]), show that the chemical composition of the remaining unevaporated water can be highly sensitive to the starting water composition. Furthermore, they suggest that the relative humidity threshold assumption may not be conservative in some instances. These results, summarized below, illustrate the importance of chemical divides that are encountered when mineral phases precipitate (Mariner 2001 [DIRS 155041]).

Evaporation of water is the net transfer of water molecules from liquid to vapor. As water evaporates from an aqueous solution, each solute concentrates until it becomes supersaturated with respect to a mineral phase and precipitates. Continued evaporation and precipitation causes the composition and properties of the remaining aqueous solution to evolve into a solution that is markedly different from the starting composition.

A chemical divide is demonstrated in the following example. If halite (NaCl) reaches saturation and begins to precipitate, and the sodium:chloride molar ratio is greater than one, then chloride will become depleted in solution while excess sodium will continue to concentrate. Inversely, if the ratio is less than one, then sodium will become depleted while excess chloride will continue to concentrate. This mechanism implies that a small difference in the original sodium:chloride ratio can determine whether a sodium or a chloride brine develops beyond the halite chemical divide.

For the sensitivity analysis, evaporation calculations were performed for several waters observed at Yucca Mountain or predicted to potentially occur in the drift. These calculations are described in detail in Mariner (2001 [DIRS 155041]). The waters evaluated include the following:

- In situ J-13 ground water; that is, average J-13 well water from Harrar et al. (1990 [DIRS 100814]) corrected for carbon dioxide degassing (DTN: MO0006J13WTRCM.000 [DIRS 151029])
- Topopah Spring tuff pore water (CRWMS M&O 2001 [DIRS 154426], Table 3, p. 36; DTN: LB0101DSTTHCR1.001 [DIRS 154656])
- Water perched on top of the Calico Hills formation at the base of the Topopah Spring tuff (CRWMS M&O 2000 [DIRS 144986], Table 8)

- Water collected from the Single Heater Test (Borehole 16, collected 2/3/97, Suite 2) (CRWMS M&O 1997 [DIRS 101540], Table 5-19, p. 5-49)

- Water collected from the Drift Scale Test (Borehole 60-3, collected 1/26/99) (CRWMS M&O 2001 [DIRS 154426] Table 9, p. 89; DTN: LL990702804244.100 [DIRS 144922])

- Water predicted by the THC model (CRWMS M&O 2000 [DIRS 142022] to seep into the drift (DTN: MO9912SPAPAI29.002 [DIRS 148596])

- Water predicted to result from reaction with cement within the drift (CRWMS M&O 2000 [DIRS 151951], Table 6.3-3, pp. 79 to 80).

Evaporation of the first five waters was evaluated at three different fixed fugacities of carbon dioxide: 10^{-1}, 10^{-3}, and 10^{-6}. The last two waters were evaluated for periods 2, 3, and 4 of the THC abstraction, (CRWMS M&O 2000 [DIRS 123916]). Figures showing the evaporative evolution of these waters are presented in Mariner (2001 [DIRS 155041]). Only selected figures are provided here. The most recent evaporation calculations (see Section 6.3.3.6) are not directly included in this sensitivity analysis. However, in many ways these calculations are well represented by water #2, which was used to initialize the Topopah Spring tuff pore water composition in the THC model for the current TSPA calculations.

The calcite chemical divide generally occurs during the early stages of evaporation because calcite is not highly soluble in water and the starting waters are either saturated or nearly saturated with respect to calcite. Figure 6.3.3-4 shows the precipitates/salts model prediction of the evaporative evolution of in situ J-13 ground water (water #1 above) at a carbon dioxide fugacity of 10^{-3}. For this water, a carbonate-rich, calcium-poor water evolves similar to that observed in the laboratory for synthetic J-13 well water. Waters #3, #4, and #5 above give similar results. In each of these cases, regardless of the fixed fugacity of carbon dioxide, sodium becomes the dominant cation and carbonate (with one exception) becomes the dominant anion. For the Drift Scale Test water (#5), chloride either becomes or is always predicted to be the dominant anion, but carbonate still concentrates in the solution (at the expense of calcium) and achieves or maintains the position of second most abundant anion in solution. These waters are predicted to evolve in a manner consistent with the relative humidity threshold assumption of 50 percent established for a sodium nitrate brine.

For waters #2, #6, and #7, the calcite chemical divide causes depletion of carbonate and concentration of aqueous calcium with increased evaporation. Figure 6.3.3-5 shows the predicted evolution of an observed Topopah Spring tuff pore water. The reason carbonate is depleted instead of calcium is that these waters have excess calcium relative to carbonate alkalinity. Beyond the calcite divide, excess calcium concentrates until the solutions become supersaturated with respect to gypsum ($CaSO_4 \cdot 2H_2O$). At this point, either calcium or sulfate will deplete depending on their molar ratio in solution. The chemical divides of other calcium minerals, such as fluorite and calcium (hydroxy) silicates, may be encountered anywhere during the reaction progress, but they do not affect the calcium concentration appreciably unless the concentrations of the non-calcium reactants are within about a factor of 10 of calcium or are greater than calcium. In waters #2, #6, and #7, calcite and gypsum are by far the most important

divides within the range of the high relative humidity model. For #6 and #7, there is excess sulfate compared to calcium, so calcium becomes depleted. For #2, there is excess calcium, so calcium continues to concentrate in solution while sulfate becomes depleted.

After the calcite and gypsum chemical divides, the divides for halite (NaCl) and sylvite (KCl) are encountered. If there is more chloride than the sum of sodium and potassium when halite and sylvite reach saturation, then sodium and potassium will be depleted and a calcium chloride brine will likely develop instead of a sodium/potassium nitrate brine. A calcium chloride brine would lower the relative humidity threshold, as discussed in Section 6.3.3.3. This scenario would also allow for high concentrations of magnesium chloride.

Whether a calcium (or magnesium) chloride brine is likely to develop in the repository is uncertain. Of the seven waters in this sensitivity analysis, only evaporation of water #2 is likely to generate such a brine. However, this water was used to initialize the Topopah Spring tuff matrix and fracture water composition in the THC model for the current TSPA calculations (Section 6.3.1). The low relative humidity model of the current precipitates/salts model is based on the assumption that a nitrate brine will develop, as predicted in *Environment on the Surfaces of the Drip Shield and Waste Package Outer Barrier* (CRWMS M&O 2000 [DIRS 151568], Section 6.4.2). With the discovery that a chloride brine may develop, this assumption may no longer be appropriate in all cases. In fact, the latest THC model results predict that waters in the vicinity of the drift will have compositions during the thermal period conducive to generating a calcium chloride brine (Section 6.3.3.6). Future development of the low relative humidity model will focus on accommodating this possibility.

6.3.3.5.1.2 Sensitivity of Mineral Suppressions on Evaporative Chemical Evolution

In a complicated hydrogeochemical system such as pore water in tuff, it is difficult to predict each mineral that will or will not precipitate as a result of evaporation. Some minerals may be inhibited by a lack of nucleation sites or by slow kinetics. Often, however, data needed to determine what will likely happen for potential minerals are either unavailable or inconclusive. In this sensitivity analysis, the sensitivity of mineral suppressions to precipitates/salts model output was assessed by varying the set of minerals suppressed and evaluating the effects on the precipitates/salts model predictions for pH, ionic strength, and chloride concentration.

The first sensitivity analysis on mineral suppressions is documented in Section 5.4 of *In-Drift Precipitates/Salts Analysis* (CRWMS M&O 2001 [DIRS 153265]). Albite-low was suppressed in one set of calculations and then unsuppressed in an identical set of calculations. The results indicated that while the mineral assemblage changed (albite-low precipitated in one set but not in the other) and the aluminum concentration was affected, this mineral suppression had no effect on the output (pH, chloride, and ionic strength) to the TSPA. Aluminum was a minor constituent in the incoming seepage water, so albite-low was a minor constituent of the mineral assemblage. This analysis suggests that minerals that involve minor constituents will not markedly affect chloride and ionic strength predictions. However, it is theoretically possible that suppression of minor constituents may affect pH because the hydrogen ion activity may also be low (e.g., 10^{-8} at pH 8) and poorly buffered.

The addition of several minerals to the Pitzer database provided another opportunity to assess the sensitivity of mineral suppressions on output feeding the TSPA-SR calculations (CRWMS M&O 2000 [DIRS 153246]). The largest change in these calculations resulted from the precipitation of gyrolite, a calcium hydroxysilicate not present in the original Pitzer database. During the boiling period (period 2) of the THC abstraction (CRWMS M&O 2000 [DIRS 123916]), precipitation of gyrolite lowered the pH nearly a full unit, from around 9.3 to around 8.5. However, chloride and ionic strength were essentially unaffected. For periods 3 and 4, the pH was nearly unaffected by the different set of minerals because gyrolite was no longer favored to precipitate. In periods 2, 3, and 4, several new minerals precipitated, while several minerals originally predicted to precipitate did not. The corresponding negligible differences in pH, chloride, and ionic strength predictions suggest that these outputs are not highly sensitive to the set of mineral suppressions chosen. This analysis is presented in detail in Mariner (2001 [DIRS 155041]).

While the above analysis suggests that the uncertainty in mineral suppressions have only minor effects on the pH, chloride, and ionic strength outputs to the TSPA, more work is warranted to evaluate the uncertainty and sensitivity of mineral suppressions on TSPA calculations.

6.3.3.5.2 Seepage/Invert Interactions Model

6.3.3.5.2.1 Results of Analyses

Table 6.3.3-1 shows the results of an example simulation that could be run on the in-drift ANC/pH mixing model given the input data available from the TSPA model at the time of calculation. The approach was to examine a hypothetical case where pH differences might be expected between the three different water sources entering the drift at about the 50,000-year time frame.

The initial solution fluxes are $W_{wpl} = 0.15$ kg/yr (BSC 2001 [DIRS 153724], Attachment 1), $W_{iw} = 0.54$ kg/yr (DTN: SN0007T0872799.014 [DIRS 152545]), and $W_{cs} = 100$ kg/yr (CRWMS M&O 2000 [DIRS 153246], Figure 4.1-14). The actual mean value in bin is 140 kg/yr, and although the lower resolution Figure 4.1-14 looks like about 200 kg/yr, the final value is abstracted to 100 kg/yr. which is abstracted to 100 kg/yr. The pH values are 3.98, 7.90, and 7.89, respectively. Chemistry concentrations for model inputs were obtained from the 50,798 year input of file CSNF_20.6i for the waste package, which is at 25°C and the high carbon dioxide case (BSC 2001 [DIRS 153724], Attachment 1). The file supplying model input for the invert is HHi5.xls, which is the 25,000 to 100,000 year, higher-temperature, high-carbon dioxide case; the file for the crown is HHc5.xls, which is the 25,000 to 100,000 year, higher-temperature, high-carbon dioxide case (Jolley 2001 [DIRS 154762]). For the crown and the invert, it was assumed that relative humidity was greater than 85 percent and that there was no evaporation or condensation. Metcalf (2001 [DIRS 154842]) provides the documentation of the calculations.

One important result is that it takes large waste package leakage fluxes (1251 kg/yr) to decrease the mixed solution pH to below pH 7.0. Additional Monte Carlo runs may identify lower fluxes that could generate acidic pH values in the mixed solutions. However, it appears likely that any such fluxes will be tens to hundreds of times the given waste package leakage flux rate of 0.15 kg/yr.

Another important result is that the mixed solution becomes more acidic (lower pH) with the addition of the pH 4.0 waste package solution to the pH 7.9 invert wicking and crown seepage solutions. This is what would be expected, and is analogous to an ANC titration in the laboratory.

However, examination of Table 6.3.3.5.2-1 shows that there are some rows which have quite variable pH values for a constant W_{wpl} value (Table 6.3.3.5.2-1, range of pH). This is because the waste package leakage flux is multiplied by the percentage mixing factor (F_{mixing}) to give a variable waste package solution mass, which is mixed with the other two solutions during the Monte Carlo simulations. As the mixing factor gets closer to one (100 percent mixing of the waste package solutions), the resulting pH in this case will be more acidic.

In the bottom row of the table, pH values of 7.0, 7.8, 7.6, 7.7, 7.7, and 4.3 correspond to F_{mixing} values of 0.231, 0.079, 0.122, 0.102, 0.087, and 0.800, respectively. The highest pH value of 7.8 corresponds to the lowest mixing percentage from the waste package (7.9 percent), and the lowest pH value of 4.3 corresponds to the highest mixing percentage from the waste package (80.0 percent). One strength of the model is that it will provide pH distributions for various amounts of mixing and changing flux from the waste packages.

Two validation test cases were performed using the examples from Morel and Hering (1993 [DIRS 151052], pp. 194 to 195) and Stumm and Morgan (1996 [DIRS 125332], pp. 170 to 172), as shown in Table 6.3.3.5.2-2. Both test cases show reasonable agreement between calculated results and the mixing results in the literature.

The first case from Morel and Hering (1993 [DIRS 151052], pp. 194 to 195) is best suited to test the capability of the model because it has the needed species concentrations for the carbonate alkalinity, as required by Equation 6-49 in the in-drift ANC/pH model. Two volumes of River A, with a pH of 8.2 and ANC = 10^{-3} equivalents/liter (Eq/L), are mixed with three volumes of River B, with a pH of 5.7 and ANC = 10^{-5} Eq/L. The assumption is made that the solutions have a density of 1.00 gm/cm^3 in order to convert volume to mass needed in the model and that the waters are at 25°C. The pH is within 0.01 pH unit of the reference value and the mixed ANC value is within one percent of the reference value.

The second case, from Stumm and Morgan (1996 [DIRS 125332], pp. 170 to 172), shown in Table 6.3.3.5.2-2, mixes acid lake water with alkaline river water in a 1:1 mixing ratio. It does not, however, specify the exact bicarbonate and carbonate ion concentrations needed for the model, instead assuming all ANC is bicarbonate and there is negligible carbonate concentration. It was not stated with certainty which equilibrium constants had been used for the Stumm and Morgan (1996 [DIRS 125332]) calculation. Nevertheless, the pH agreed with the reference value (pH = 7.2 versus 7.20), and the mixed ANC value was equal to the reference value.

For the carbonate contribution to ANC, the model is reasonably accurate and precise, given quality input data. Efforts continue to find other validation cases for the silicate and molybdate contributions. Since the model is only an abstraction of all of the species contributing alkalinity and acidity to a solution, model pH values will only be given to 0.1 pH units. In some instances, this abstraction error will dominate calculation error for model applications in complicated chemical systems. One example may be seen in the first row of Table 6.3.3.5.2-1, where all

mixtures are a pH of 8.5, yet the highest source water pH is 7.9 and no carbon dioxide gas is considered lost from solution. This difference may be caused by having only seven species contributing to the abstracted model pH values in Table 6.3.3.5.2-1, as opposed to the tens or hundreds of species in the EQ3/6 V7.2b speciation calculations they were abstracted from.

6.3.3.5.3 Microbial Communities Model

Improvements to the microbial communities model, dealing with microbial sorption and transport as colloids, are described in Section 10.3.6.

6.3.3.6 Abstraction for the Total System Performance Assessment

6.3.3.6.1 Precipitates/Salts Model

Preliminary performance assessment calculations called for a new set of precipitates/salts model lookup tables. These lookup tables were prepared to represent the effects of relative humidity and fluxes of evaporation and seepage on invert water composition. The abstracted THC invert water compositions presented in Section 6.3.1 were used as input. As recommended in Section 6.3.1.6.3, the fugacity of carbon dioxide was not taken from the invert abstraction. Rather, it was taken from the fracture crown abstraction for the corresponding case and time period.

The precipitates/salts model calculations begin with the high relative humidity submodel. EQ3NR (EQ3/6 V7.2b) input files were prepared for each period and thermal/carbon dioxide mode. After adding the input data from the abstractions in Section 6.3.1, nitrate, which is not included in the THC model, was added at a NO_3:Cl molar ratio of 0.1. On a log scale, this order of magnitude appears to be representative of the NO_3:Cl ratio in Topopah Spring tuff pore water analyses (CRWMS M&O 2000 [DIRS 144986], Table 6). Nitrate is added because its occurrence in Yucca Mountain waters presents the possibility that a nitrate brine may develop by evaporative processes (CRWMS M&O 2000 [DIRS 151568], Section 6.4.2). Because nitrate, like chloride, is highly unreactive, it is assumed that the NO_3:Cl ratio would remain constant in the THC calculations had it been included. The input files were set up to require electrical balancing on sodium, except when electrical balancing on another component would have caused a smaller change in the concentration of a component. This only happened for the cooldown period of each higher-temperature case, when sulfate was the better choice for electrical balancing. Finally, K-feldspar, maximum microcline, dolomite, quartz, albite, tridymite, diaspore, enstatite, wollastonite, anorthite, and anhydrite were suppressed from precipitating. These minerals were suppressed because their formation is likely too slow at the temperatures and pressures modeled (CRWMS M&O 2001 [DIRS 153265], Table 16; Klein and Hurlbut 1999 [DIRS 124293]) or because their precipitation would be inconsistent with the minerals predicted by the THC model to precipitate. An example of the latter is that gypsum is used in the THC model instead of anhydrite. Several of the suppressed minerals likely never became supersaturated in the calculations; they were included as suppressed minerals in the input files simply to prevent rerunning calculations in the event an undesired mineral became supersaturated. Suppression of a mineral in the input files has no effect on the outcome unless the mineral becomes supersaturated.

The EQ3N/R (EQ3/6 V7.2b) runs produced pickup files that initialized sets of EQ6 runs designed to evaporate water (remove water) incrementally, precipitate supersaturated unsuppressed minerals, and equilibrate the solution with the fugacity of carbon dioxide of the crown for the corresponding time period and thermal/carbon dioxide mode. Reaction progress was limited to that required to produce an activity of water of 0.85, which corresponds to an aqueous solution equilibrated with air having a relative humidity of 85 percent. At this activity, ionic strength ranges between about 4 and 10 molal, depending on the dominant ions and pH. The pickup files from these runs were then used to initialize solid-centered flow-through EQ6 calculations in which both seepage and evaporation occur. The ratio of evaporation rate to seepage rate was varied from –9.0 to 0.999 to cover all realistic possibilities for this ratio. The value of –9.0 represents condensation (negative evaporation) at a rate that is 9 times that of seepage, while the value of 0.999 represents an evaporation rate that is 99.9 percent of the seepage rate. In some cases, the latter value resulted in water activity values less than 0.85, so the ratio was reduced to prevent the activity from exceeding 0.85. These runs generated steady-state water compositions that were independent of the starting solution (CRWMS M&O 2001 [DIRS 153265]). For each ratio of evaporation rate to seepage rate, steady-state results were added to the lookup tables. These results included pH, ionic strength, the molalities of each component, and the molalities of a set of aqueous species that potentially contribute to alkalinity. An example lookup table for the subset of output parameters is presented in Table 6.3.3-1.

For precipitates/salts model results at relative humidity values less than 85 percent, the low relative humidity model was used, following the same procedure outlined in *In-Drift Precipitates/Salts Analysis* (CRWMS M&O 2001 [DIRS 153265]). It was used to predict pH, ionic strength, and chloride concentration as a function of relative humidity. These predictions were also added to each lookup table and to the example in Table 6.3.3-1. The complete set of lookup tables and supporting model input and output files were transmitted to the TSPA implementation team (Jolley 2001 [DIRS 154762]).

The results show some new trends for pH compared to the trends observed in the calculations performed for the TSPA-SR (CRWMS M&O 2000 [DIRS 153246]). Unlike the previous boiling period predictions, where the pH increased above 9 (CRWMS M&O 2001 [DIRS 153995], Figure 2), the preliminary performance assessment pH calculations never increase much above 8. The pH instead generally remains in the range of 6.5 to 8, except during the thermal periods of the higher-temperature scenarios. Under these conditions, the pH falls to around 5 or slightly lower as evaporation produces ionic strengths above 1 molal. These lower pH predictions are caused by the differences in the abstracted seepage and gas compositions used as input. The changes in these abstracted input compositions are discussed at length in Section 6.3.1.

Predictions of the chloride and ionic strength do not show new trends. Their molalities increase in approximately the same proportions as previously observed when relative humidity decreases and ratios of the rates of evaporation and seepage increase (CRWMS M&O 2001 [DIRS 153995]). However, as discussed in Section 6.3.3.5.1.1, the results of the high relative humidity model show that during the thermal period, a calcium chloride brine could possibly develop due to predicted chemical divides and the excess of chloride in the seepage water during the thermal periods. This possibility is not captured in the low relative humidity model results for chloride concentration or in the relative humidity threshold assumption, which assumes dry

conditions below a relative humidity of 50 percent. Future development of the low relative humidity model and relative humidity threshold assumption will focus on predicting and incorporating the possibility of generating a chloride brine.

6.3.3.6.2 Seepage/Invert Interactions Model

Only the sections dealing with the precipitates/salts model have been incorporated into the TSPA model at this time.

6.3.3.6.3 Microbial Communities Model

See Section 10.3.6 for details on the TSPA abstraction for microbial transport and sorption.

6.3.3.6.4 Multiple Lines of Evidence

For the precipitates/salts model, a number of natural analogues and models for evaporation and chemical divides are discussed in *In-Drift Precipitates/Salts Analysis* (CRWMS M&O 2001 [DIRS 153265], Section 6.1) and *Environment on the Surfaces of the Drip Shield and Waste Package Outer Barrier* (CRWMS M&O 2000 [DIRS 151568], Section 6.5). They include laboratory evaporation studies and studies of the formation of natural brines and evaporites. These studies support the conceptual model and demonstrate the general trends predicted by the precipitates/salts model.

The most rigorously studied lines of evidence for the precipitates/salts model currently include three sets of laboratory evaporation experiments and handbook solubility values of highly soluble salts. The laboratory experiments, conducted on synthetic J-13 well water and Topopah Spring tuff pore water, provide measurements of how the aqueous composition changes upon evaporation. These data, which were not used to calibrate or develop the precipitates/salts model, are predicted within acceptable limits of accuracy by the model (CRWMS M&O 2001 [DIRS 153265], Section 6.5).

Additional evidence that may be applicable to some of the processes discussed in this section can be found in Sections 7.3.1, 8, and 10.

6.3.3.7 Summary of Remaining Uncertainties

6.3.3.7.1 Precipitates/Salts Model

The sensitivity analyses performed in support of the unquantified uncertainties analysis and documented in Mariner (2001 [DIRS 155041]) provide preliminary assessments of uncertainties associated with starting water composition, carbon dioxide fugacity, and mineral suppressions. While these assessments provide insight into some of the uncertainties of the current model, especially with regard to the relative humidity threshold assumption and the potential evolution of a calcium/magnesium chloride brine, more work is needed in these areas to quantify the uncertainties.

An initial low order approximation on the probability of the formation of magnesium and calcium chloride brines can be estimated. The probability is estimated from the combination of

the different modeling runs done on the seven different water compositions described in Section 6.3.3.5.1.1. Out of the seven starting waters tested there were three different model runs done for each water for a total of 21 different starting waters. The results in Section 6.3.3.5.1.1 indicate that only the three modeling runs associated with the Topopah Spring Tuff pore water could proceed through the chemical divide where calcium and magnesium chlorides would form. Assuming equal weighting to each of the modeled runs would indicate that there would be a 14 percent chance of the starting water composition going toward a calcium/magnesium chloride brine due to evaporative processes. Different weighting from additional analyses will affect the probability of producing high chloride brines.

To caveat the 14 percent probability, an exhaustive list of all possible starting water compositions is not included. Nor does it preclude that the Topopah Spring pore water is the most likely end member composition for water dripping on a waste package, and thus could be weighted to be the most representative. Evidence to perhaps negate selecting the Topopah Spring pore water as the most representative is the results from the cement-modified waters. The cement-modified waters use as the initial starting water composition Topopah Spring pore water yet the reactions with the cement grout prior to evaporation change the chemistry sufficiently to preclude the formation of the magnesium chloride brine. Other EBS materials or byproducts that could modify the composition of waters before they contact the waste package include corrosion products, dust, and biofilms.

Remaining unquantified uncertainties include uncertainties in the representation of processes that govern the evaporative evolution of seepage under repository conditions. These include the physical model representation (currently assumed to be a simple flow-through mixing cell), steady-state and equilibrium assumptions, chemical activity models, and thermodynamic database constants. For simple evaporation of synthesized J-13 well water and Topopah Spring tuff pore water in a beaker, uncertainties in thermodynamic constants, activity models, and equilibrium assumptions do not prevent reasonably accurate predictions of pH, chloride concentration, and ionic strength (Section 6.3.3.3.1). However, the question remains whether the uncertainties observed for these laboratory experiments are representative of the dominant evaporative processes in a repository.

6.3.3.7.2 Seepage/Invert Interactions Model

With only a conceptual model discussed and model development in its initial stages (see Section 6.3.3.4.2), any further discussion on uncertainties can only be speculation.

6.3.3.7.3 Microbial Communities Model

In addition to the uncertainty already discussed in Section 6.3.3.3.3, any future design changes will introduce some programmatic uncertainty (i.e., the potential for material masses, compositions, and locations to be changed is possible prior to finalization for the license applications of future designs). However, parameters such as degradation rates and the potential for spatial variability in microbial colonization are much more important sources of modeling uncertainty, since these can have a greater direct impact on waste package degradation and radionuclide transport. The potential impacts include things like increased corrosion of waste packages due to MIC or increased solubility of waste forms due to production of siderophores.

Calculations performed using this model may need to be revisited as the repository design matures and/or process modeling matures, particularly as these changes are effected by the materials committed to the repository after closure.

6.3.3.8 Summary and Conclusions

6.3.3.8.1 Precipitates/Salts Model

As demonstrated by model validation summarized in Section 6.3.3.3.1, the precipitates/salts model predicts the effects of simple evaporation in laboratory experiments within a factor of 2 or less for chloride concentrations and ionic strength and within a pH unit for pH predictions. In addition, handbook solubilities for a set of ten salts having solubilities greater than 1 molal are easily predicted within a factor of 10 and almost always within a factor of 2. While all three parameters (pH, chloride, and ionic strength) were provided to TSPA-SR (CRWMS M&O 2000 [DIRS 153246]), only pH and ionic strength predictions were used.

According to the precipitates/salts model results for the TSPA-SR calculations, the relative humidity threshold assumption of 50 percent, corresponding to a sodium nitrate brine, holds as a valid assumption. The starting water compositions used for these TSPA-SR calculations were provided by *Abstraction of Drift-Scale Coupled Processes* (CRWMS M&O 2000 [DIRS 123916]). Evaporation of these waters (identified as water #6 in Section 6.3.3.5 above) will not result in the development of a calcium (or magnesium) chloride brine because of an excess of sulfate, carbonate, and/or silica in these waters (Mariner 2001 [DIRS 155041]). Calcium is depleted by precipitation of gypsum (or anhydrite if not suppressed), calcite, and calcium (hydroxy)silicates (and magnesium is largely depleted by analogous mineral precipitation) due to this excess.

This assumption may not be valid for the calculations presented in Section 6.3.3.6. These results indicate that during the thermal periods, especially in the higher-temperature scenarios, the relative concentrations of the dominant ions (i.e., sodium, chloride, calcium, and magnesium) would likely give rise to a calcium/magnesium chloride brine (Section 6.3.3.5.1.1). The uncertainty associated with the evolution of such a brine is borne largely in the uncertainty of the starting water composition. Therefore, any future efforts to quantify the uncertainty of developing a calcium/magnesium chloride brine must include quantification of the uncertainty of the input starting water composition.

6.3.3.8.2 Seepage/Invert Interactions Model

Since the in-drift ANC/pH mixing model will not be implemented for uncertainty analysis in this version of the TSPA model, a calculation employing the waste package chemistry as the only fluid in the invert should be used to check the maximum effect possible (zero mixing of the waste package leaking with more dilute invert or crown waters) when the ANC/pH mixing model is implemented. Any future work should also consider that evaporation fluxes from the mixing invert and waste package solutions may concentrate solution chemistry values above present maximum values in the TSPA model.

6.3.3.8.3 Microbial Communities Model

The *In-Drift Microbial Communities* model (CRWMS M&O 2000 [DIRS 151561]) addresses a significant portion of the uncertainty discussed briefly in Section 6.3.3.3.3. However, the biggest source of uncertainty lies in further investigating issues that are discussed in 6.3.3.3.3. Although there are important uncertainties associated with organic complexation and production of siderophores, the models produced seem to address enough of the uncertainty that they would not significantly change the results of the TSPA-SR (CRWMS M&O 2000 [DIRS 153246]). As an example, the new microbial transport model reported in Section 10.3.6 would not affect the conclusions of the TSPA-SR because sorption was conservatively excluded from the calculations.

6.3.4 Rockfall

6.3.4.1 Introduction

The deterioration of the rock mass surrounding the potential repository emplacement drifts was predicted based on a probabilistic key-block analysis. Key blocks are formed at the surrounding rock mass of an excavation by the intersection of three or more planes of structural discontinuities. The *Drift Degradation Analysis* (CRWMS M&O 2000 [DIRS 151635]) provides an assessment of the possible formation of key blocks within the potential repository horizon that is based on the orientations of discontinuities present in the ESF main loop and in ECRB Cross Drift. Block failure due to seismic and thermal effects has also been analyzed.

The rockfall analyses provide data to the EBS postclosure performance assessment that may modify estimates of seepage into the emplacement drifts due to the mechanical effects of rockfall during the period of compliance (see Section 4.3.4). These data also support disruptive events analyses (see Section 14.4). Additionally, the rockfall analyses provide data and information to support repository design, including both waste package and subsurface design.

Technical literature was reviewed to determine the most appropriate approach to developing a key-block analysis (CRWMS M&O 2000 [DIRS 151635], Section 6.5). As a result of this review, the discrete region key block analysis (DRKBA V3.3) software was selected for the development of the rockfall model. The DRKBA V3.3 probabilistic approach is unique, and is distinguished from traditional key-block analyses in that it not only assesses the maximum size of key blocks, but it also predicts the number of potential key blocks that will be formed within a referenced length of tunnel. The approach also allows for a variety of tunnel and jointing configurations. DRKBA V3.3 simulates structural discontinuities as circular discs placed in the rock mass according to probabilistic distributions determined from tunnel-mapping data. Joint planes are simulated by a Monte Carlo technique from probability distributions representing the orientation, spacing, and trace length of the corresponding joint set. DRKBA V3.3 determines where joint planes intersect to form blocks, then analyzes these blocks to determine if they are geometrically feasible (i.e., if the shape of the block is such that it is physically possible to slide or fall into the tunnel opening). If the blocks are geometrically feasible, DRKBA V3.3 then determines if they are mechanically stable (i.e., if the gravitational forces that cause the block to move into the tunnel opening are less than the frictional forces on the sliding surfaces of the block).

6.3.4.2 Goal of Model

DRKBA rockfall model predicts size ranges and quantities of rock that may fall into drifts in order to assess the effects of fallen rocks on the in-drift physical and chemical environment.

6.3.4.3 Discussion of Total System Performance Assessment-Site Recommendation Results and Identification of Unquantified Uncertainties

Uncertainties in the model for rockfall were not quantified in the treatment in the TSPA-SR (CRWMS M&O 2000 [DIRS 153246]).

The usefulness of the rockfall model is affected by how well the data inputs describe the actual fracture conditions. The natural variability of fractures within a rock mass always represents uncertainty in the design of structures in rock. The extensive fracture data collected at Yucca Mountain provide a good representation of fracturing at the emplacement drift horizon. Fracture data have been represented in the DRKBA model by simulating joint radii, spacings, and positioning with beta distributions based on field mapping data (CRWMS M&O 2000 [DIRS 151635], Section 6.3.2). Individual joints within each joint set are represented as circular discs in three-dimensional space with radii drawn from a distribution estimated on the assumption that the radius is equal to twice the mapped trace length (CRWMS M&O 2000 [DIRS 151635], Section 5.1). All joint spacing data have been corrected for "true" spacing, that is, the spacing measured normal to the plane of the joint sets (CRWMS M&O 2000 [DIRS 152286], Section 6.4.2.1). This correction for true spacing is referred to as a Terzaghi correction. The range of fracture variability from tunnel mapping has been captured in the rockfall model through multiple Monte Carlo simulations of the rock mass. To account for uncertainties associated with seismic, thermal, and time-dependent effects on rockfall, a conservative reduction of joint strength parameters has been included in the approach.

Unquantified Uncertainties Selected for Quantification–Selected for quantification are uncertainties in values for M, a multiplier of fracture trace lengths to determine the radius of the joint plane, and a Terzaghi correction for subhorizontal fractures in the DRKBA model. Uncertainty in the range of fracture variability was also selected. Quantification was done at the subsystem level with sensitivity studies on M, the Terzaghi correction, and the number of Monte Carlo simulations.

The uncertainties described above are not affected by temperature variation. The *Drift Degradation Analysis* (CRWMS M&O 2000 [DIRS 151635], Section 7.1) showed that thermal effects have a minor impact on rockfall. Uncertainties associated with alternative thermal operating modes are qualitatively the same as those for the higher-temperature mode described in the TSPA-SR report (CRWMS M&O 2000 [DIRS 153246]).

6.3.4.4 Model Development

The DRKBA rockfall model was developed prior to the TSPA-SR (CRWMS M&O 2000 [DIRS 153246]). There has been no subsequent rockfall model development.

6.3.4.5 Results of the Analysis

Values of M and the Terzaghi correction were sampled over suitable ranges, and the resulting rockfall quantities and size ranges were determined. The number of Monte Carlo simulations was also varied to test the sensitivity of the model to the number of simulations. The results of the sensitivity analyses are described in this section. Details of the calculations associated with the sensitivity analyses are provided in the *Rockfall Sensitivity Calculations* (BSC 2001 [DIRS 154537]).

6.3.4.5.1 Sensitivity of Fracture Size in the Discrete Region Key Block Analysis Rockfall Model

The *Drift Degradation Analysis* (CRWMS M&O 2000 [DIRS 151635], Attachment XIV) presents the results of a sensitivity calculation for the extent of the modeled joint plane based on the mapped joint trace length. It is recognized that the actual extent of a joint plane cannot be fully known based on field mapping data; the mapped trace length of a joint represents some portion of the overall joint plane. Underrepresenting the extent of the joint plane would not be conservative in a key-block analysis. Since the underrepresented joint planes may not extend or connect to adjacent joint planes, underrepresentation would limit the number of blocks otherwise generated in the model. Conversely, overstating the extent of the joint plane would increase connectivity among joint planes, creating more blocks in the model and resulting in an increased, or conservative, estimate of block development. However, infinite joint planes would not be an accurate representation of the jointed rock mass. The basis to sufficiently model the extent of the joint plane based on the available field data is provided in the *Drift Degradation Analysis* (CRWMS M&O 2000 [DIRS 151635], Attachment XIV).

Joint planes are represented as circular discs in the DRKBA rockfall model with the assumption that the radius of the joint plane is equal to twice the mapped trace length (CRWMS M&O 2000 [DIRS 151635], Section 5.1). The multiplier M is used to obtain the radius of the circular fracture disc from the trace length:

$$R = M * TL \qquad \text{(Eq. 6.3.4-1)}$$

where R is the radius of the circular fracture disc and TL is the trace length of the mapped fracture.

The sensitivity calculation in the *Drift Degradation Analysis* (CRWMS M&O 2000 [DIRS 151635], Attachment XIV) showed that for a circular joint plane described using a radius equal to twice the mapped trace length (i.e., $M = 2$), there is an approximate 3 percent probability that the actual joint radius is greater than the modeled value. Based on these findings, it was concluded that the fracture size used in the DRKBA rockfall model is conservative.

To further document the sensitivity of the size of the joint plane in the DRKBA rockfall model, a series of rockfall analyses was developed for the Tptpmn and Tptpll units, with the joint radius multiplier (M) incrementally varied for each analysis. Values of M were set equal to 1.0, 1.5, 2.0, 2.5, and 3.0. With the exception of the joint radius, all inputs for these analyses were consistent with inputs for the static condition presented in the *Drift Degradation Analysis* (CRWMS M&O 2000 [DIRS 151635], Sections 6.3.1, 6.3.2, and 6.3.3).

Figures 6.3.4-1 and 6.3.4-2 present the key-block analysis results in the format of cumulative frequency of occurrence for the Tptpmn and Tptpll units. The DRKBA V3.3 input and output files and associated calculation files are provided in the *Rockfall Sensitivity Calculations* (BSC 2001 [DIRS 154537]). The cumulative frequencies of occurrence corresponding to the 50, 75, 90, 95, and 98 percentile block volume for each unit are listed in Tables 6.3.4-1 and 6.3.4-2. The maximum block sizes predicted from the analyses are also presented in these tables. The predicted numbers of key blocks per unit length of emplacement drift are listed in Table 6.3.4-3. For radius multipliers greater than 1.5, the cumulative block size distributions are relatively similar (Figures 6.3.4-1 and 6.3.4-2). The greatest sensitivity from the variation of the joint radius is in the frequency of blocks developed. As shown in Table 6.3.4-3, block development is limited when the radius of the joint plane is equal to the fracture trace length (i.e., $M = 1$). As the radius multiplier increases, the number of blocks increases, with a substantial increase in the number of blocks when the multiplier exceeds 2.0. This trend illustrates that as the extent of the joint plane increases, there is an increased connectivity among joint planes, creating a higher frequency of block development in the model.

6.3.4.5.2 Sensitivity of the Number of Monte Carlo Simulations in the Discrete Region Key Block Analysis Rockfall Model

In the DRKBA rockfall model, random joint patterns are generated with joint centers positioned in three-dimensional space, then each joint set is considered in sequence for each Monte Carlo simulation. The forming of key blocks is therefore different in each Monte Carlo simulation. To document the sensitivity of the model to the number of Monte Carlo simulations for the sensitivity analyses, a series of test runs was conducted. The test runs were intended to show sensitivity to the number of Monte Carlo simulations in the prediction of block size distribution, maximum block size, and the number of blocks. The DRKBA V3.3 input and output files, and associated calculation files, are provided in the *Rockfall Sensitivity Calculations* (BSC 2001 [DIRS 154537]).

Test runs were conducted for the Tptpmn unit with 100, 200, 400, 600, and 800 Monte Carlo simulations. Figure 6.3.4-3 shows the block size distribution curves in the form of cumulative frequency of occurrence. The prediction of block size distribution is similar for all simulations, as indicated in Figure 6.3.4-3. The predicted numbers of blocks per 10 simulations for the 5 Monte Carlo simulation cases are presented in Figure 6.3.4-4. The results are in good agreement for the 400, 600, and 800 simulation cases. The maximum block sizes predicted for each case are shown in Figure 6.3.4-5. The 98 percentile blocks are nearly identical for all Monte Carlo simulation cases. The maximum block size remains consistent after 400 simulations.

For the Tptpll unit, test runs with 100, 200, 400, 600, and 800 Monte Carlo simulations were conducted. Figure 6.3.4-6 shows the block size distribution curves for each case. The prediction of block size distribution is similar for all simulations. The predicted numbers of blocks per 10 simulations for each case are presented in Figure 6.3.4-7. The results show a relatively low number of blocks per 10 simulations for all cases, with the number of blocks remaining consistent after 400 simulations. The maximum block sizes predicted for each of the Monte Carlo simulation cases are shown in Figure 6.3.4-8. The maximum blocks predicted are similar for all simulations, with the maximum block size typically between 1 and 2 m^3.

6.3.4.5.3 Sensitivity of the Terzaghi Correction for Spacing of Subhorizontal Fractures in the Discrete Region Key Block Analysis Rockfall Model

The procedure for determining joint set spacing is documented in *Fracture Geometry Analysis for the Stratigraphic Units of the Repository Host Horizon* (CRWMS M&O 2000 [DIRS 152286], Section 6.4.2). A Terzaghi correction, which is a mathematical correction to determine the "true" spacing measured normal to the joint plane, was applied to the mapped joint spacing data. For vertical joints striking perpendicular to the axis of the tunnel, the Terzaghi correction factor would be 1, that is, the mapped spacing is equal to the true spacing, without a correction. Correction factors are most significant for subhorizontal fractures. For the subhorizontal fracture set from mapped fractures in the Tptpmn unit, the average Terzaghi correction factor is approximately 15, indicating that the true spacing of subhorizontal joints is 15 times less than the mapped spacing (BSC 2001 [DIRS 154537]). These Terzaghi correction factors with an average of approximately 15 were used in the *Drift Degradation Analysis* (CRWMS M&O 2000 [DIRS 151635]). For joints mapped along a horizontal scanline, a subhorizontal joint dipping 8 degrees or more will have a maximum Terzaghi correction factor of approximately 7 (i.e., 1/(sin 8) is approximately 7). For joints dipping less than 8 degrees, the Terzaghi correction factor ranges from 7 to infinity. Therefore, the uncertainty associated with the correction factor increases within this range.

To document the sensitivity of the DRKBA rockfall model to the Terzaghi correction factor, analyses were conducted with a maximum correction factor of 7. The joint spacing distributions for the original true joint spacing and the modified true spacing (i.e., with a Terzaghi correction factor less than or equal to 7) are shown in Figures 6.3.4-9 and 6.3.4-10, respectively. The beta distribution parameters for joint spacing, which are required input for the DRKBA V3.3 program (CRWMS M&O 2000 [DIRS 151635], Sections 6.3.1 and 6.3.2), are provided in Table 6.3.4-4. The details for the calculation of each beta parameter are provided in the *Rockfall Sensitivity Calculations* (BSC 2001 [DIRS 154537]). With the exception of the beta distribution parameters for the subhorizontal joint set of the Tptpmn unit, all inputs for these analyses were consistent with inputs for the static condition presented in the *Drift Degradation Analysis* (CRWMS M&O 2000 [DIRS 151635], Sections 6.3.1, 6.3.2, and 6.3.3).

Figure 6.3.4-11 presents the key-block analysis results in the format of cumulative frequency of occurrence for the Tptpmn unit. The DRKBA V3.3 input and output files and associated calculation files are provided in the *Rockfall Sensitivity Calculations* (BSC 2001 [DIRS 154537]). The cumulative frequencies of occurrence corresponding to the 50, 75, 90, 95, and 98 percentile block volume for the Tptpmn unit are listed in Table 6.3.4-5. The maximum block sizes predicted from the analysis are also presented in this table. The predicted numbers of key blocks per unit length of emplacement drift are, under static condition with modified Terzaghi correction in the Tptpmn, 50 and 33 km, respectively, for the original and modified cases (BSC 2001 [DIRS 154537]).

As shown in Figures 6.3.4-9 and 6.3.4-10, the frequency of widely spaced joints increases with the modified Terzaghi correction. The impact of this change in the DRKBA rockfall model is a reduction in the number of blocks per kilometer and a slight increase in the overall distribution of block sizes (Figure 6.3.4-11). The increased spacing of the subhorizontal joint set in the Tptpmn unit resulted in the development of fewer blocks with a slightly larger volume.

6.3.4.6 Abstraction for Total System Performance Assessment

The subsystem sensitivity analysis presented above quantifies the sensitivity of parameters in the DRKBA rockfall model. Since the sensitivity analysis does not change the results of the rockfall model presented in the *Drift Degradation Analysis* (CRWMS M&O 2000 [DIRS 151635], Section 6), an abstraction for TSPA is not applicable.

6.3.4.7 Multiple Lines of Evidence

The number of blocks predicted by the DRKBA static rockfall model for the various stratigraphic units within the potential repository horizon is consistent with field observations in the ESF (CRWMS M&O 2000 [DIRS 151635], Section 6.5). The DRKBA rockfall model predicts the highest frequency of blocks in the Tptpmn unit and the lowest frequency of blocks in the Tptpll unit. Field observations are consistent with this trend.

The size of key blocks observed in the ECRB Cross Drift is generally less than 0.5 m^3. The maximum size block observed in the ECRB Cross Drift is captured within the range of predicted block sizes from the DRKBA rockfall model (CRWMS M&O 2000 [DIRS 151635], Table 44).

The seismic component of the DRKBA rockfall model predicts that the seismic effect on both the size and number of blocks is minor. Natural analogues from mines, tunnels, and caves can be used to test this prediction. There have been several compilations of effects on underground openings in response to earthquakes (Stevens 1977 [DIRS 154501]; Pratt et al. 1978 [DIRS 151817]; Carpenter and Chung 1986 [DIRS 154504]; Sharma and Judd 1991 [DIRS 154505]).

The damage from earthquakes results from shear waves. These are generated when the energy from an earthquake passes through a density contrast; the largest one is between air and rock at the surface of the earth. If the dimensions of an underground opening are considerably less than the wavelength of a shear wave, the amplitude of motion will be about twice as large at the surface as at depth (Stevens 1977 [DIRS 154501], p. 20). In addition, the effects of surface waves decrease with increasing depth, much in the same way that the effects of ocean waves decrease with depth of water. A consequence of this is that the damage reported in shallow near-surface tunnels is greater than that reported in deep mines (Pratt et al. 1978 [DIRS 151817]). Data presented by Sharma and Judd (1991 [DIRS 154505], Figure 7) indicate that damage to underground facilities at the depth for the potential repository is rare, even at accelerations of 0.4 g.

Pratt et al. (1978 [DIRS 151817], p. 20) report that peak accelerations less than 0.2 g have caused no reported damage to tunnels. Sharma and Judd (1991 [DIRS 154505], p. 275) note that their database of 192 reports of underground observations contains 98 cases with no damage, and that there are probably hundreds of other undocumented cases of no damage. In fact, damage to underground openings is inevitable only when the underground facility is displaced by a fault (Carpenter and Chung 1986 [DIRS 154504]; Stevens 1977 [DIRS 154501]).

Stevens (1977 [DIRS 154501]) and Pratt et al. (1978 [DIRS 151817], p. 26) both suggest that the host material for an underground facility may be important in predicting the amount of damage caused by shaking. Competent rock is expected to outperform unconsolidated material.

Carpenter and Chung (1986 [DIRS 154504]) discuss potential problems for deep geologic disposal sites in response to earthquakes. They strongly recommend that faults with the potential for movement be avoided, which is consistent with design criteria for the potential repository at Yucca Mountain. They also note that modeling studies suggest potential problems for waste handling equipment in shafts. The potential facility at Yucca Mountain would avoid this problem by using inclines for the emplacement of waste.

As noted earlier, there are several examples of the performance of underground facilities during earthquakes. The following paragraphs contain a few specific, well-documented examples.

On July 28, 1976, a magnitude 7.8 earthquake occurred in Tang-Shan, China, a city with substantial mining and industrial facilities. Surface intensities at Tang-Shan were such that in the area where the strongest shaking occurred, 80 to 90 percent of the surface structures collapsed. However, there was generally no serious damage to important engineered structures immediately below the surface, regardless of their depth or size (Wang 1985 [DIRS 151821], p. 741).

The U.S. Geological Survey reported in the lessons and conclusions of the Alaskan earthquake on March 28, 1964, that no significant damage was reported to underground facilities, including mines and tunnels, as a result of the earthquake, although some rocks were shaken loose in places. Included in this analysis were studies of the coal mines in the Matanuska Valley (which were undamaged), the railroad tunnels near Whittier, the tunnel and penstocks at the Eklutna hydroelectric project, and the Chugach Electric Association tunnel between Cooper Lake and Kenai Lake. There were also no reports of damage to the oil and gas wells in and along Cook Inlet. These reports of no damage from the Alaskan earthquake are significant; it was one of the largest (magnitude 8.5) to occur in this country, and surface damage was extreme (Pratt et al. 1978 [DIRS 151817], p. 32).

Tunnels in the epicentral region of the Kobe, Japan, earthquake (January 16, 1995; magnitude 6.9) experienced no major damage (partial or total collapse) for peak ground accelerations measured at the surface of approximately 0.6 g (Savino et al. 1999 [DIRS 148612]).

On June 29, 1992, a magnitude 5.6 earthquake occurred at Little Skull Mountain, which is about 20 km from Yucca Mountain. Within days of the earthquake, a team of scientists examined the interior of the tunnel 125 m deep in the epicentral region of the earthquake. The team reported no evidence of damage in the tunnel that could be associated with the earthquake (Savino et al. 1999 [DIRS 148612]).

6.3.4.8 Summary of Remaining Uncertainties

The remaining uncertainties within the DRKBA rockfall analyses are associated with the assessment of seismic, thermal, and long-term degradation effects on block development. Currently, these uncertainties are accounted for by applying a conservative reduction in joint strength properties in the rockfall model (CRWMS M&O 2000 [DIRS 151635], Section 7.2). To provide a better understanding and quantification of these uncertainty sources, additional rockfall analyses are planned in support of the license application. The additional activities include:

- Appropriate boundary conditions for thermal and seismic loading
- Critical fracture patterns from the rockfall Monte Carlo simulations
- Appropriate thermal and mechanical properties of rock blocks and joints
- Long-term degradation of joint strength parameters
- Site-specific ground motion time histories appropriate for the postclosure period.

6.3.4.9 Summary and Conclusions

Previously unquantified uncertainties associated with the DRKBA rockfall model have been identified, including the extent of fracture planes, the Terzaghi correction for spacing of subhorizontal joints, and the number of Monte Carlo simulations. The quantification of these uncertainties and the multiple lines of evidence presented in Section 6.3.4.7 provide additional confidence that the DRKBA model for rockfall can adequately predict the size ranges and quantities of rock that may fall into emplacement drifts.

As described in Section 6.3.4.5.1, uncertainty about the extent of the fracture planes has been quantified by varying the radius of the fracture plane. The results indicate that increasing the joint radius has a marginal impact on the block size distribution, and the maximum block size increases only slightly. The number of blocks, however, increases significantly with increasing joint radius. An increase in fracture extent in the DRKBA model causes greater fracture connectivity, resulting in an increase in block development. The radius multiplier in the DRKBA rockfall model, M, acts as a calibrator of the actual extent of the joint plane. Based on the field occurrence of blocks presented in the *Drift Degradation Analysis* (CRWMS M&O 2000 [DIRS 151635], Section 6.5), a radius multiplier of 2, as originally used in the DRKBA rockfall model, provides a reasonable yet conservative estimate of the number of blocks. The sensitivity study presented in Section 6.3.4.5.1 indicates that the frequency of blocks substantially increases when the radius multiplier exceeds 2. Therefore, a radius multiplier of 2.5 or greater would result in an excessive, inappropriate number of blocks, based on field evidence of block development in the ESF.

As described in Section 6.3.4.5.2, uncertainty about the impact on block development of the number of Monte Carlo simulations used in the DRKBA rockfall model has been quantified. The results indicate that 400 Monte Carlo simulations are sufficient to capture the range of block development in the rockfall model.

As described in Section 6.3.4.5.3, uncertainty about the correction factor applied to the spacing of the subhorizontal joint set has been quantified. The results indicate that a reduction in the correction factor from a mean value of 15 to a maximum value of 7 causes a decrease in the

number of blocks simulated and a slight increase in the distribution of block sizes. Given the significant reduction in the Terzaghi correction factor, the resulting impact on block development is minor.

The sensitivity analyses for the DRKBA rockfall model presented in this section confirm the appropriateness of the analysis parameter selection in the *Drift Degradation Analysis* report (CRWMS M&O 2000 [DIRS 151635]). These sensitivity analysis results indicate no impact to the repository subsystems potentially affected by rockfall.

6.4 SUMMARY AND PARAMETERS PROVIDED TO TOTAL SYSTEM PERFORMANCE ASSESSMENT

6.4.1 Summary of the Total System Performance Assessment Implementation of the Precipitates/Salts Model Lookup Tables

The TSPA parameters provided by the precipitates/salts model are summarized in the set of lookup tables presented in Section 6.3.3.6.1. The important independent variables are the design operating mode, time period, relative humidity, and relative evaporation rate (Q^e/Q^s, also known as R^{es}). Given values for each of these inputs, the lookup tables can be used to estimate output values for pH, ionic strength, and molalities of selected dissolved components and individual aqueous species.

The lookup tables include results for each possible design operating mode and time period, but they do not include values for each possible value of relative humidity, and the relative evaporation rate (Q^e/Q^s). Relative humidity and Q^e/Q^s are allowed to vary within each time period; thus, only results for a subset of values for these inputs that cover the expected ranges of these parameters are included in the tables. When relative humidity is less than 85 percent, pH is interpolated as a linear function of relative humidity, while each molality output (e.g., ionic strength, Cl molality, etc.) is interpolated as a linear function of relative humidity and the logarithm of the output value (e.g., log [ionic strength]). When relative humidity is greater than or equal to 85 percent, pH is interpolated as a linear function of the logarithm of one minus Q^e/Q^s (i.e., log $(1 - Q^e/Q^s)$) while each molality output is interpolated as a linear function of the logarithm of $(1 - Q^e/Q^s)$ and the logarithm of the output (e.g., log [ionic strength]). Log-log plots of the non-pH outputs versus $(1 - Q^e/Q^s)$ show a high degree of linearity, which supports these linearizations.

6.4.2 Summary of the Total System Performance Assessment Implementation of the Acid Neutralizing Capacity/pH Mixing Model

The in-drift mixing model attempts to establish a unified water chemistry model within the drift, which fits seamlessly with prior TSPA model development by producing integrated output feeds of pH, ionic strength, and acid neutralizing capacity (ANC) for mixed solutions in the drift. These in-drift solutions are mixtures of seepage fluxes from the crown above the drift, the water wicked through the rock and corroded metals in the invert, and the diffusion film or flux from a waste package after failure.

The necessary variable inputs to the in-drift ANC/pH mixing model from other source components of the TSPA model are the incoming water fluxes from the crown seepage, invert

wicking, and waste package leakage, and the associated major species concentrations that comprise the ANC: $[HCO_3^-]$, $[CO_3^{-2}]$, $[OH^-]$, $[H^+]$, $[MgOH^+]$, $[H_3SiO_4^-]$, $[H_2SiO_4^{-2}]$, $[UO_2CO_3^{-2}]$, and $[MoO_4^{-2}]$.

The new aspects of this ANC/pH in-drift mixing model integrate process model chemistry (CRWMS M&O 2001 [DIRS 153265]; BSC 2001 [DIRS 154620]; CRWMS M&O 2000 [DIRS 129283]) to provide consistent solution chemistry for use in modeling radionuclide solubilities, colloidal properties and transport, radionuclide sorption, and carbon dioxide gas equilibria within and leaving the repository drift for the TSPA model. Additionally, ionic strength is evaluated as part of the combined water source mixtures to provide values to the TSPA model. The integrated outputs of this model are designed to be the same TSPA model feeds: pH, ionic strength, plus ANC values in solutions that are mixed from three sources (i.e., crown seepage, invert wicking, and waste package leakage).

For most of the TSPA submodels (e.g., sorption, solubility, and colloids), the appropriate output feeds will be the mixed solution variables from three sources: $pH_{3Source}$, and $I_{3Source}$, produced from Equations 6-55 and 6-57, respectively. The mixing ANC parameter, $ANC_{3Source}$ (computed from Equation 6-5), is an important variable that may help describe chemistry in future subroutines when it is available. Cl^- may be linearly mixed exactly like ANC if it is needed in other subroutines.

6.4.3 Incoming Liquid and Gas Abstraction Results

Tables of water chemistry and carbon dioxide gas abundance for use in TSPA calculations are found in Sections 6.3.1.6.3.1 and 6.3.1.6.3.2 (with the appropriate lookup tables). Implementation of the tables, and guidelines for their use, are discussed in Section 6.3.1.6.3. If ionic strengths are needed for TSPA calculations based on the chemistries presented in Sections 6.3.1.6.3.1 and 6.3.1.6.3.2, they can be calculated for each period using Equation 4 from the *In-Drift Precipitates/Salts Analysis* (CRWMS M&O 2001 [DIRS 153265], p. 45).

6.4.4 Integration of Water Chemistries in the Drift between Total System Performance Assessment Model Components

In the TSPA-SR model (CRWMS M&O 2000 [DIRS 153246]), carbon dioxide levels in the drift were not coordinated between EBS component models and no integration was attempted within the TSPA model. This led to different assumed carbon dioxide levels in the same place at the same time during TSPA model runs. The overall effect of these differences are uncertain, although in the cases where coordination of carbon dioxide levels between models did not occur, parameters were selected to maximize radionuclide solubility and create a bounding condition. However, many systems in the drift are influenced by the fugacity of carbon dioxide in the drift air. Radionuclide solubilities depend on carbon dioxide fugacities. Aqueous solutions in and near the drift will have a pH that depends on the carbon dioxide fugacity. While some integration can be obtained by alterations of the TSPA model, full integration will require the incorporation of ongoing development and analyses of the various models that make up the EBS.

6.4.5 In-Drift Salts and Precipitates Modeling

The in-drift precipitates/salts model was developed to predict solution chemistry in the drift and invert external to the waste package. The input parameters to this model are the concentration (or activity) of each incoming model component in the water entering at the crown of the drift, temperature, relative humidity, carbon dioxide fugacity, the seepage rate, and the relative evaporation rate (CRWMS M&O 2001 [DIRS 153265], Section 4.1.3). The outputs of the model are the pH and ionic strength of the solution and the chloride concentration (CRWMS M&O 2001 [DIRS 153265], Sections 6.6.3 and 6.6.4).

The original model utilized the average composition of well J-13 water as a source of incoming model component concentrations (or activities) (CRWMS M&O 2001 [DIRS 153265], Section 4.1.3). Later work (CRWMS M&O 2001 [DIRS 153995]) applied the salts/precipitates model to abstracted THC water compositions developed in the *Abstraction of Drift-Scale Coupled Processes* (CRWMS M&O 2000 [DIRS 123916], Section 6.1). These are the only waters that have been documented. Further study continues on different input waters, and these continuing efforts should further reduce uncertainty in this input.

The output water chemistry of this model should serve as an input to other models in the drift in some cases, including the chemistry inside the waste package and the models that determine waste form dissolution and radionuclide solubility. At present, these models use well J-13 water or other waters as input. In addition, other inputs to the precipitates/salts model are currently being analyzed. This will give a wider range of modeled data and reduce uncertainty. More information on these efforts can be found in Section 6.3.3.

6.4.6 In-Package Chemistry Models

The chemistry inside the waste package is modeled in the *In-Package Chemistry for Waste Forms* (BSC 2001 [DIRS 153724]) and abstracted in the *In-Package Chemistry Abstraction* (CRWMS M&O 2000 [DIRS 129287]). This pair of reports uses a set carbon dioxide fugacity and a standard well J-13 water composition to predict water chemistry inside the waste package. Comparisons are made in the modeling effort to two other water types to determine the influence of water chemistry variation (CRWMS M&O 2000 [DIRS 111880], Section 6.3.2). These predictions are standardized for different time periods (CRWMS M&O 2000 [DIRS 129287], Section 6) to facilitate incorporation in the TSPA. These compositions, which include pH, total carbonate, Eh, ionic strength, F, and Cl parameters, are then used to model the degradation rates of waste package contents.

While this model is relatively insensitive to predicted variations in input water chemistry (CRWMS M&O 2000 [DIRS 111880], Section 6.2.3), any future work should consider the results of the in-drift precipitates/salts model applied to various drift waters as input to the in-package chemistry model, at least in the cases where it is predicted that these high ionic strength waters will enter the waste package. This consideration will lead to a more internally consistent model. Variation of carbon dioxide as an input by coordinating time periods with the in-drift precipitates/salts analysis would also make the model more internally consistent. These waters, as they emerge from the waste package, should be mixed with other predicted waters in the drift to form a more complete model of the EBS chemistry.

As in the in-drift precipitates/salts model, work continues for various input waters and some variation in the fugacity of carbon dioxide in the drift. These efforts will improve understanding of in-package chemical environment and lead to better predictive modeling of the environment.

6.4.7 Integration of Model Inputs

For certain elements, radionuclide solubility depends on temperature and the fugacity of carbon dioxide (CRWMS M&O 2001 [DIRS 154286], Section 6), as does waste form dissolution rate (CRWMS M&O 2000 [DIRS 136060], Section 6). The chemical composition of water inside the waste package depends on flux through the waste package (CRWMS M&O 2000 [DIRS 111880], Section 6). Water composition in the waste package also depends on carbon dioxide concentrations, although this can be conservatively ignored (CRWMS M&O 2000 [DIRS 111880], Section 6.2). Even if the model output is not sensitive to a particular input, it is important that common input parameters be consistent across the different models for a particular space and time. If the inputs for a parameter such as carbon dioxide fugacity are different for the different models in the same space and time, it will call into question the validity of the total system model, even if the parameter has little or no effect on the final output of the component model. In addition, models that are sensitive to carbon dioxide fugacity cannot be varied to demonstrate this sensitivity because the input data does not exist for relevant waters.

Another problem occurs because there is no attempt to coordinate the chemistries of different waters in the TSPA model. Because there is no mixing of waters and no coordination of carbon dioxide chemistry within the drift between models, a complete picture of drift conditions is not formed in the model. While parameters were selected to be conservative or bounding, improvement in and integration between EBS submodels improves confidence in them. The integration of carbon dioxide will require more information from the component models, as will mixing of the waters in the EBS. However, some integration can be accomplished with available information. One potential method is the ANC model (Section 6.3.3.4.2.3), which would take available data and provide a more complete picture of EBS chemistry by mixing waters from the in-drift water chemistry analyses and the in-package chemistry analyses. A complete explanation of this model is found in Section 6.3.3.4.2.3.

INTENTIONALLY LEFT BLANK

Table 6.3.1.5-1. Thermal-Hydrologic-Chemical Seepage Simulations

Infiltration-Property Set	Geochemical System	Simulation Type	Temperature Case	CO_2 Case	Initial Water Composition	Run ID
Mean Infiltration	NA	TH	Higher	NA	NA	th6_ht1
			Lower	NA	NA	th6_lt3
Mean Infiltration	Extended	THC	Higher	High	Alcove 5 (Pore)	thc6_ht1
			Higher	Low	Alcove 5 (Pore)	thc6_ht1L
			Higher	High	UZ-14 (Perched)	thc6_ht1w3
			Lower	High	Alcove 5 (Pore)	thc6_lt3
			Lower	Low	Alcove 5 (Pore)	thc6_lt3L
			Lower	High	UZ-14 (Perched)	thc6_lt3w3
			Ambient	Low	Alcove 5 (Pore)	thc6_ambL
			Ambient	High	UZ-14 (Perched)	thc6_ambw3

Source: Bodvarsson 2001 [DIRS 154669], Attachment 5, pp. 10 to 59. Unless indicated otherwise in the text, the input data are identical to those for the Tptpll model (BSC 2001 [DIRS 154677], Section 6.6).

NOTE: NA = Not Applicable. See text for additional information.

Table 6.3.1.5-2. Composition of Selected Pore Water and Other Waters from Yucca Mountain

Parameter	Units	HD-PERM-1 Tptpmn	HD-PERM-2 Tptpmn	HD-PERM-3 Tptpmn	DXD042 Tptpll	SD-6 Ptn	TSw-Avg TSw	UZ-14-Pore Tptpln/ Tptpv	UZ-14-Perch Tptpln/ Tptpv	J-13 TSw/ CHn
pH	pH	7.79	8.32	8.31	8.10[a]	7.52[a] (7.2)	8.2	7.66[a]	7.8	7.41
Na^+	mg/L	61	61	62	47.3	51.6	91	67	35	45.8
K^+	mg/L	6	7	9	0.2[a] (<0.5)	1.8	4[c]	2[a]	4.1	5.04
Ca^{+2}	mg/L	98	106	97	15.5[a] (9.1)	62.4	27	43	31	13
Mg^{+2}	mg/L	25.7	16.6	17.4	0.98	12	5	3.7	2.5	2.01
SiO_2	mg/L	79	66	75	95.6	92.8	60	35	40.7	60.1
Cl^-	mg/L	123	110	123	16.4	33	41	88	7	7.14
SO_4^{-2}	mg/L	124	111	120	8.5	101	40	19	24.2	18.4
HCO_3^-	mg/L	211[a]	233[a]	178[a]	128[a]	154[a] (95)	219[a] (191)	144[a] (170)	146.4	138[a] (128.9)
NO_3^-	mg/L	22	3	10	10[c]	57	13	16	17.1	8.78
F^-	mg/L	0.36	0.96	0.76	N/A	N/A	N/A	N/A	N/A	2.18
$\log(P_{CO2})$[a]	bars	-2.51	-3.00	-3.1	-3.00[b]	-2.37	-2.88	-2.53	-2.65	-2.29
CO_2 (approx.)[a, e]	ppmv	3500	1100	900	1100	4800	1500	3400	2500	5800
Calcite S.I.[a, d]	log(Q/K)	0.56	1.16	1.00	0.00[b]	0.00[b]	0.50	0.00[b]	0.03	-0.75

Sources: HD-PERM-x (DTN: MO0005PORWATER.000 [DIRS 150930]); UZ-14D (Yang et al. 1996 [DIRS 100194], Table 6, Sample UZ-14D, 8/21/93); DXD042 (DTN: LA9909JF831222.004 [DIRS 145598]; LA9909JF831222.006 [DIRS 146231]); SD-6 (DTN: LA0002JF12213U.001 [DIRS 154760]); TSw-Avg (CRWMS M&O 1999 [DIRS 129261], Table 4.5.1); UZ-14-Pore (DTN: LA0002JF12213U.001 [DIRS 154760]); UZ-14-Perch (Yang et al. 1996 [DIRS 100194], Table 6, Sample UZ-14D]); mean J-13 (DTN: MO0006J13WTRCM.000 [DIRS 151029]).

NOTES: [a] Calculated (values in parenthesis, if any, are the original data) - See text and Bodvarsson 2001 [DIRS 154669], Attachment 5, pp. 38 to 43, 47 to 49, 55 to 58.
[b] Fixed condition in order to compute pH - See text.
[c] Assumed.
[d] Saturation index at 25°C.
[e] At the drift atmospheric pressure (near 0.88 bars).
N/A = Not Available.

Table 6.3.1.6-1. Abstraction Results for High Temperature and Low Carbon Dioxide Partial Pressure in the Tptpll Lithology for Seepage at the Crown of the Drift

	Preclosure	Boiling	Cool Down	Extended Cool Down	Transition to Ambient	Ambient
	(0-50 yr)	(51-1,500 yr)	(1,501-4,000 yr)	(4,001-25,000 yr)	(25,001-100,000 yr)	(100,001-1,000,000 yr)
Actual THC Model Run Time (yr)	49.97	300.00	1,800.01	10,000.00	50,001.50	Averaged
Temperature (°C)	79.30	122.87	95.80	54.02	27.37	23.60
PCO_2 (v.frac)	9.20E-04	8.91E-06	1.66E-05	1.62E-03	5.71E-04	4.39E-04
pH	7.90	7.23	8.42	7.92	8.45	8.55
Ca (mol/L)	1.17E-03	2.34E-02	4.51E-03	1.48E-03	1.88E-03	1.97E-03
Mg (mol/L	5.94E-04	4.75E-02	6.50E-04	9.69E-05	2.50E-04	2.57E-04
Na (mol/L)	5.24E-03	4.23E-01	4.48E-03	4.30E-03	4.52E-03	4.39E-03
Cl (mol/L)	4.36E-03	3.72E-01	6.62E-03	3.27E-03	3.29E-03	3.29E-03
SiO_2(aq) (mol/L)	3.66E-03	3.45E-01	1.02E-02	2.55E-03	1.45E-03	1.44E-03
HCO_3 (mol/L)	4.96E-04	3.08E-04	3.34E-05	1.36E-03	2.53E-03	2.58E-03
SO_4 (mol/L)	1.59E-03	9.28E-02	2.86E-03	1.20E-03	1.20E-03	1.21E-03
K (mol/L)	2.39E-04	3.96E-02	5.33E-04	1.95E-04	1.04E-04	9.23E-05
AlO_2 (mol/L)	3.75E-08	2.45E-13	1.06E-08	6.27E-09	1.12E-09	6.74E-10
F (mol/L)	5.64E-04	3.32E-03	3.96E-04	4.06E-04	3.28E-04	3.11E-04
$HFeO_2$ (mol/L)	4.01E-11	6.09E-10	1.55E-09	4.54E-11	4.58E-12	1.97E-12

Source: Data derived from THC simulations thc6_ht1L and thc6_ambL (Table 6.3.1.5-1) as archived in Jolley (2001 [DIRS 154762]).

Table 6.3.1.6-2. Abstraction Results for High Temperature and High Carbon Dioxide Partial Pressure in the Tptpll Lithology for Seepage at the Crown of the Drift

	Preclosure	Boiling	Cool Down	Extended Cool Down	Transition to Ambient	Ambient
	(0-50 yr)	(51-1,500 yr)	(1,501-4,000 yr)	(4,001-25,000 yr)	(25,001-100,000 yr)	(100,001-1,000,000 yr)
Actual THC Model Run Time (yr)	49.97	300.00	1,800.01	10,000.00	50,001.50	Averaged
Temperature (°C)	79.30	122.86	95.80	54.02	27.37	23.2
PCO_2 (v.frac)	9.20E-04	8.92E-06	2.26E-05	3.45E-03	1.06E-03	7.67E-04
pH	7.90	7.23	8.37	7.74	8.29	8.41
Ca (mol/L)	1.17E-03	2.34E-02	4.35E-03	1.61E-03	2.08E-03	2.18E-03
Mg (mol/L)	5.94E-04	4.75E-02	5.90E-04	5.38E-05	1.87E-04	1.98E-04
Na (mol/L)	5.24E-03	4.23E-01	4.71E-03	4.57E-03	4.83E-03	4.68E-03
Cl (mol/L)	4.36E-03	3.72E-01	6.65E-03	3.28E-03	3.31E-03	3.31E-03
SiO_2(aq) (mol/L)	3.66E-03	3.45E-01	1.05E-02	2.80E-03	1.57E-03	1.55E-03
HCO_3 (mol/L)	4.96E-04	3.08E-04	3.76E-05	1.92E-03	3.22E-03	3.25E-03
SO_4 (mol/L)	1.59E-03	9.28E-02	2.86E-03	1.20E-03	1.20E-03	1.21E-03
K (mol/L)	2.39E-04	3.96E-02	5.55E-04	2.09E-04	1.12E-04	9.74E-05
AlO_2 (mol/L)	3.75E-08	2.45E-13	8.85E-09	4.31E-09	7.86E-10	4.59E-10
F (mol/L)	5.64E-04	3.32E-03	4.08E-04	3.91E-04	3.14E-04	2.97E-04
$HFeO_2$ (mol/L)	4.01E-11	6.09E-10	1.41E-09	4.40E-11	4.47E-12	1.87E-12

Source: Data derived from THC simulations thc6_ht1 (Table 6.3.1.5-1) and thc6_16_25_g4_amb (DTN: LB0011DSTTHCR1.001 [DIRS 154759]) as archived in Jolley (2001 [DIRS 154762]).

Table 6.3.1.6-3. Abstraction Results for Low Temperature and Low Carbon Dioxide Partial Pressure in the Tptpll Lithology for Seepage at the Crown of the Drift

	Preclosure	Post Closure Hot	Cool Down	Transition to Ambient	Ambient
	(0-300 yr)	(301-10,000 yr)	(10,001-30,000 yr)	(30,001-100,000 yr)	(100,001-1,000,000 yr)
Actual THC Model Run Time (yr)	53.00	700.00	20,000.00	51,411.30	Averaged
Temperature (°C)	52.92	73.40	35.59	25.89	23.60
PCO_2 (v.frac)	1.19E-03	1.48E-03	8.75E-04	5.11E-04	4.39E-04
pH	8.02	7.84	8.26	8.50	8.55
Ca (mol/L)	1.33E-03	1.08E-03	1.66E-03	1.92E-03	1.97E-03
Mg (mol/L)	5.00E-04	1.60E-04	1.81E-04	2.60E-04	2.57E-04
Na (mol/L)	4.08E-03	4.66E-03	4.65E-03	4.48E-03	4.39E-03
Cl (mol/L)	3.43E-03	3.40E-03	3.28E-03	3.29E-03	3.29E-03
SiO_2(aq) (mol/L)	2.44E-03	3.24E-03	1.69E-03	1.43E-03	1.44E-03
HCO_3 (mol/L)	1.29E-03	7.60E-04	2.15E-03	2.59E-03	2.58E-03
SO_4 (mol/L)	1.26E-03	1.24E-03	1.20E-03	1.20E-03	1.21E-03
K (mol/L)	1.37E-04	2.66E-04	1.35E-04	9.83E-05	9.23E-05
AlO_2 (mol/L)	7.28E-09	2.88E-08	2.12E-09	9.51E-10	6.74E-10
F (mol/L)	3.91E-04	4.69E-04	3.60E-04	3.21E-04	3.11E-04
$HFeO_2$ (mol/L)	6.08E-12	4.91E-11	3.17E-12	2.03E-12	1.97E-12

Source: Data derived from THC simulations thc6_lt3L and thc6_ambL (Table 6.3.1.5-1) as archived in Jolley (2001 [DIRS 154762]).

Table 6.3.1.6-4. Abstraction Results for Low Temperature and High Carbon Dioxide Partial Pressure in the Tptpll Lithology for Seepage at the Crown of the Drift

	Preclosure (0-300 yr)	Post Closure Hot (301-10,000 yr)	Cool Down (10,001-30,000 yr)	Transition to Ambient (30,001-100,000 yr)	Ambient (100,001-1,000,000 yr)
Actual THC Model Run Time (yr)	53.00	700.00	20,000.00	51,411.30	Averaged
Temperature (°C)	52.92	73.40	35.59	25.89	23.2
PCO_2 (v.frac)	1.19E-03	1.48E-03	1.71E-03	9.38E-04	7.67E-04
pH	8.02	7.84	8.09	8.35	8.41
Ca (mol/L)	1.33E-03	1.08E-03	1.87E-03	2.14E-03	2.18E-03
Mg (mol/L)	5.00E-04	1.60E-04	1.19E-04	1.97E-04	1.98E-04
Na (mol/L)	4.08E-03	4.66E-03	4.95E-03	4.79E-03	4.68E-03
Cl (mol/L)	3.43E-03	3.40E-03	3.30E-03	3.31E-03	3.31E-03
SiO_2(aq) (mol/L)	2.44E-03	3.25E-03	1.84E-03	1.55E-03	1.55E-03
HCO_3 (mol/L)	1.29E-03	7.61E-04	2.84E-03	3.31E-03	3.25E-03
SO_4 (mol/L)	1.26E-03	1.24E-03	1.20E-03	1.20E-03	1.21E-03
K (mol/L)	1.37E-04	2.66E-04	1.44E-04	1.06E-04	9.74E-05
AlO_2 (mol/L)	7.28E-09	2.87E-08	1.47E-09	6.64E-10	4.59E-10
F (mol/L)	3.91E-04	4.69E-04	3.42E-04	3.06E-04	2.97E-04
$HFeO_2$ (mol/L)	6.08E-12	4.91E-11	3.10E-12	2.00E-12	1.87E-12

Source: Data derived from THC simulations thc6_lt3 (Table 6.3.1.5-1) and thc6_16_25_g4_amb (DTN: LB0011DSTTHCR1.001 [DIRS 154759]) as archived in Jolley (2001 [DIRS 154762]).

Table 6.3.1.6-5. Abstraction Results for High Temperature and Low Carbon Dioxide Partial Pressure in the Tptpll Lithology for Matrix Imbibition into the Invert

	Preclosure	Boiling	Cool Down	Extended Cool Down	Transition to Ambient	Ambient
	(0-50 yr)	(51-1,500 yr)	(1,501-4,000 yr)	(4,001-25,000 yr)	(25,001-100,000 yr)	(100,001-1,000,000 yr)
Actual THC Model Run Time (yr)	5.00	250.01	2,000.00	10,000.00	49,806.80	Averaged
Temperature (°C)	75.02	120.69	93.89	53.96	27.48	23.69
PCO_2 (v.frac)	1.56E-03	2.20E-05	1.08E-05	1.44E-03	5.06E-04	4.07E-04
pH	7.86	8.10	8.36	7.89	8.49	8.57
Ca (mol/L)	8.75E-04	1.29E-02	1.34E-02	1.85E-03	1.79E-03	1.92E-03
Mg (mol/L)	3.54E-04	7.66E-03	1.84E-03	2.69E-05	1.99E-04	2.07E-04
Na (mol/L)	4.40E-03	5.82E-02	2.44E-03	3.46E-03	4.71E-03	4.54E-03
Cl (mol/L)	3.26E-03	5.88E-02	1.33E-02	3.26E-03	3.29E-03	3.29E-03
SiO_2(aq) (mol/L)	3.78E-03	3.80E-02	6.49E-03	3.07E-03	1.41E-03	1.35E-03
HCO_3 (mol/L)	8.30E-04	2.90E-05	2.53E-05	1.15E-03	2.44E-03	2.52E-03
SO_4 (mol/L)	1.17E-03	2.06E-02	8.94E-03	1.19E-03	1.20E-03	1.21E-03
K (mol/L)	4.39E-04	1.10E-02	3.74E-04	1.98E-04	1.17E-04	9.83E-05
AlO_2 (mol/L)	1.24E-08	3.53E-11	5.11E-08	3.04E-09	1.01E-09	7.30E-10
F (mol/L)	5.53E-04	3.30E-04	2.12E-04	3.74E-04	3.41E-04	3.19E-04
$HFeO_2$ (mol/L)	5.47E-11	2.01E-09	1.25E-09	4.49E-11	4.66E-12	1.97E-12

Source: Data derived from THC simulations thc6_ht1L and thc6_ambL (Table 6.3.1.5-1) as archived in Jolley (2001 [DIRS 154762]).

Table 6.3.1.6-6. Abstraction Results for High Temperature and High Carbon Dioxide Partial Pressure in the Tptpll Lithology for Matrix Imbibition at the Base of the Invert

	Preclosure	Boiling	Cool Down	Extended Cool Down	Transition to Ambient	Ambient
	(0-50 yr)	(51-1,500 yr)	(1,501-4,000 yr)	(4,001-25,000 yr)	(25,001-100,000 yr)	(100,001-1,000,000 yr)
Actual THC Model Run Time (yr)	5.00	250.01	2,000.00	10,000.00	50,001.50	Averaged
Temperature (°C)	75.02	120.68	93.89	53.96	27.44	23.26
PCO_2 (v.frac)	1.56E-03	2.15E-05	4.60E-05	3.40E-03	9.44E-04	7.13E-04
pH	7.86	8.27	8.04	7.70	8.33	8.43
Ca (mol/L)	8.75E-04	2.30E-02	1.37E-02	1.97E-03	2.01E-03	2.13E-03
Mg (mol/L)	3.54E-04	2.87E-02	2.45E-03	1.50E-05	1.35E-04	1.53E-04
Na (mol/L)	4.40E-03	2.24E-01	3.96E-03	3.71E-03	5.02E-03	4.82E-03
Cl (mol/L)	3.26E-03	2.24E-01	1.60E-02	3.27E-03	3.31E-03	3.31E-03
SiO_2(aq) (mol/L)	3.78E-03	7.10E-02	6.32E-03	3.40E-03	1.52E-03	1.46E-03
HCO_3 (mol/L)	8.30E-04	2.35E-05	4.13E-05	1.73E-03	3.15E-03	3.19E-03
SO_4 (mol/L)	1.17E-03	5.35E-02	9.67E-03	1.19E-03	1.20E-03	1.21E-03
K (mol/L)	4.39E-04	4.20E-02	6.11E-04	2.12E-04	1.24E-04	1.03E-04
AlO_2 (mol/L)	1.24E-08	3.93E-12	2.59E-08	2.05E-09	7.25E-10	5.06E-10
F (mol/L)	5.53E-04	4.18E-04	2.15E-04	3.66E-04	3.24E-04	3.04E-04
$HFeO_2$ (mol/L)	5.47E-11	2.81E-09	8.49E-10	4.36E-11	4.53E-12	1.86E-12

Source: Data derived from THC simulations thc6_ht1 (Table 6.3.1.5-1) and thc6_16_25_g4_amb (DTN: LB0011DSTTHCR1.001 [DIRS 154759]) as archived in Jolley (2001 [DIRS 154762]).

Table 6.3.1.6-7. Abstraction Results for Low Temperature and Low Carbon Dioxide Partial Pressure in the Tptpll Lithology for Matrix Imbibition into the Invert

	Preclosure (0-300 yr)	Post Closure Hot (301-10,000 yr)	Cool Down (10,001-30,000 yr)	Transition to Ambient (30,001-100,000 yr)	Ambient (100,001-1,000,000 yr)
Actual THC Model Run Time (yr)	49.97	750.01	20,000.00	51,411.30	Averaged
Temperature (°C)	50.89	72.11	35.63	25.96	23.69
PCO_2 (v.frac)	1.05E-03	1.27E-03	8.17E-04	4.57E-04	4.07E-04
pH	8.06	7.79	8.28	8.53	8.57
Ca (mol/L)	1.22E-03	1.64E-03	1.60E-03	1.84E-03	1.92E-03
Mg (mol/L)	3.78E-04	9.72E-05	1.24E-04	2.07E-04	2.07E-04
Na (mol/L)	4.22E-03	3.47E-03	4.83E-03	4.67E-03	4.54E-03
Cl (mol/L)	3.25E-03	3.43E-03	3.28E-03	3.29E-03	3.29E-03
SiO_2(aq) (mol/L)	3.02E-03	4.52E-03	1.67E-03	1.36E-03	1.35E-03
HCO_3 (mol/L)	1.28E-03	6.02E-04	2.11E-03	2.50E-03	2.52E-03
SO_4 (mol/L)	1.19E-03	1.26E-03	1.20E-03	1.20E-03	1.21E-03
K (mol/L)	2.21E-04	3.22E-04	1.58E-04	1.10E-04	9.83E-05
AlO_2 (mol/L)	1.89E-09	6.68E-09	1.61E-09	9.37E-10	7.30E-10
F (mol/L)	4.57E-04	4.08E-04	3.78E-04	3.33E-04	3.19E-04
$HFeO_2$ (mol/L)	1.33E-11	4.45E-11	3.19E-12	2.03E-12	1.97E-12

Source: Data derived from THC simulations thc6_lt3L and thc6_ambL (Table 6.3.1.5-1) as archived in Jolley (2001 [DIRS 154762]).

Table 6.3.1.6-8. Abstraction Results for Low Temperature and High Carbon Dioxide Partial Pressure in the Tptpll Lithology for Matrix Imbibition at the Base of the Invert

	Preclosure (0-300 yr)	Post Closure Hot (301-10,000 yr)	Cool Down (10,001-30,000 yr)	Transition to Ambient (30,001-100,000 yr)	Ambient (100,001-1,000,000 yr)
Actual THC Model Run Time (yr)	30.00	750.01	20,000.00	51,411.30	Averaged
Temperature (°C)	53.52	72.11	35.63	25.96	23.26
PCO_2 (v.frac)	1.09E-03	1.28E-03	1.66E-03	8.53E-04	7.13E-04
pH	8.05	7.79	8.10	8.38	8.43
Ca (mol/L)	1.19E-03	1.64E-03	1.83E-03	2.06E-03	2.13E-03
Mg (mol/L)	3.89E-04	9.71E-05	6.70E-05	1.44E-04	1.53E-04
Na (mol/L)	4.25E-03	3.47E-03	5.11E-03	4.99E-03	4.82E-03
Cl (mol/L)	3.26E-03	3.43E-03	3.30E-03	3.31E-03	3.31E-03
SiO_2(aq) (mol/L)	3.08E-03	4.53E-03	1.82E-03	1.47E-03	1.46E-03
HCO_3 (mol/L)	1.26E-03	6.03E-04	2.82E-03	3.22E-03	3.19E-03
SO_4 (mol/L)	1.19E-03	1.26E-03	1.20E-03	1.20E-03	1.21E-03
K (mol/L)	2.40E-04	3.23E-04	1.67E-04	1.17E-04	1.03E-04
AlO_2 (mol/L)	2.41E-09	6.67E-09	1.14E-09	6.67E-10	5.06E-10
F (mol/L)	4.67E-04	4.08E-04	3.57E-04	3.17E-04	3.04E-04
$HFeO_2$ (mol/L)	1.37E-11	4.45E-11	3.11E-12	2.00E-12	1.86E-12

Source: Data derived from THC simulations thc6_lt3 (Table 6.3.1.5-1) and thc6_16_25_g4_amb (DTN: LB0011DSTTHCR1.001 [DIRS 154759]) as archived in Jolley (2001 [DIRS 154762]).

Table 6.3.1.8-1. Summary of Uncertainty Issues Related to Predicted Composition of Fluids Entering Drifts

Category	Uncertainty Issue	Treatment of Uncertainty Issue	Affected Goals
Conceptual Uncertainties	Geochemical system considered (minerals, gases, and aqueous species)	Treated by including major rock-forming minerals, major aqueous species, and major gases of interest (carbon dioxide, air, and steam) in the system Effects of secondary mineral phase precipitation is most uncertain at higher temperatures and may require further evaluation Uncertainty is limited under ambient conditions if ambient water concentrations can be reproduced Trace minerals and aqueous species are not considered (not in the current scope for the THC model)	Precipitation of secondary phases not currently included in simulations could significantly affect the predicted composition of waters around the drift at high temperature. Reactions between trace minerals and aqueous species could affect predicted concentrations of major species through pH change
	Drift wall is closed to advective fluid flow (but open to carbon dioxide diffusive fluxes)	Case of open drift wall is not addressed Infiltration rates (even at high rates indicative of future wet climates) are below seepage thresholds, so there is no effect on water percolation fluxes around the drift Effect of carbon dioxide diffusive transport across the wall is taken into account and may be more important than advective fluxes Evaporative concentration effects (due to ventilation) are indirectly taken into account by the salts and precipitates model (Section 6.3.3) Effects of atmospheric carbon dioxide in the drift during ventilation (through diffusive fluxes) were investigated and determined to be short-lived after ventilation ends	Boundary conditions of pressure and relative humidity in the drift could affect evaporative concentration effects at the drift wall, most particularly during ventilation. Such boundary conditions have not been determined Carbon dioxide advective fluxes into the drift are not calculated, which could affect the pH of pore water at the drift wall In-drift interactions are not considered (this was not a goal of the THC seepage models)
	Precipitation/ nucleation kinetics	Not treated This affects minerals such as silica and calcite, which have fast reaction rates. Reaction of calcite at equilibrium with a supersaturation gap may approximate nucleation processes Silica precipitation is modeled with a very fast reaction rate	In areas where rapid boiling occurs, predicted silica concentrations are overestimated and silica precipitation is underestimated. However, the water saturation in these areas is very small such that the actual amounts of silica are minute
	Water chemistry is not computed below a set water saturation (10^{-4}) or above a set ionic strength (4) (Activity coefficient model limitations)	Salts precipitation in the last remaining water, when boiling or evaporating is not considered The composition of the last aqueous phase for which geochemical speciation is computed (prior to dryout) is saved by the model. This composition is assumed to mix instantly with percolating water during rewetting	Some solid phases precipitated upon dryout may not dissolve instantly upon rewetting. In this case, assuming instant dissolution may overpredict dissolved salt concentrations when rewetting occurs

Table 6.3.1.8-1. Summary of Uncertainty Issues Related to Predicted Composition of Fluids Entering Drifts (Continued)

Category	Uncertainty Issue	Treatment of Uncertainty Issue	Affected Goals
Conceptual Uncertainties (Continued)	Vapor pressure lowering due to changes in water activity caused by dissolved salts	Not treated This effect would only become significant once most of the water has already evaporated (i.e., when ionic strength becomes large - for example, at 3m NaCl, the reduction in vapor pressure would only be approximately 10%)	By neglecting this effect, evaporative concentration is overestimated
	Vapor pressure lowering due to capillary pressure	Not treated The effect on evaporative concentration is mostly bounded by the higher- and lower-temperature cases (without vapor pressure lowering)	Neglecting vapor pressure lowering increases the effect of evaporative concentration around the drift (resulting in overestimated water salinities)
	Oxidation-reduction processes are neglected	Not treated (considers only oxidized conditions) Oxidizing conditions prevail in the unsaturated zone at Yucca Mountain such that the redox species considered in the THC seepage model (iron and sulfate) occur only in their oxidized state	Limited anticipated effect. Likely no effect for iron and sulfate in the current models. Redox reactions involving microbial processes and species not presently modeled (nitrates, phosphates) could have some effect on pH
	Mineral solid-solutions	Treated as ideal for clays; no treatment for other minerals Taken indirectly into account through calibration of thermodynamic data such that ambient water compositions can be reproduced Compositions of primary solid solution phases, when known, are indirectly taken into account in the amounts of individual end-members input into the model Individual mineral phases with fixed solid-solution compositions (determined by analysis) are included in simulations (e.g., zeolites)	Limited anticipated effect. In the current THC seepage models, this would primarily affect the composition of precipitating alkali feldspars (thus affecting predicted Na and K concentrations). However, these minerals typically form nearly pure secondary phases in nature (i.e., as modeled). Zeolites in the repository host units (mostly stellerite) are not abundant and not particularly variable in composition
	Ion-exchange and surface complexation	Not treated Dominant primary rock minerals in the rock wall around the drifts are not strong ion exchangers THC seepage simulations do not include trace elements that could be strongly affected by surface complexation	Limited effect for the current application range of the THC seepage models. Could shift somewhat the predicted concentrations of Na, K, Ca, and Mg
	Capillary pressure effect on chemical potentials of reacting species	Not treated It is taken indirectly into account through calibration of thermodynamic data such that ambient water compositions can be reproduced	Could potentially shift predicted concentrations of some species

Table 6.3.1.8-1. Summary of Uncertainty Issues Related to Predicted Composition of Fluids Entering Drifts (Continued)

Category	Uncertainty Issue	Treatment of Uncertainty Issue	Affected Goals
Data Uncertainties	Infiltration water and initial pore-water composition	Alternate water analyses are used in recent analyses Additional systematic evaluations may be needed with additional compositions Uncertainty can be assessed by comparing predictions of ambient water compositions with measured ambient pore-water compositions and pore-gas CO_2 concentrations	Currently one of the main uncertainties affecting predicted water compositions around the drift (and likely more so through infiltration/transport than through reaction)
	Carbon dioxide partial pressures at top model boundary	Treated in recent analyses Composition of infiltration-water input into the model essentially dictates the boundary carbon dioxide pressure; therefore the uncertainty in infiltrating water composition overcomes this uncertainty	Within the investigated range (750 and 3700 ppmv), no effect until 800-1000 years, then small pH effect (0.4 units) at the drift wall, and negligible effect on other predicted concentrations
	Thermodynamic and kinetic data	Treated partly through sensitivity studies on long-term behavior of ambient system chemistry, assuming a fixed infiltration rate When possible within the uncertainty of the original data, treated through calibration with observed water composition and mineralogical data Other uncertainties treated through model validation (Drift Scale Test and laboratory experiments)	One of the main uncertainties affecting predicted water compositions around the drift. However, it can be constrained by calibration and model validation against observed data, such that ambient simulations predict concentrations consistent with observed values
	Host rock mineralogy	Treated in updated model (Tptpmn versus Tptpll host rock unit) Bulk chemical composition of the potential repository host units do not differ significantly	No significant effect on the predicted compositions of major aqueous species. Small amounts of fast reacting minerals containing elements present in minor quantities in pore water (e.g., fluorite) can have a large effect on the predicted concentrations of these minor species (e.g., F^-)
	Infiltration rates	Alternate infiltration rate scenarios are used in original analysis. Stepwise increase in infiltration rates are used in all analyses At high infiltration rate conditions most conducive to in-drift seepage, water compositions are more function of transport than reaction such that the uncertainty regarding the composition of infiltration, rather than the rate, becomes more important	Affects predicted concentrations at the drift wall. However, the effect is stronger under low infiltration conditions least susceptible to cause in-drift seepage

Table 6.3.1.8-1. Summary of Uncertainty Issues Related to Predicted Composition of Fluids Entering Drifts (Continued)

Category	Uncertainty Issue	Treatment of Uncertainty Issue	Affected Goals
Parameter Uncertainties	Heterogeneity	Fracture permeability heterogeneity treated in updated model Heterogeneity in matrix properties not treated Local heterogeneity in mineralogical properties not treated Heterogeneity in initial water geochemistry not treated directly; treated indirectly through alternate compositions used	Possible local changes in predicted water compositions around the drift. However, the bulk composition of waters around the drift is not expected to be significantly affected
	Transport parameters (diffusion coefficients and tortuosity)	Carbon dioxide diffusion coefficient changed by a factor of 30 between initial and updated analyses Sensitivity to diffusion coefficient for aqueous species was not investigated; however, tortuosity factor was changed from 0.2 to 0.7 between initial and updated analyses	Affects predicted concentrations of carbon dioxide at the drift wall during dryout; otherwise, the effect appears limited

NOTE: See also Table 4.3.6-2.

Table 6.3.2-1. Summary of Uncertainties on the Effects of Engineered Materials in the In-Drift Chemical Environment and any Associated Model Improvements

Key Uncertainty Not Included in TSPA-SR Models	Model Improvements Discussed in SSPA Vol. 1
Trace elemental compositions and effects on chemistry	No
Radionuclide or metal sorption onto corrosion products	Yes (Section 10)
Oxygen gas depletion (generation of sub-oxic conditions)	No
Cement leachate effects on in-drift chemistry	Yes (Section 6.3.3.5.1.1)
Generation of colloids from corrosion products	Yes (Section 10)
Alkaline plumes interacting with EBS	No

Source: TSPA-SR refers to CRWMS M&O 2000 [DIRS 153246].

Table 6.3.3-1. Example Precipitates/Salts Model Lookup Table for Selected Outputs

Input Parameters		Precipitates/Salts Model Output for:				Invert	Low Temp, Low CO2		Preclosure Period (0-300 yr)				
RH (%)	Qe/Qs[a]	pH	Ionic Strength (molal)	Total Cl (molal)	Total F (molal)	Total N (molal)	HCO3- (molal)	CO32- (molal)	OH- (molal)	H+ (molal)	H2SiO42- (molal)	H3SiO4- (molal)	MgOH+ (molal)
< 50.3	na[b]	NA	NA	NA	NA	NA	NA	NA	NA	NA	NA	NA	NA
50.3	NA	7.30	2.61E+01	2.70E-02	NA	NA	NA	NA	NA	NA	NA	NA	NA
51.0	NA	7.30	2.38E+01	3.72E-01	NA	NA	NA	NA	NA	NA	NA	NA	NA
53.1	NA	7.30	1.49E+01	1.69E+00	NA	NA	NA	NA	NA	NA	NA	NA	NA
55.2	NA	7.30	1.15E+01	2.20E+00	NA	NA	NA	NA	NA	NA	NA	NA	NA
60.5	NA	7.30	6.26E+00	2.99E+00	NA	NA	NA	NA	NA	NA	NA	NA	NA
65.7	NA	7.30	4.68E+00	3.22E+00	NA	NA	NA	NA	NA	NA	NA	NA	NA
71.0	NA	7.30	4.32E+00	3.28E+00	NA	NA	NA	NA	NA	NA	NA	NA	NA
76.2	NA	7.30	4.24E+00	3.29E+00	NA	NA	NA	NA	NA	NA	NA	NA	NA
81.5	NA	7.30	4.33E+00	3.27E+00	NA	NA	NA	NA	NA	NA	NA	NA	NA
85.0	NA	7.30	4.29E+00	3.17E+00	3.87E-04	3.17E-01	5.88E-04	2.17E-05	2.84E-06	2.24E-08	1.85E-10	4.18E-06	7.38E-08
> 85	-9.00	6.75	9.62E-04	3.25E-04	4.54E-05	3.25E-05	6.99E-05	2.99E-08	3.28E-07	1.87E-07	1.85E-14	7.04E-08	1.74E-10
> 85	0.00	7.71	9.63E-03	3.25E-03	4.54E-04	3.25E-04	6.88E-04	3.38E-06	3.24E-06	2.18E-08	2.06E-11	6.84E-06	1.22E-08
> 85	0.90	7.53	7.46E-02	3.24E-02	3.18E-04	3.24E-03	5.23E-04	2.74E-06	2.51E-06	3.81E-08	1.64E-11	5.11E-06	2.20E-08
> 85	0.99	7.44	5.34E-01	3.18E-01	3.42E-04	3.18E-02	5.58E-04	5.33E-06	2.61E-06	5.40E-08	3.35E-11	4.87E-06	3.83E-08
> 85	0.999	7.38	3.92E+00	2.72E+00	4.47E-04	2.72E-01	7.10E-04	2.75E-05	3.24E-06	2.37E-08	2.25E-10	5.02E-06	6.37E-08
> 85	> 0.999	7.30	4.29E+00	3.17E+00	3.87E-04	3.17E-01	5.88E-04	2.17E-05	2.84E-06	2.24E-08	1.85E-10	4.18E-06	7.38E-08

Source: Jolley 2001 [DIRS 154762]. This reference also presents a complete set of lookup tables.

NOTES: [a] Q_e/Q_s is the evaporative flux divided by the seepage flux.

[b] Not applicable to model (dry conditions at relative humidity less than 50.3 percent).

Table 6.3.3.5.2-1. Sensitivity Analysis of the In-Drift ANC/pH Model

W_{wpl} (kg/yr)	Run 1 pH	Run 2 pH	Run 3 pH	Run 4 pH	Run 5 pH	Run 6 pH	Range of pH	Mean pH
1.15	8.5	8.5	8.5	8.5	8.5	8.5	8.5	8.5
251.15	8.5	8.5	7.9	8.4	8.3	8.2	7.9-8.5	8.3
501.15	7.9	8.5	7.6	8.2	7.6	8.0	7.6-8.5	8.0
751.15	7.4	8.4	7.2	7.9	8.1	8.0	7.2-8.4	7.8
1001.15	8.4	8.4	8.1	7.9	7.3	7.4	7.3-8.4	7.9
1251.15	8.4	7.4	7.9	6.3	7.2	8.4	6.3-8.4	7.6
1501.15	8.4	7.4	7.9	7.3	6.4	5.9	5.9-8.4	7.2
1751.15	6.0	7.2	4.7	4.7	8.4	8.4	4.7-8.4	6.6
2001.15	7.3	8.4	7.7	4.6	8.3	7.3	4.6-8.4	7.3
2251.15	7.6	8.2	7.6	4.6	8.1	8.2	4.6-8.2	7.4
2501.15	8.2	7.9	8.4	4.5	4.4	4.4	4.4-8.4	6.3
2751.15	8.2	4.3	7.8	4.4	4.6	4.3	4.3-8.2	5.6
3001.15	7.5	5.1	7.4	4.5	7.4	7.7	4.5-7.7	6.6
3251.15	4.3	4.6	4.3	7.9	7.9	8.1	4.3-8.1	6.2
3501.15	4.6	4.4	6.6	8.3	5.4	7.0	4.4-8.3	6.1
3751.15	6.0	4.6	4.2	6.4	8.2	4.5	4.2-8.2	5.7
4001.15	7.0	7.8	7.6	7.7	7.7	4.3	4.3-7.8	7.0

Source: Metcalf 2001 [DIRS 154842].

NOTE: Sensitivity analysis of in-drift ANC/pH model showing variation of mixed solution pH as a function of waste package leakage flux (W_{wpl}) and percentage waste package mixing (F_{mixing}) with other water sources by Monte Carlo simulation (seen as variation across a row of pH for a given W_{wpl}).

Table 6.3.3.5.2-2. Validation Analyses of In-Drift ANC/pH Model Showing Agreement Between Mixing Model Results and Literature Mixing Examples

Parameter	Morel and Hering[a]	Stumm and Morgan[b]	In-drift ANC/pH Mixing Model-1[c]	In-drift ANC/pH Mixing Model-2
Water pH (mixed)	7.91	7.2	7.90	7.20
ANC_{mixed} (Eq/L)	4.06 E-04	9.5 E-05	4.04 E-04	9.50 E-05

Sources: [a] Morel and Hering 1993 [DIRS 151052], pp. 194 to 195.
[b] Stumm and Morgan 1996 [DIRS 125332], pp. 170 to 172.
[c] Metcalf 2001 [DIRS 154842].

Table 6.3.4-1. Block Volume Corresponding to Various Levels of Predicted Cumulative Frequency of Occurrence, Emplacement Drift in Tptpmn Unit, Static Condition

Cumulative Frequency of Occurrence (%)	Joint Radius Multiplier (*M*)				
	1.0	1.5	2.0	2.5	3.0
50	0.16	0.01	0.04	0.01	0.01
75	0.30	0.16	0.21	0.16	0.16
90	0.61	0.44	0.55	0.52	0.50
95	1.35	0.67	1.06	0.98	0.98
98	1.35	1.18	1.86	1.86	2.17
Maximum	1.35	1.86	14.30	20.87	13.05

Source: BSC 2001 [DIRS 154537].

NOTE: Block volume measured in m^3.

Table 6.3.4-2. Block Volume Corresponding to Various Levels of Predicted Cumulative Frequency of Occurrence, Emplacement Drift in Tptpll Unit, Static Condition

Cumulative Frequency of Occurrence (%)	Joint Radius Multiplier (*M*)				
	1.0	1.5	2.0	2.5	3.0
50	0.24	0.04	0.01	0.01	0.01
75	0.24	0.16	0.07	0.16	0.10
90	0.24	0.38	0.24	0.38	0.24
95	0.24	1.49	0.86	0.86	0.47
98	0.24	1.49	1.29	3.36	0.86
Maximum	0.24	1.49	1.29	3.36	3.36

Source: BSC 2001 [DIRS 154537].

NOTE: Block volume measured in m^3.

Table 6.3.4-3. Predicted Number of Key Blocks per Unit Length along Emplacement Drift, Static Condition

Lithologic Unit	Joint Radius Multiplier (*M*)				
	1.0	1.5	2.0	2.5	3.0
Tptpmn	1	11	50	152	265
Tptpll	0	2	2	5	6

Source: BSC 2001 [DIRS 154537].

NOTE: Blocks per unit length measured in km.

Table 6.3.4-4. Beta Distribution Parameters for Spacing of the Subhorizontal Joint Set of the Tptpmn Unit

Beta Distribution Parameters	Original True Spacing[a]	Modified True Spacing[b]
a (m)	0.0018	0.0018
b (m)	15.2606	15.2606
p	0.2010	0.3834
q	5.2988	5.8050

NOTES: [a] CRWMS M&O 2000 [DIRS 151635], Table 7, Joint Set Number 3.
[b] BSC 2001 [DIRS 154537], file New-Beta-Tptpmn V1 - modified Terzaghi.xls.

Table 6.3.4-5. Block Volume Corresponding to Various Levels of Predicted Cumulative Frequency of Occurrence, Emplacement Drift in Tptpmn Unit, Static Condition with Modified Terzaghi Correction

Cumulative Frequency of Occurrence (%)	Terzaghi Correction Factor	
	Original	Modified
50	0.04	0.04
75	0.21	0.24
90	0.55	0.81
95	1.06	1.54
98	1.85	2.36
maximum	14.29	19.35

Source: BSC 2001 [DIRS 154537].

NOTE: Block volume measured in m^3.

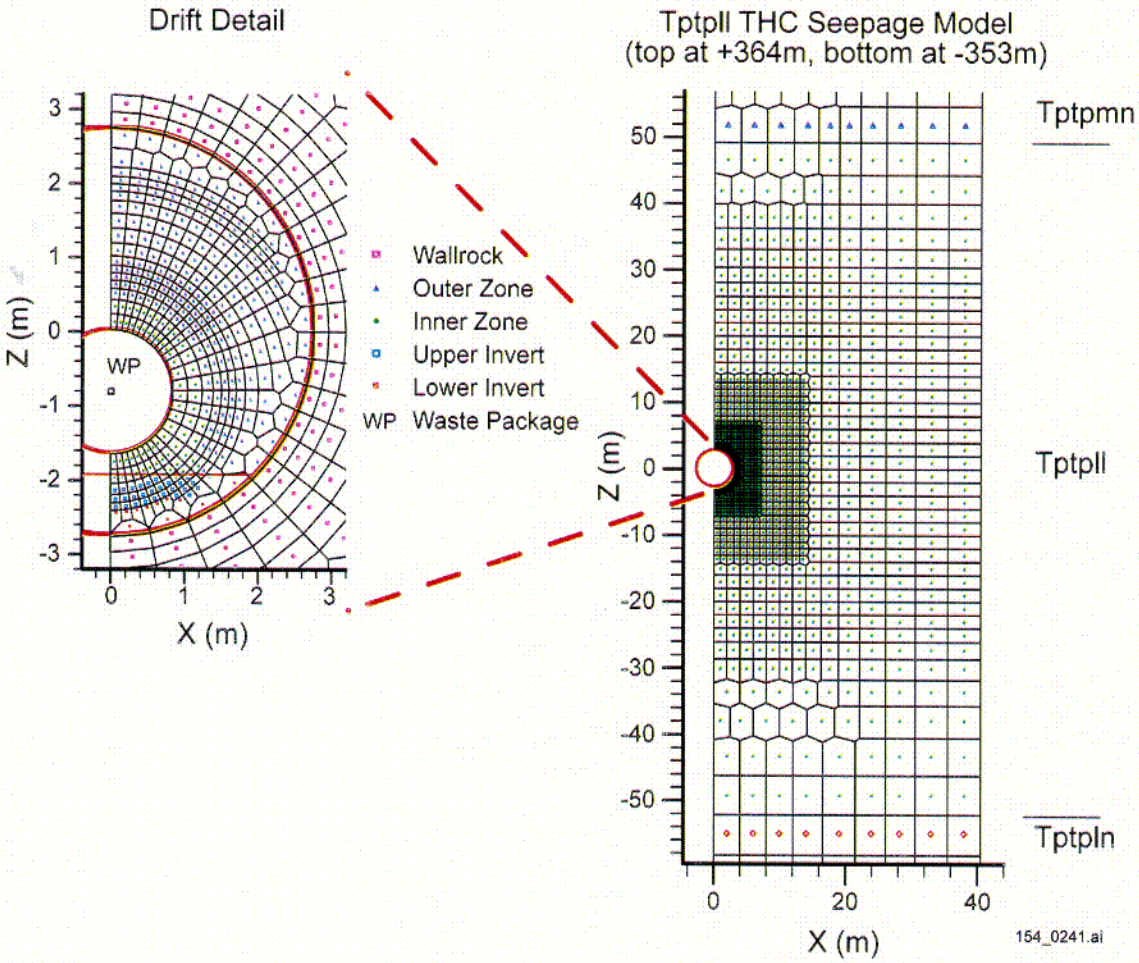

154_0241.ai

Source: Adapted from BSC 2001 [DIRS 154677], Figures 84 and 85.

NOTE: Laterally, the mesh covers half the distance between drift centers. Vertically, the mesh extends from near ground surface down to the regional water table. THC = thermal-hydrologic-chemical.

Figure 6.3.1.2-1. Example of Thermal-Hydrologic-Chemical Seepage Model Mesh with Drift in the Topopah Spring Tuff Lower Lithophysal Geologic Unit (TptpII)

C01

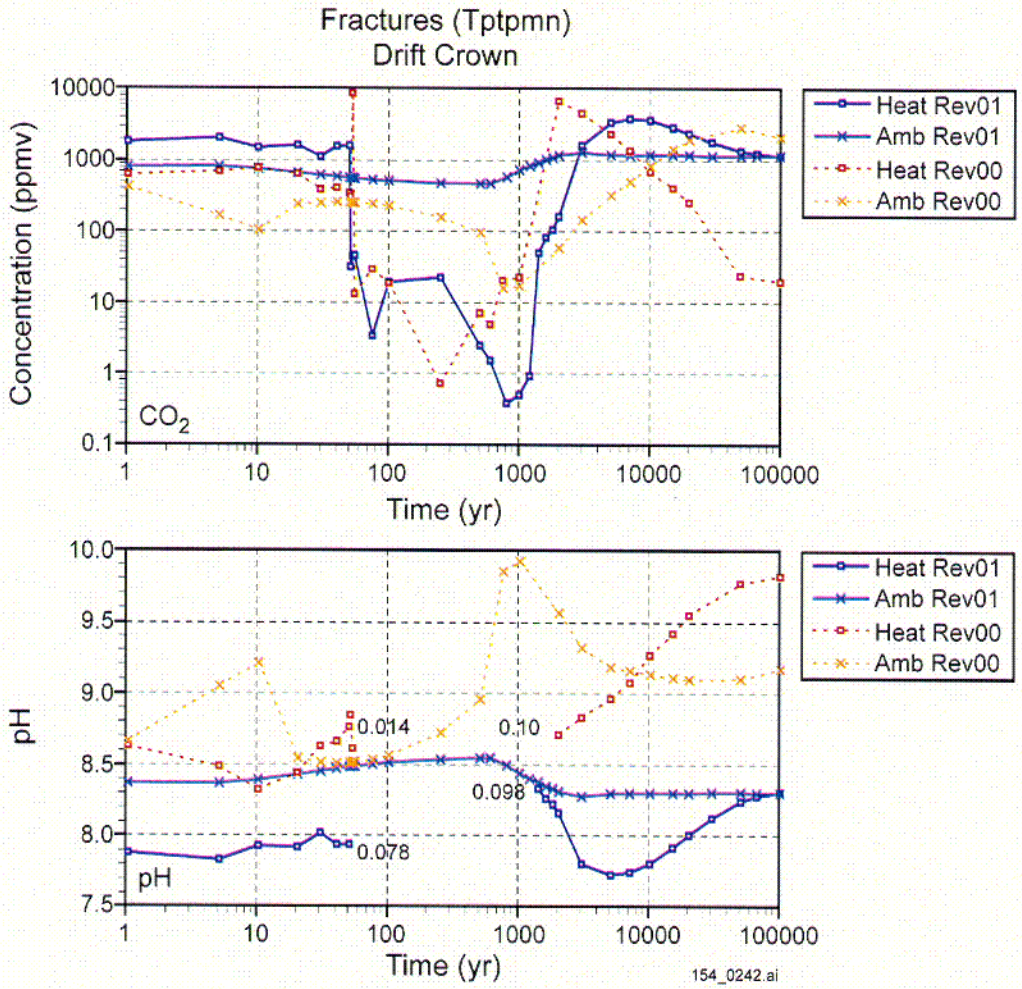

154_0242.ai

Source: CRWMS M&O 2000 [DIRS 142022]; BSC 2001 [DIRS 154677].

NOTE: Comparison of initial and updated simulation results. Results are for simulations under heat load (Heat) and ambient (Amb) conditions (extended-case geochemical system). The infiltration rate changes from 6 to 16 mm/yr at 600 years and from 16 to 25 mm/yr at 2,000 years, except for the ambient case (fixed rate of 1 mm/yr). For pH, the dryout period is left blank (no water); numbers by each curve indicate the last output liquid saturation before dryout and the first output liquid saturation during rewetting.

Figure 6.3.1.4-1. Time Profiles for Thermal-Hydrologic-Chemical Simulations of Carbon Dioxide (Pore Gas) Concentration and pH (Pore Water) in Fractures at the Drift Crown

CO2

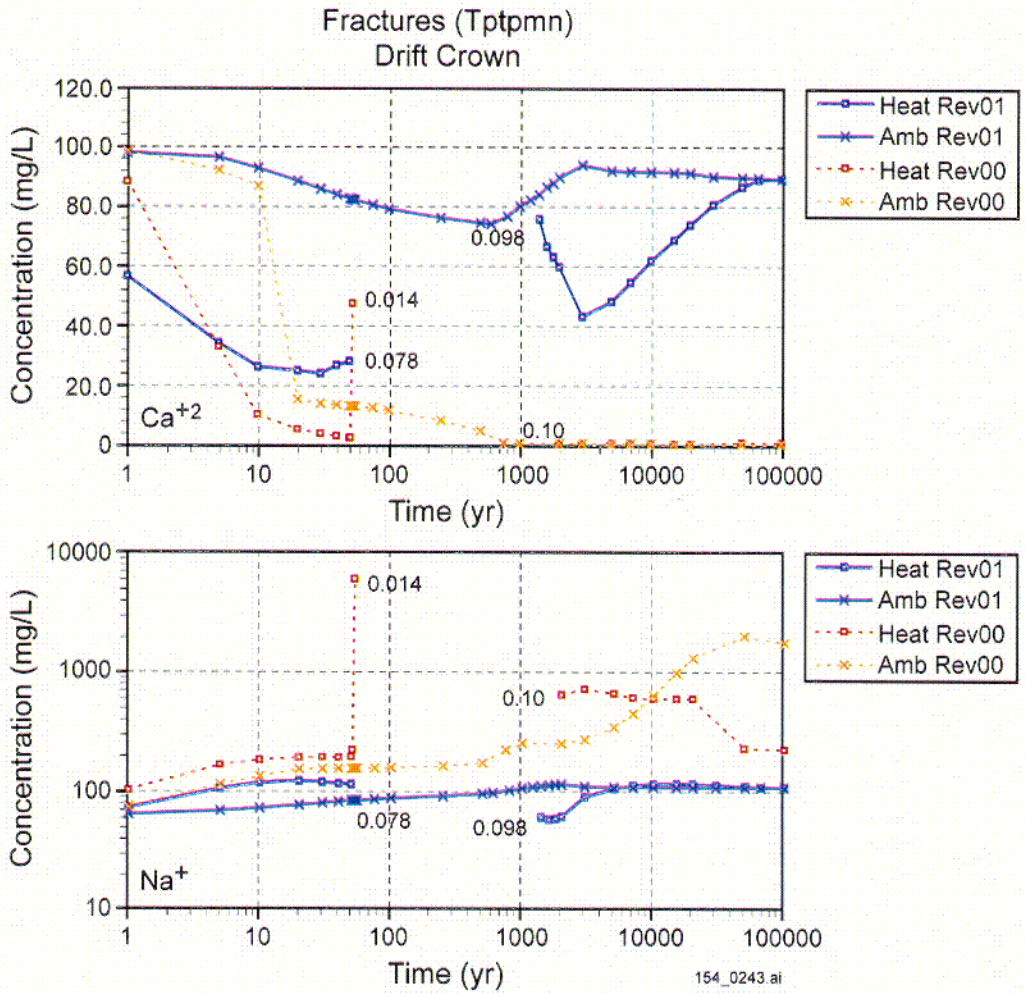

154_0243.ai

Source: CRWMS M&O 2000 [DIRS 142022]; BSC 2001 [DIRS 154677].

NOTE: Comparison of simulation results for Revision 00 and Revision 01. Results are for simulations under heat load (Heat) and ambient (Amb) conditions (extended-case geochemical system). The infiltration rate changes from 6 to 16 mm/yr at 600 years and from 16 to 25 mm/yr at 2,000 years, except for the REV 00 ambient case (fixed rate of 1 mm/yr). The dryout period is left blank (no water); numbers by each curve indicate the last output liquid saturation before dryout and the first output liquid saturation during rewetting.

Figure 6.3.1.4-2. Time Profiles for Thermal-Hydrologic-Chemical Simulations of Aqueous Calcium and Sodium Concentrations in Fractures at the Drift Crown

C03

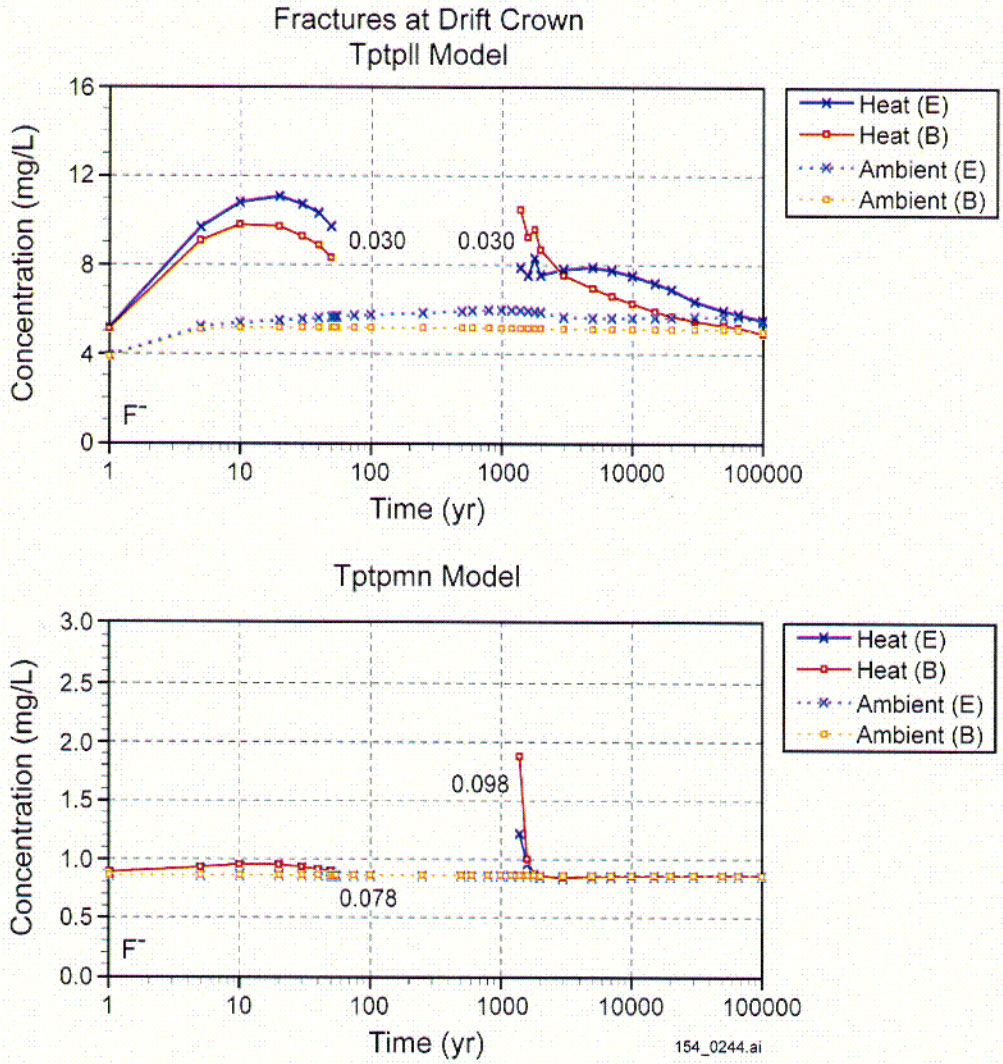

154_0244.ai

Source: BSC 2001 [DIRS 154677].

NOTE: Comparison of simulation results for Tptpll and Tptpmn in Revision 01. Results are for simulations under heat load (Heat) and ambient (Amb) conditions, for the extended-case (E) and base-case (B) geochemical systems. The infiltration rate changes from 6 to 16 mm/yr at 600 years and from 16 to 25 mm/yr at 2,000 years. The dryout period is left blank (no water); numbers by each curve indicate the last output liquid saturation before dryout and the first output liquid saturation during rewetting.

Figure 6.3.1.4-3. Time Profiles for Thermal-Hydrologic-Chemical Simulations of Total Aqueous Fluoride Concentrations in Fractures at the Drift Crown for the Tptpll and Tptpmn Hydrogeologic Units

C04

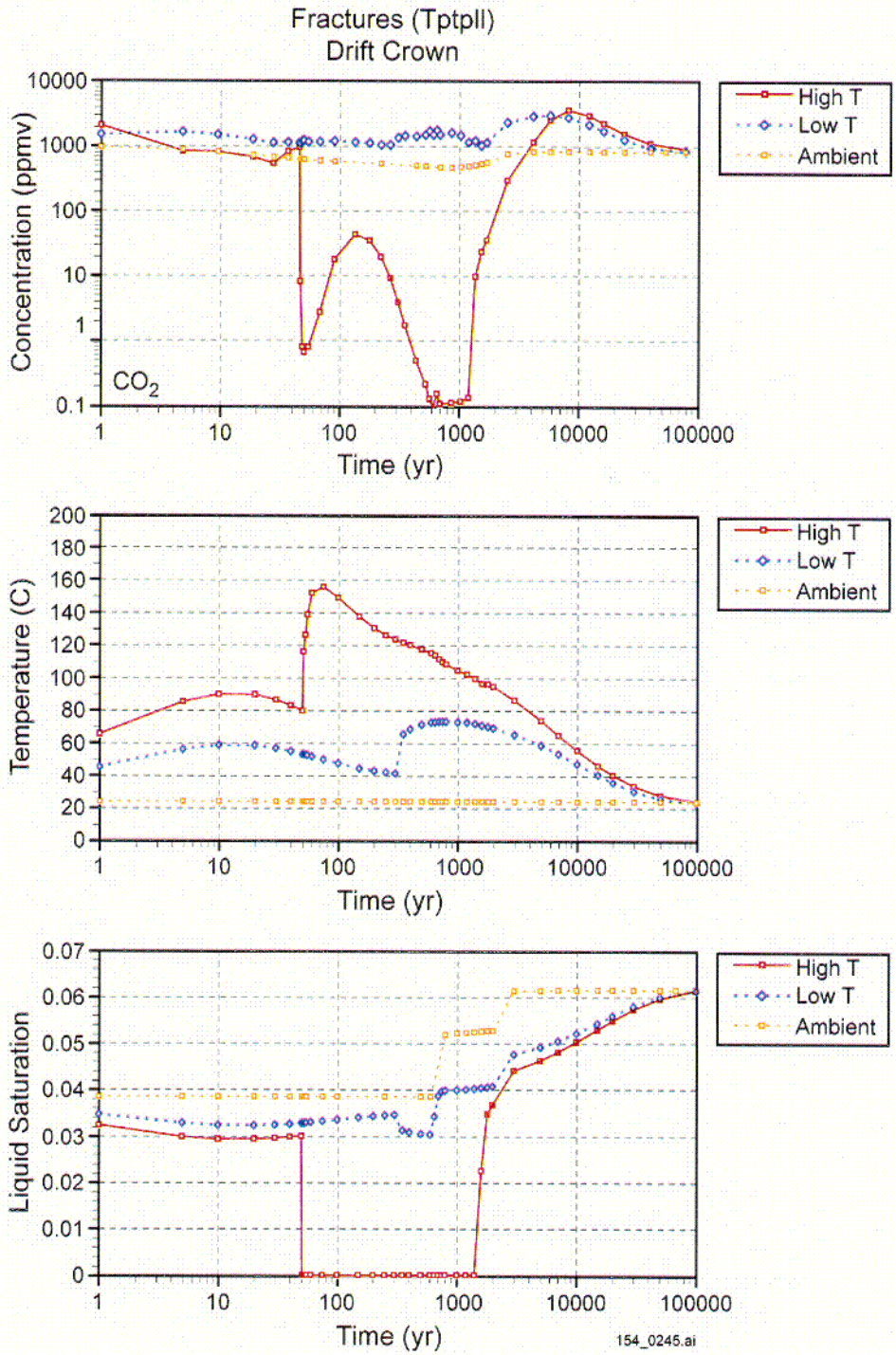

154_0245.ai

Source: Bodvarsson 2001 [DIRS 154669], Attachment 5, pp. 10 to 59).

NOTE: Comparison of simulation results for the higher-temperature versus lower-temperature case (post-Revision 01). The infiltration rate changes from 6 to 16 mm/yr at 600 years and from 16 to 25 mm/yr at 2,000 years.

Figure 6.3.1.5-1. Time Profiles of Thermal-Hydrologic-Chemical Simulations of Modeled Carbon Dioxide Concentrations (Pore Gas), Temperature, and Liquid Saturation in Fractures at the Drift Crown

C05

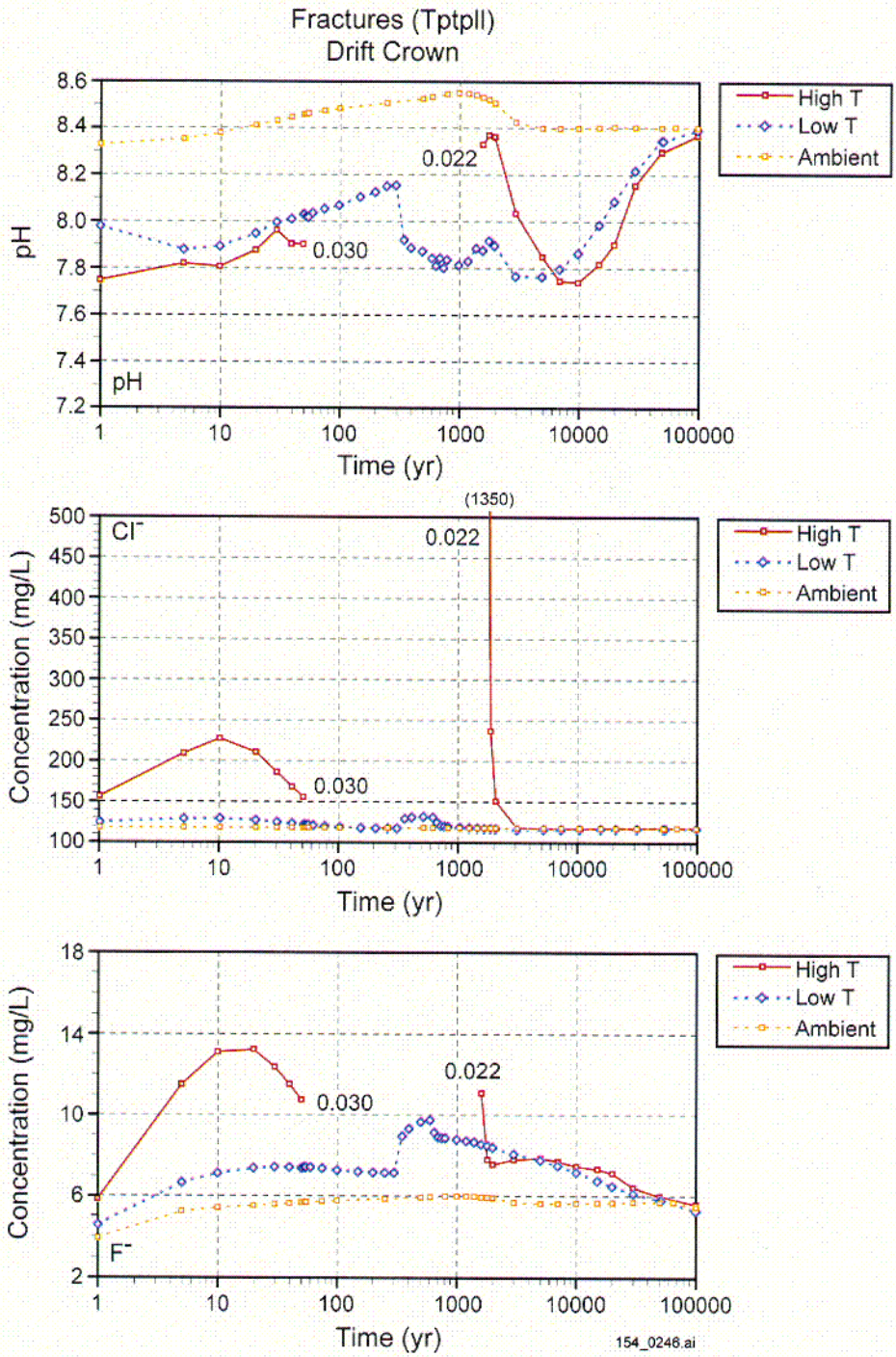

154_0246.ai

Source: Bodvarsson 2001 [DIRS 154669], Attachment 5, pp. 10 to 59).

NOTE: Comparison of simulation results for the higher-temperature versus lower-temperature case (post-Revision 01). The infiltration rate changes from 6 to 16 mm/yr at 600 years and from 16 to 25 mm/yr at 2,000 years. For the higher-temperature case, the dryout period is left blank (no water); numbers by each curve indicate the last output liquid saturation before dryout and the first output liquid saturation during rewetting.

Figure 6.3.1.5-2. Time Profiles for Thermal-Hydrologic-Chemical Simulations of Modeled pH, Total Aqueous Chloride, and Total Aqueous Fluoride Concentrations in Fractures at the Drift Crown

C06

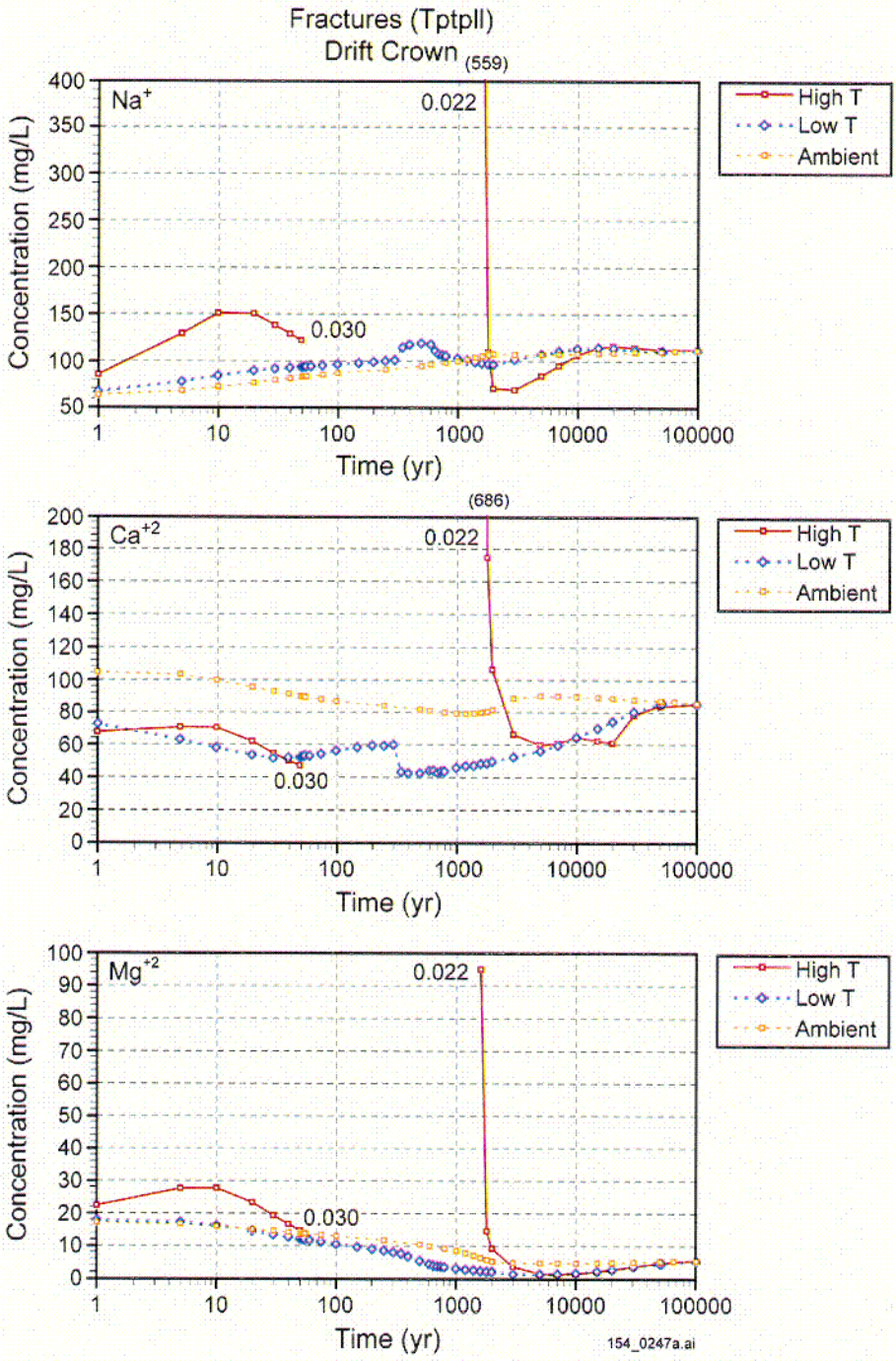

154_0247a.ai

Source: Bodvarsson 2001 [DIRS 154669], Attachment 5, pp. 10 to 59).

NOTE: Comparison of simulation results for the higher-temperature versus lower-temperature case (post-Revision 01). The infiltration rate changes from 6 to 16 mm/yr at 600 years and from 16 to 25 mm/yr at 2,000 years. For the higher-temperature case, the dryout period is left blank (no water); numbers by each curve indicate the last output liquid saturation before dryout and the first output liquid saturation during rewetting.

Figure 6.3.1.5-3. Time Profiles for Thermal-Hydrologic-Chemical Simulations for Modeled Total Aqueous Sodium, Calcium, and Magnesium Concentrations in Fractures at the Drift Crown

C07

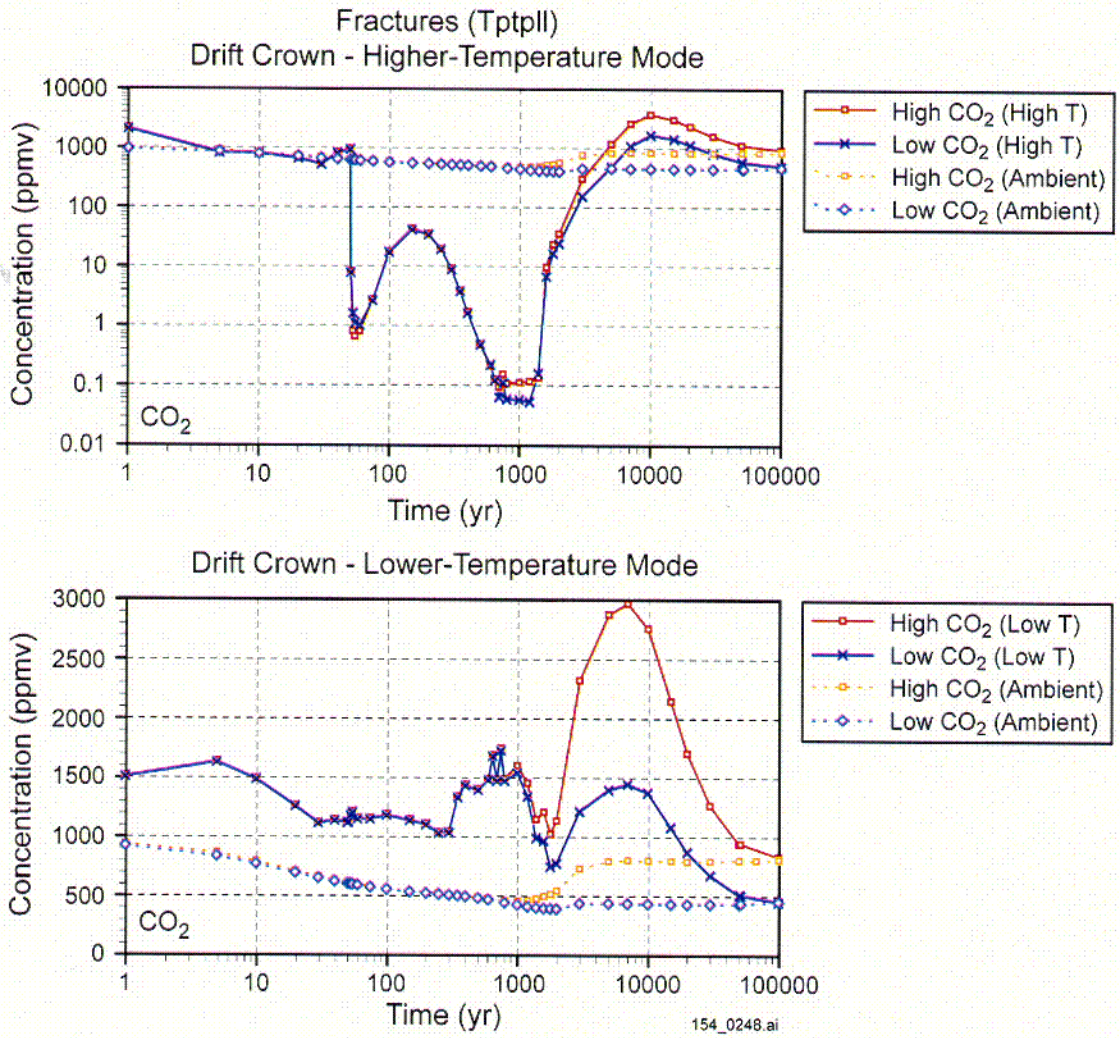

154_0248.ai

Source: Bodvarsson 2001 [DIRS 154669], Attachment 5, pp. 10 to 59).

NOTE: Comparison of simulation results for high carbon dioxide versus low carbon dioxide cases (post-Revision 01). Results are for the higher-temperature (High T) and lower-temperature (Low T) cases, and assuming approximately 3,700 ppmv (High CO_2) and 750 ppmv (Low CO_2) carbon dioxide concentrations at the top model boundary. The infiltration rate changes from 6 to 16 mm/yr at 600 years and from 16 to 25 mm/yr at 2,000 years.

Figure 6.3.1.5-4. Time Profiles for Thermal-Hydrologic-Chemical Simulations of Modeled Carbon Dioxide Concentrations (Pore Gas) in Fractures at the Drift Crown

C08

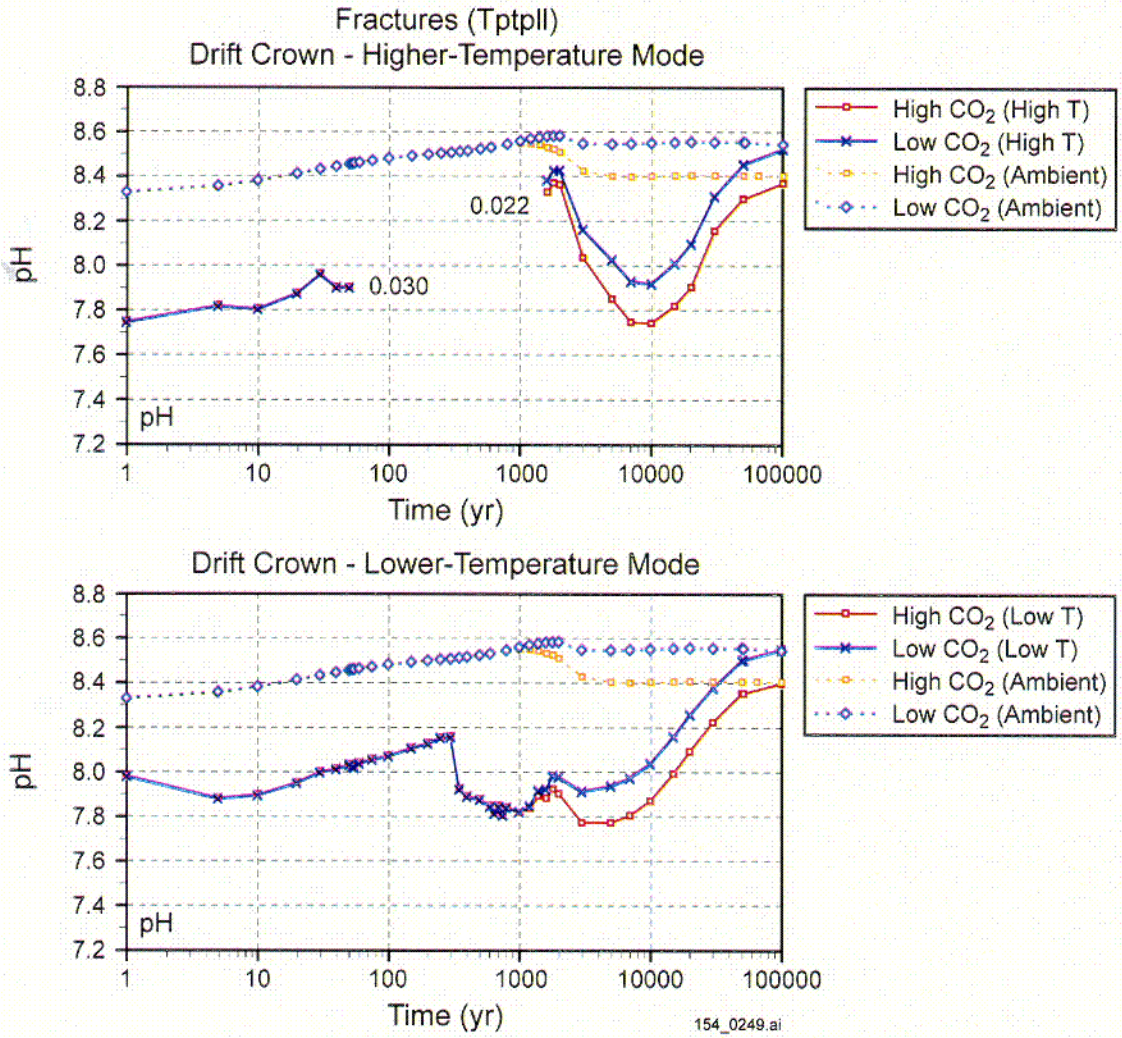

154_0249.ai

Source: Bodvarsson 2001 [DIRS 154669], Attachment 5, pp. 10 to 59).

NOTE: Comparison of simulation results for high carbon dioxide versus low carbon dioxide cases (post-Revision 01). Results are for the higher-temperature (High T) and lower-temperature (Low T) cases, and assuming approximately 3,700 ppmv (High CO_2) and 750 ppmv (Low CO_2) carbon dioxide concentrations at the top model boundary. The infiltration rate changes from 6 to 16 mm/yr at 600 years and from 16 to 25 mm/yr at 2,000 years.

Figure 6.3.1.5-5. Time Profiles for Thermal-Hydrologic-Chemical Simulations of Modeled pH in Fractures at the Drift Crown

C09

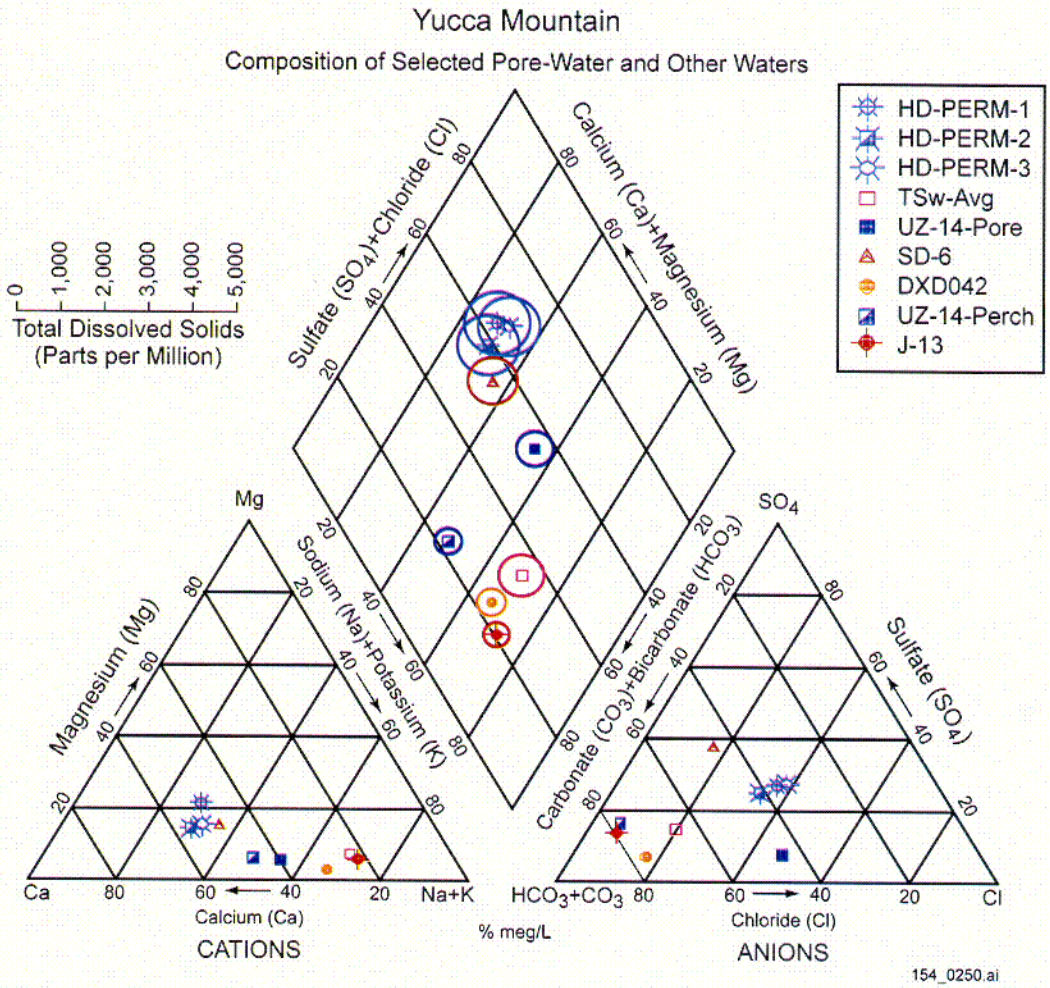

154_0250.ai

Source: MO0005PORWATER.000 [DIRS 150930]; LA9909JF831222.004 [DIRS 145598]; LA9909JF831222.006 [DIRS 146231]; LA0002JF12213U.001 [DIRS 154760]; CRWMS M&O 1999 [DIRS 129261], Table 4.5.1; Yang et al. 1996 [DIRS 100194], Table 6; MO0006J13WTRCM.000 [DIRS 151029]; Bodvarsson 2001 [DIRS 154669], Attachment 5, pp. 38 to 43, 47 to 49, 55 to 58 – (See text for additional details).

NOTE: The diameters of circles plotted around points on the diamond-shaped part of the diagram are proportional to the total salinity of the samples and drawn at the displayed scale. Samples listed in Table 6.3.1.5-2.

Figure 6.3.1.5-6. Piper Diagram for the Compositions of Selected Pore Water and Other Water

C10

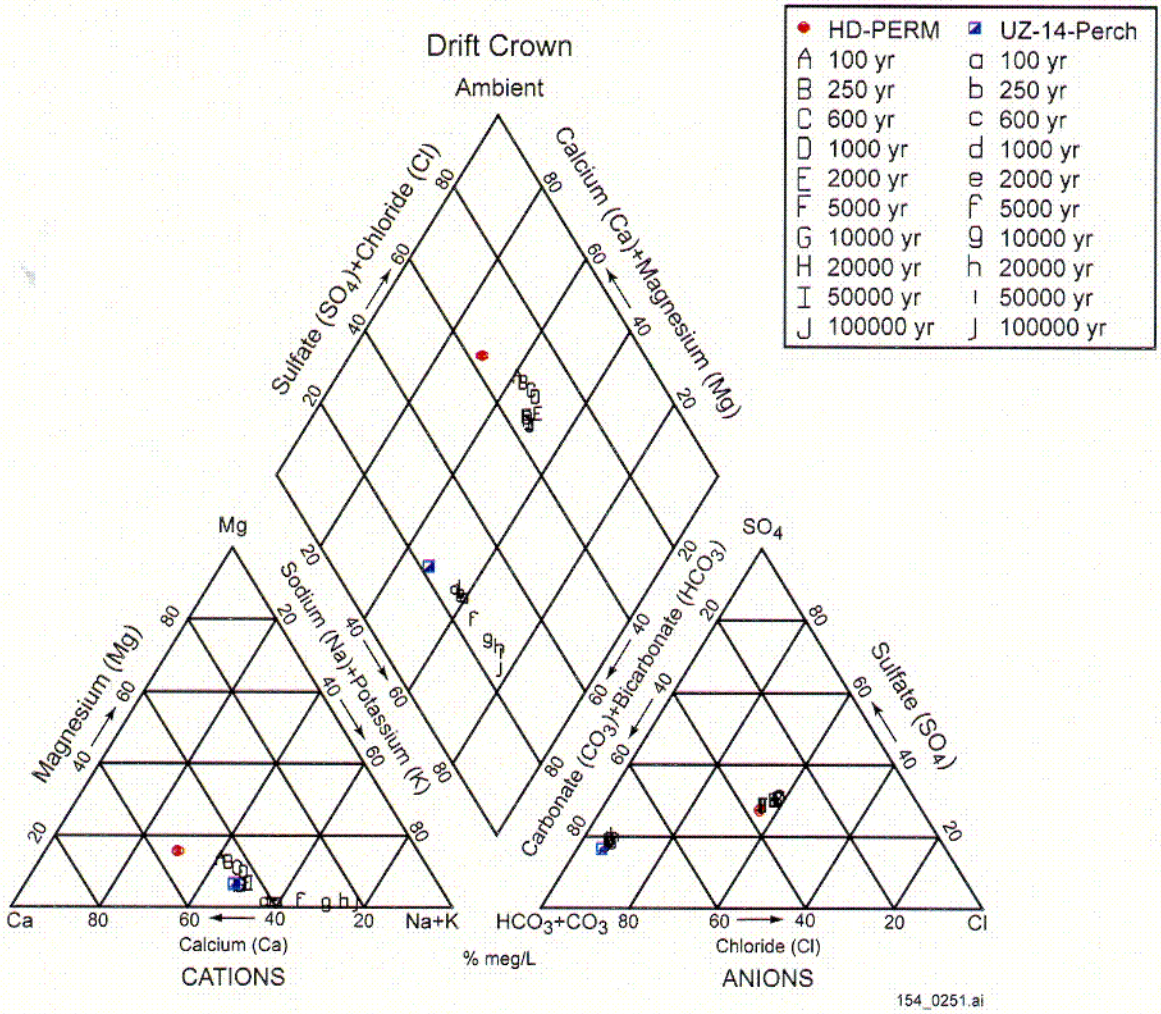

154_0251.ai

Source: Bodvarsson 2001 [DIRS 154669], Attachment 5, pp. 10 to 59).

NOTE: Thermal-hydrologic-chemical simulations for Alcove-5 pore water versus UZ-14 perched water in post-Revision 01 simulations. Evolution of water compositions modeled under ambient conditions (near 24°C; no thermal perturbation). Points are plotted for selected time intervals as shown in the legend.

Figure 6.3.1.5-7. Piper Diagram of the Modeled Evolution of Water Compositions for Two Initial Water Compositions Under Ambient Conditions

C11

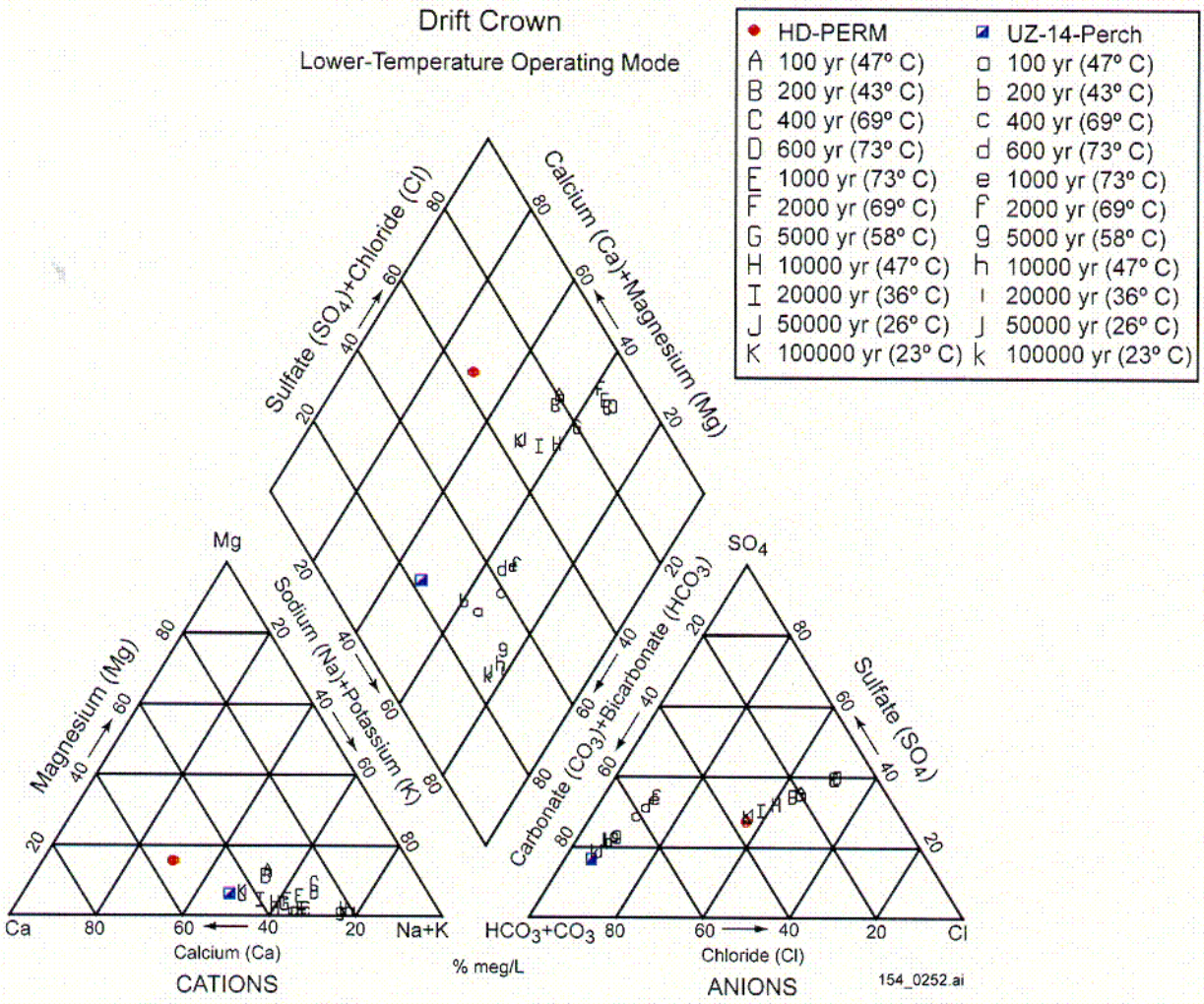

154_0252.ai

Source: Bodvarsson 2001 [DIRS 154669], Attachment 5, pp. 10 to 59.

NOTE: Thermal-hydrologic-chemical simulations for Alcove-5 pore water versus UZ-14 perched water. Results for post-Revision 01 simulations. Piper diagram showing the modeled evolution of water compositions for the lower-temperature case and two initial water compositions. Points are plotted for selected time intervals (and corresponding temperatures) as shown in the legend.

Figure 6.3.1.5-8. Piper Diagram of the Modeled Evolution of Water Compositions for the Lower-Temperature Case and Two Initial Water Compositions

C12

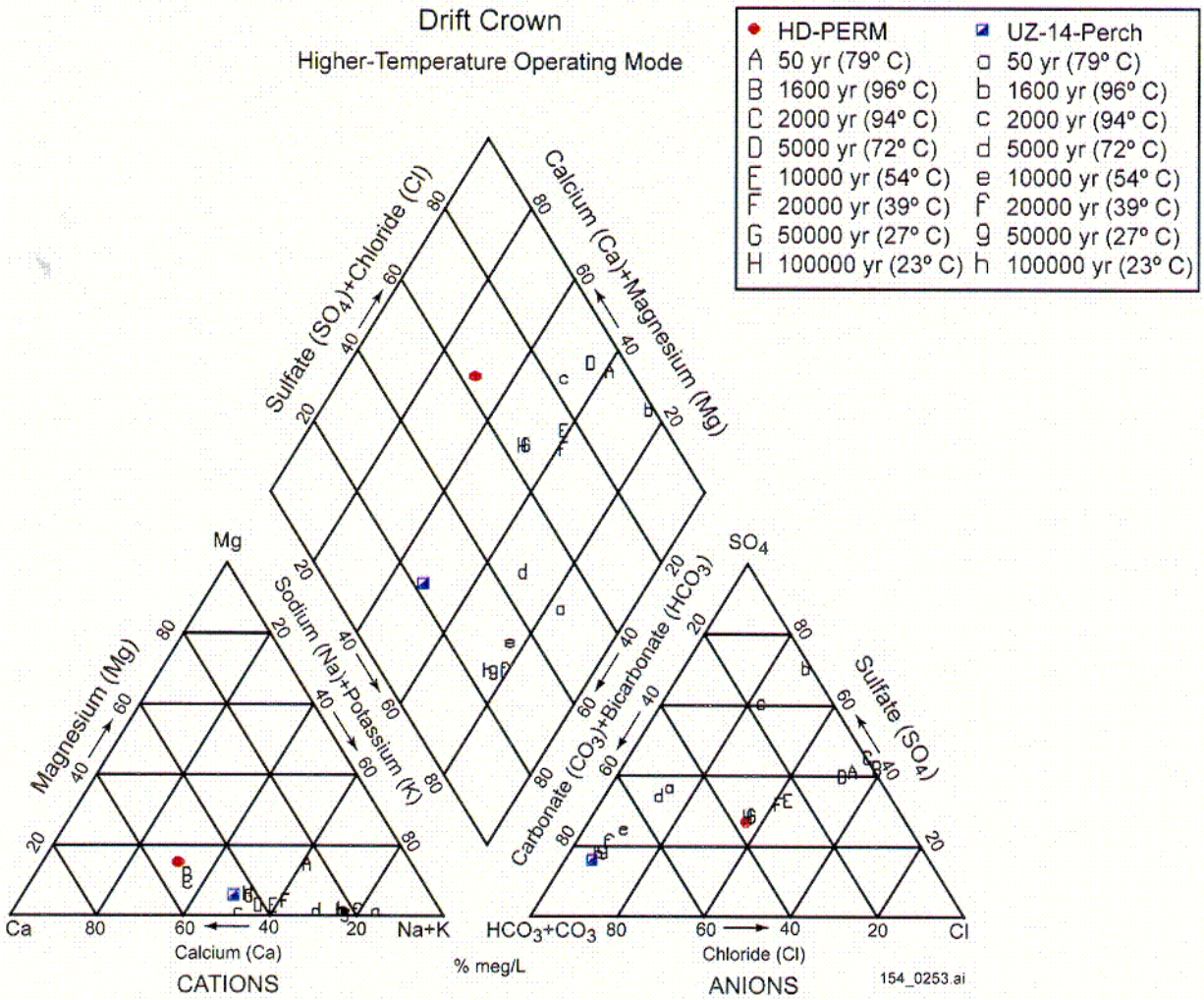

154_0253.ai

Source: Bodvarsson 2001 [DIRS 154669], Attachment 5, pp. 10 to 59).

NOTE: Thermal-hydrologic-chemical simulations for Alcove-5 pore water versus UZ-14 perched water. Results for post-Revision 01 simulations. Piper diagram showing the modeled evolution of water compositions for the higher-temperature case for two initial water compositions. Points are plotted for selected time intervals (and corresponding temperatures) as shown in the legend.

Figure 6.3.1.5-9. Piper Diagram of the Modeled Evolution of Water Compositions for the Higher-Temperature Case and Two Initial Water Compositions

C13

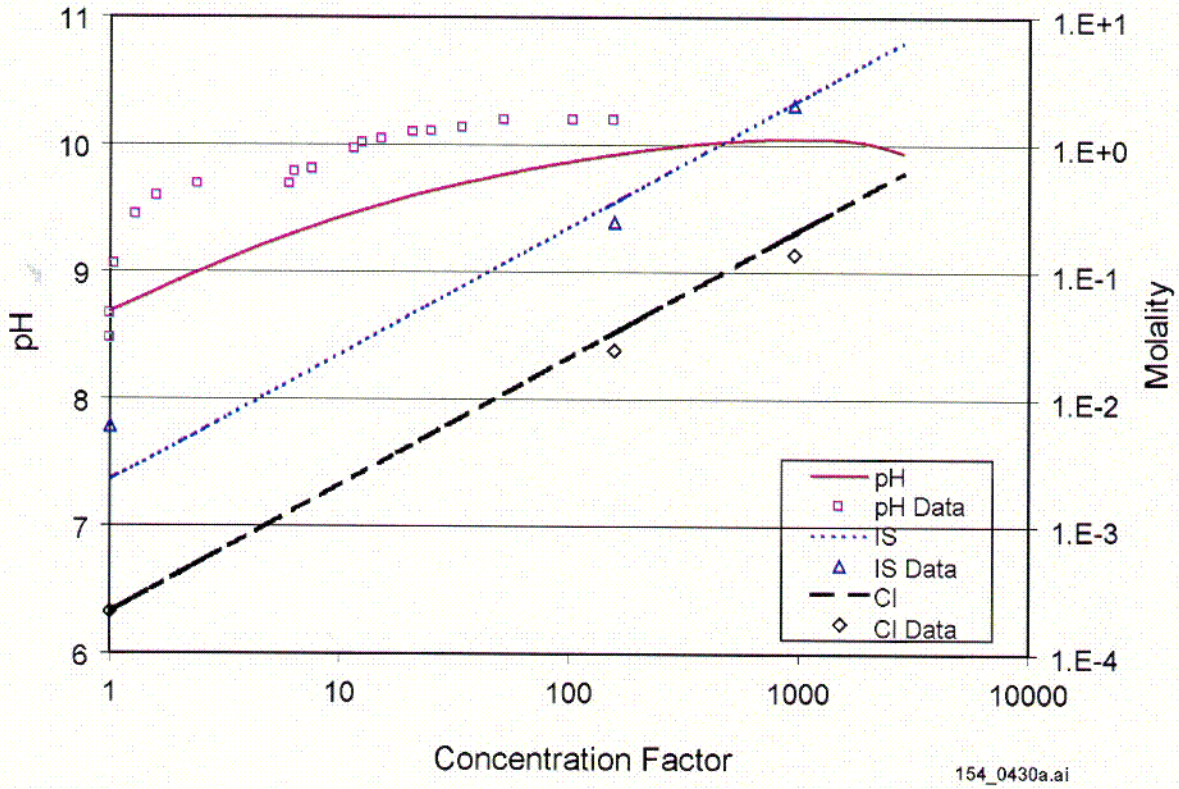

154_0430a.ai

Source: Data from Rosenberg et al. 1999 [DIRS 125338]. Model predictions from Jolley 2001 [DIRS 154762].

NOTE: IS = ionic strength; Cl = chloride.

Figure 6.3.3-1. Ionic Strength, pH, and Chloride Model Predictions versus Well J-13 Evaporation Data

C14

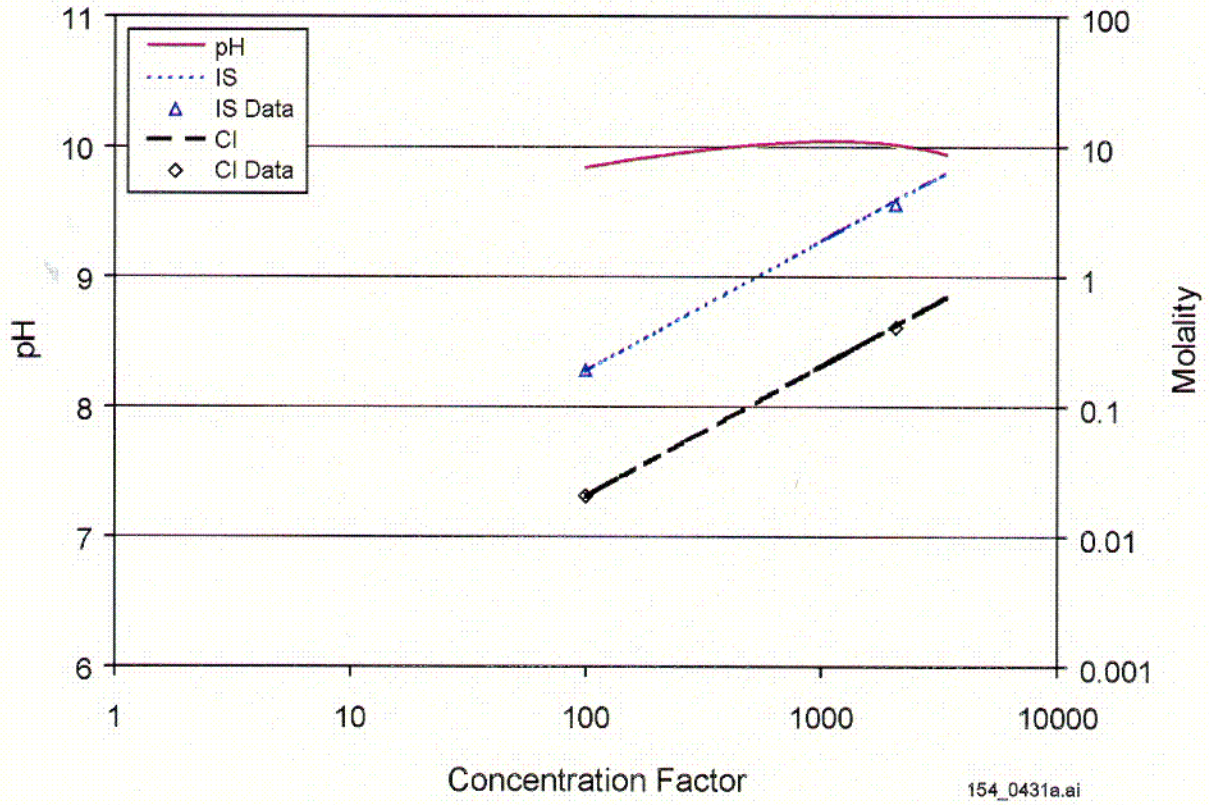

154_0431a.ai

Source: Data from CRWMS M&O 2000 [DIRS 151568]. Model predictions from Jolley 2001 [DIRS 154762].

NOTE: IS = ionic strength; Cl = chloride.

Figure 6.3.3-2. Ionic Strength, pH, and Chloride Model Predictions versus 100 x Well J-13 Evaporation Data

C15

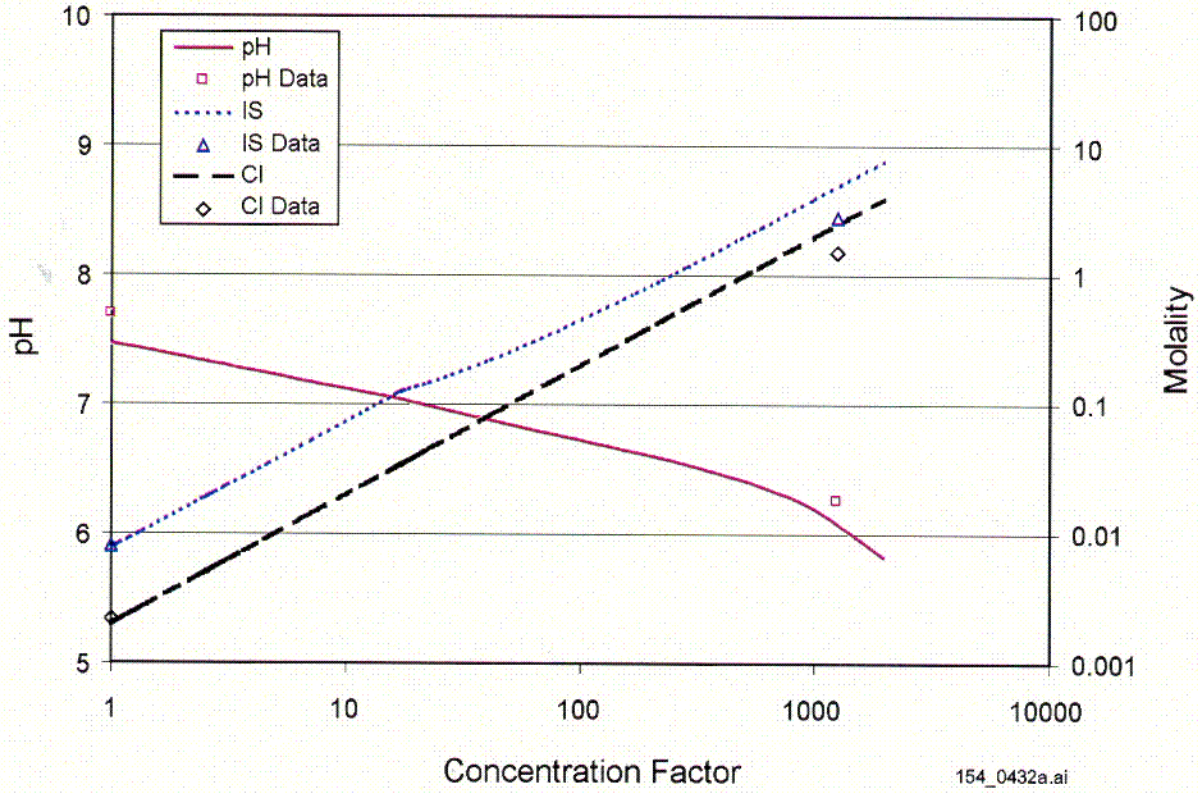

154_0432a.ai

Source: Data from Rosenberg et al. 1999 [DIRS 125339]. Model predictions from Jolley 2001 [DIRS 154762].

NOTE: IS = ionic strength; Cl = chloride.

Figure 6.3.3-3. Ionic Strength, pH, and Chloride Model Predictions versus Topopah Spring Tuff Pore Water Evaporation Data

C16

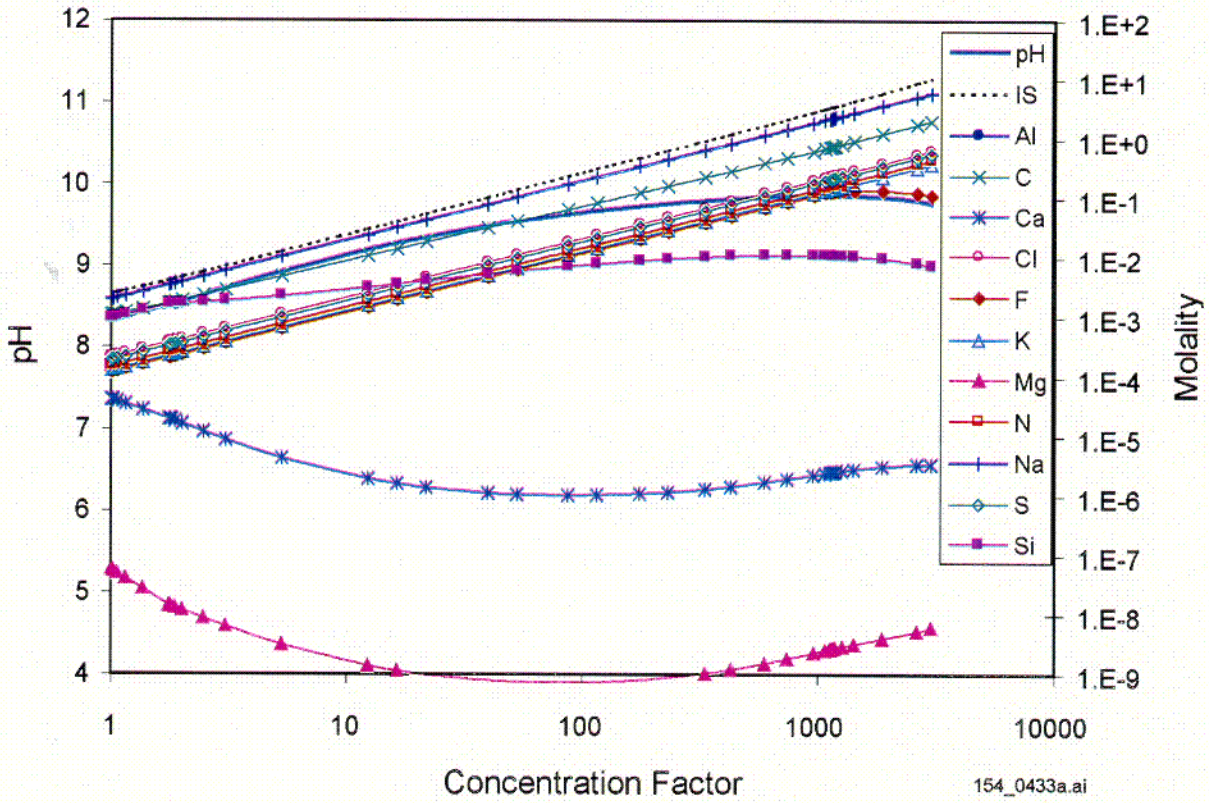

154_0433a.ai

Source: Jolley 2001 [DIRS 154762]; Mariner 2001 [DIRS 155041].

NOTE: IS = ionic strength.

Figure 6.3.3-4. Aqueous Evaporative Evolution of In Situ J-13 Well Water at f_{CO2} of 10^{-3}

C17

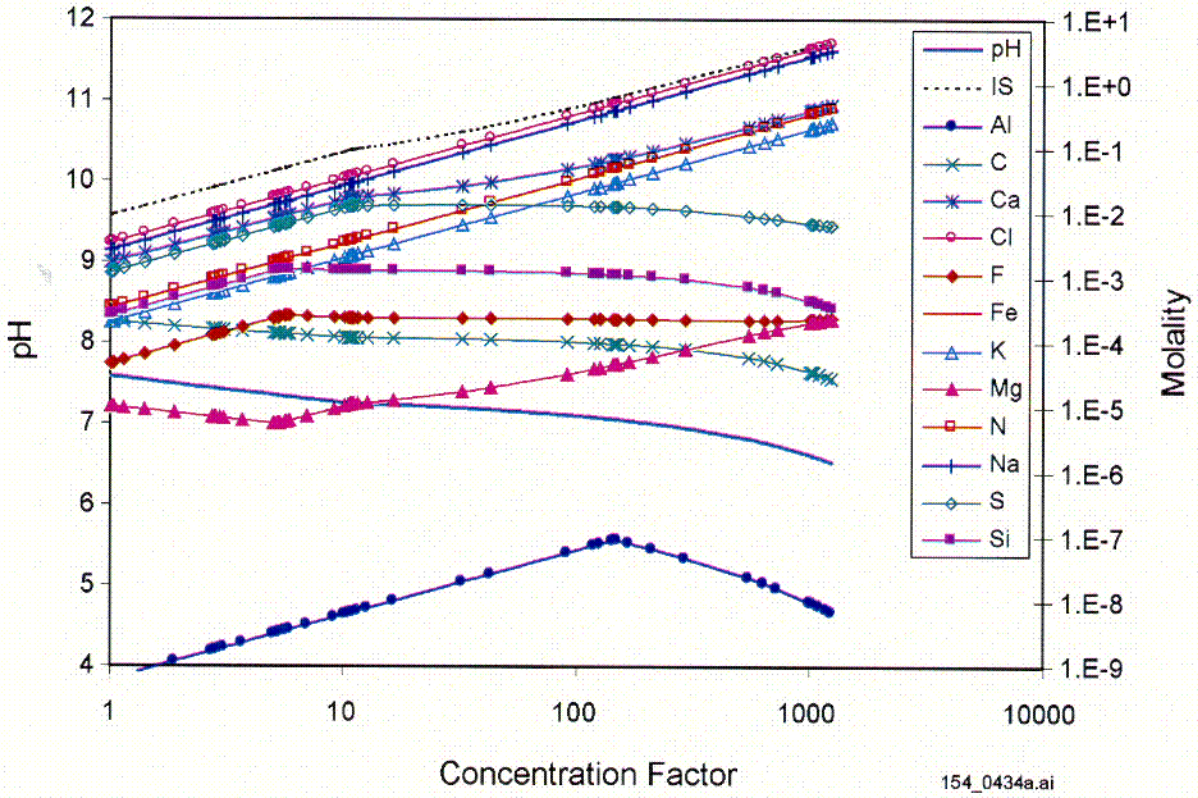

154_0434a.ai

Source: Jolley 2001 [DIRS 154762]; Mariner 2001 [DIRS 155041].

NOTE: IS = ionic strength.

Figure 6.3.3-5. Aqueous Evaporative Evolution of Topopah Spring Tuff Pore Water at f_{CO2} of 10^{-3}

C18

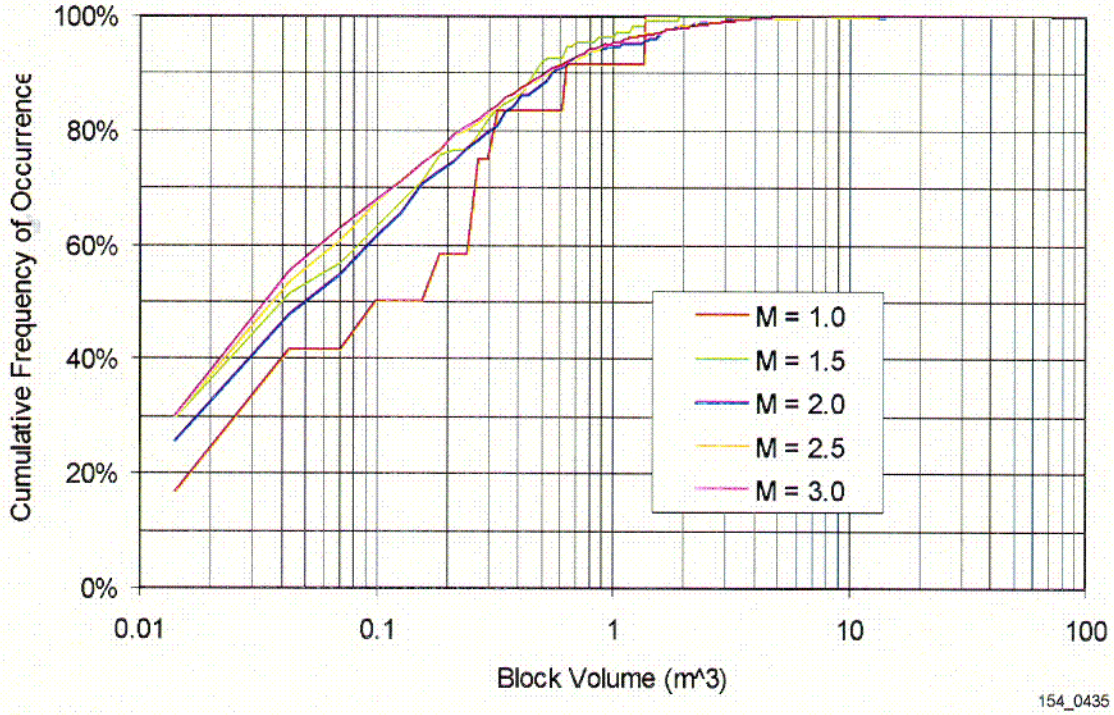

154_0435

Source: BSC 2001 [DIRS 154537].

NOTE: Data for the Tptpmn Unit, 75°-Azimuth.

Figure 6.3.4-1. Cumulative Key-Block Size Distribution for Various Sizes of Joint Planes in the Tptpmn Unit

C19

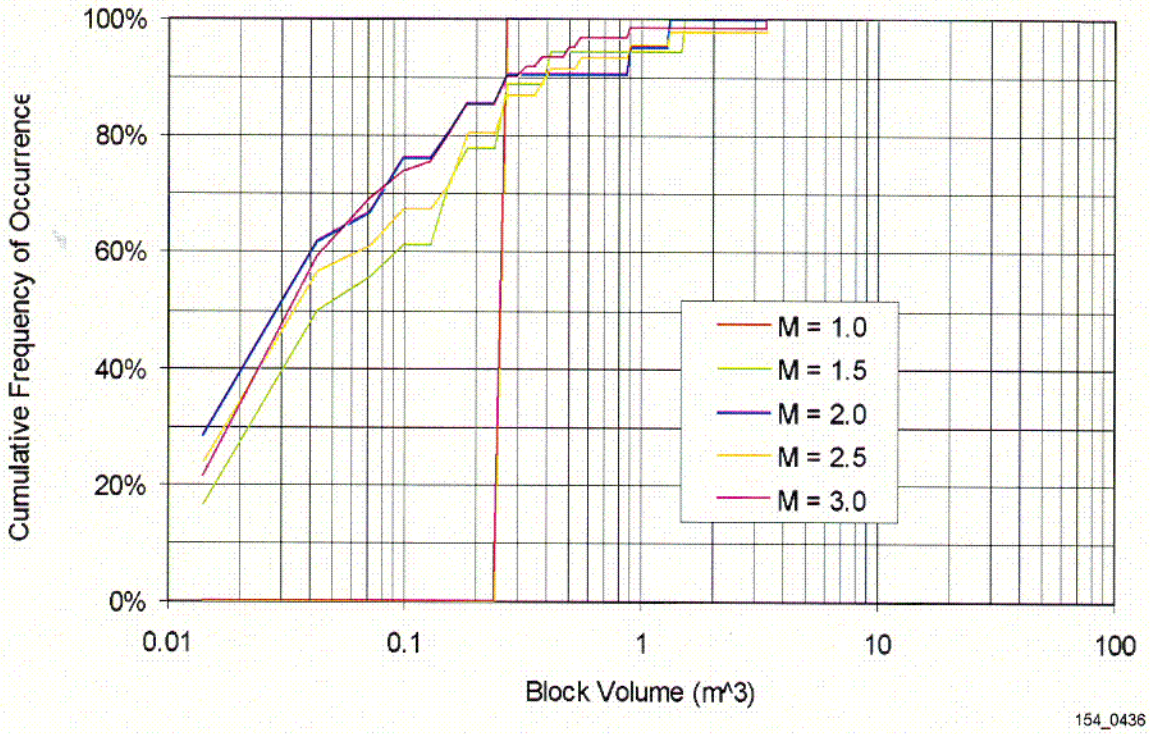

154_0436

Source: BSC 2001 [DIRS 154537].

NOTE: Data for the Tptpll Unit, 75°-Azimuth.

Figure 6.3.4-2. Cumulative Key-Block Size Distribution for Various Sizes of Joint Planes in the Tptpll Unit

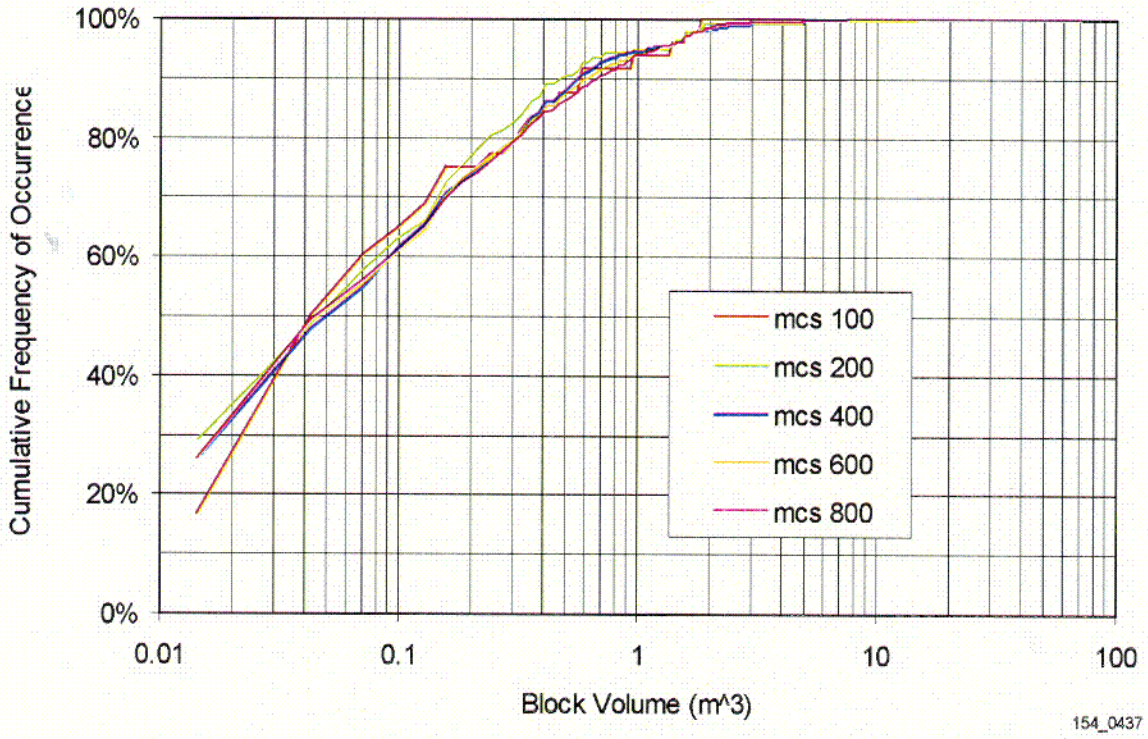

154_0437

Source: BSC 2001 [DIRS 154537].

Figure 6.3.4-3. Cumulative Block Size Distributions for Various Monte Carlo Simulations in the Tptpmn Unit

C21

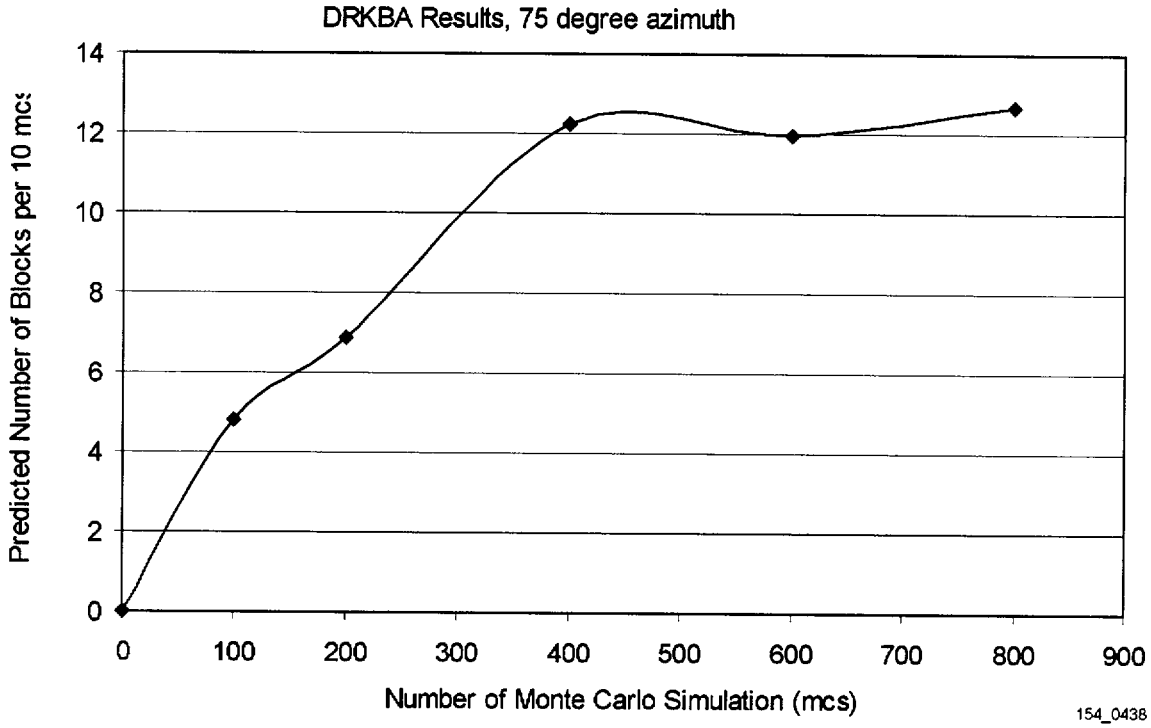

154_0438

Source: BSC 2001 [DIRS 154537].

NOTE: Data for the Tptpmn Unit, 75° azimuth, using the discrete region key-block analysis (DRKBA) software.

Figure 6.3.4-4. Predicted Number of Key-Blocks for Various Monte Carlo Simulations in the Tptpmn Unit

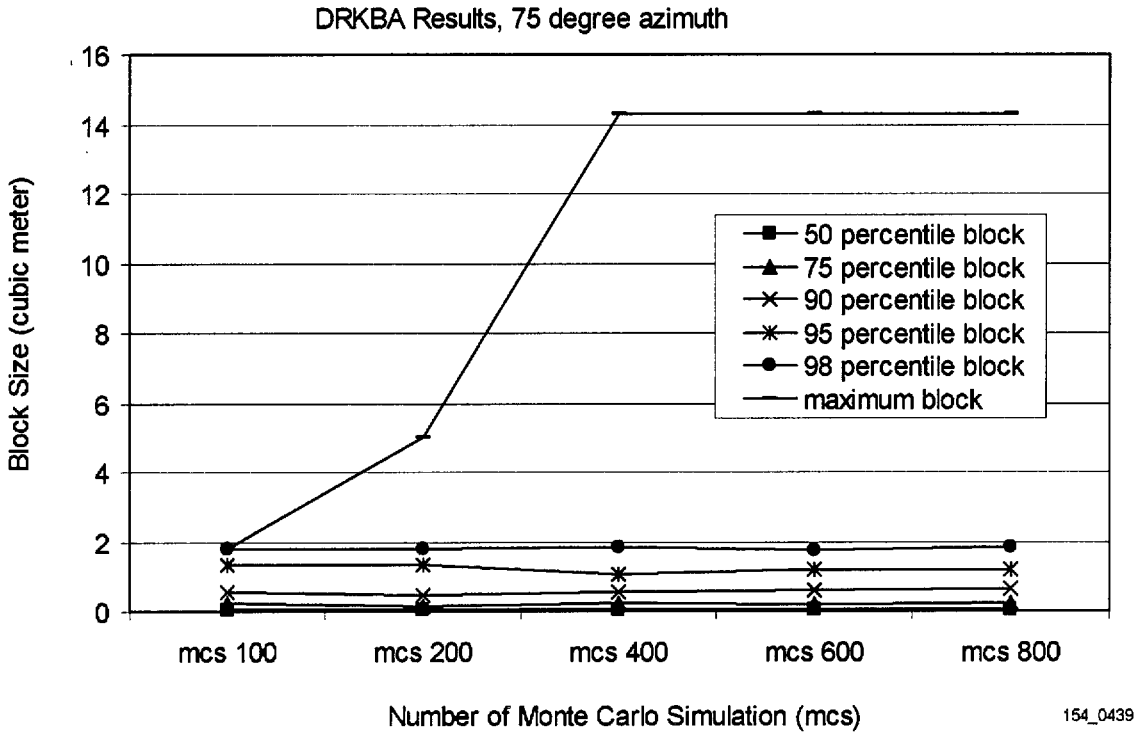

154_0439

Source: BSC 2001 [DIRS 154537].

NOTE: Data for the Tptpmn unit, 75° azimuth, using the discrete region key-block analysis (DRKBA) software.

Figure 6.3.4-5. Predicted Maximum Block Size for Various Monte Carlo Simulations in the Tptpmn Unit

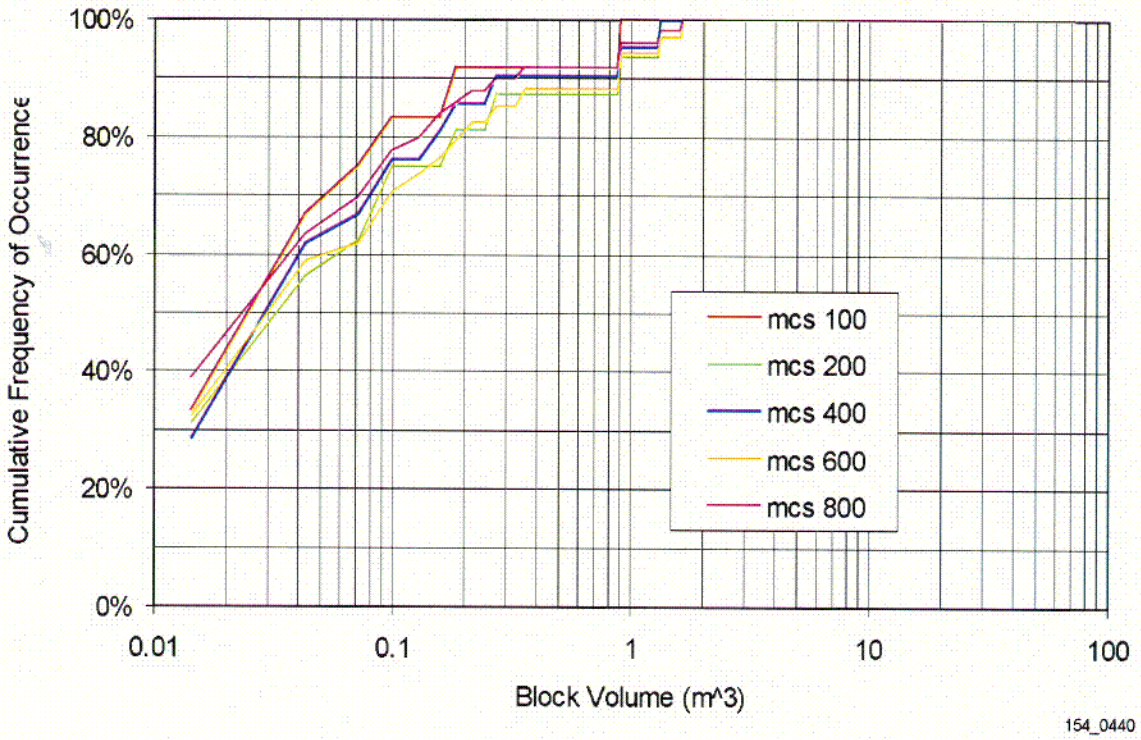

154_0440

Source: BSC 2001 [DIRS 154537].

Figure 6.3.4-6. Block Size Distributions for Various Monte Carlo Simulations in the Tptpll Unit

C22

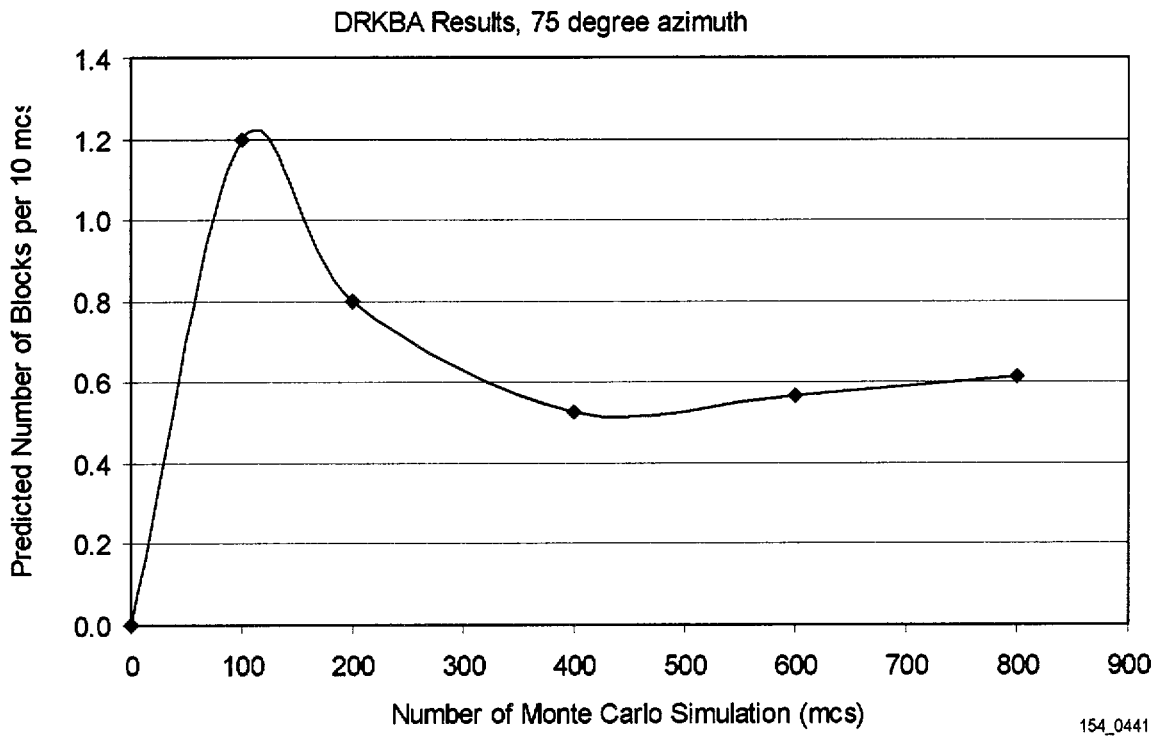

154_0441

Source: BSC 2001 [DIRS 154537].

NOTE: Data for the Tptpll unit, 75° azimuth, using the discrete region key-block analysis (DRKBA) software.

Figure 6.3.4-7. Predicted Number of Key Blocks for Various Monte Carlo Simulations in the Tptpll Unit

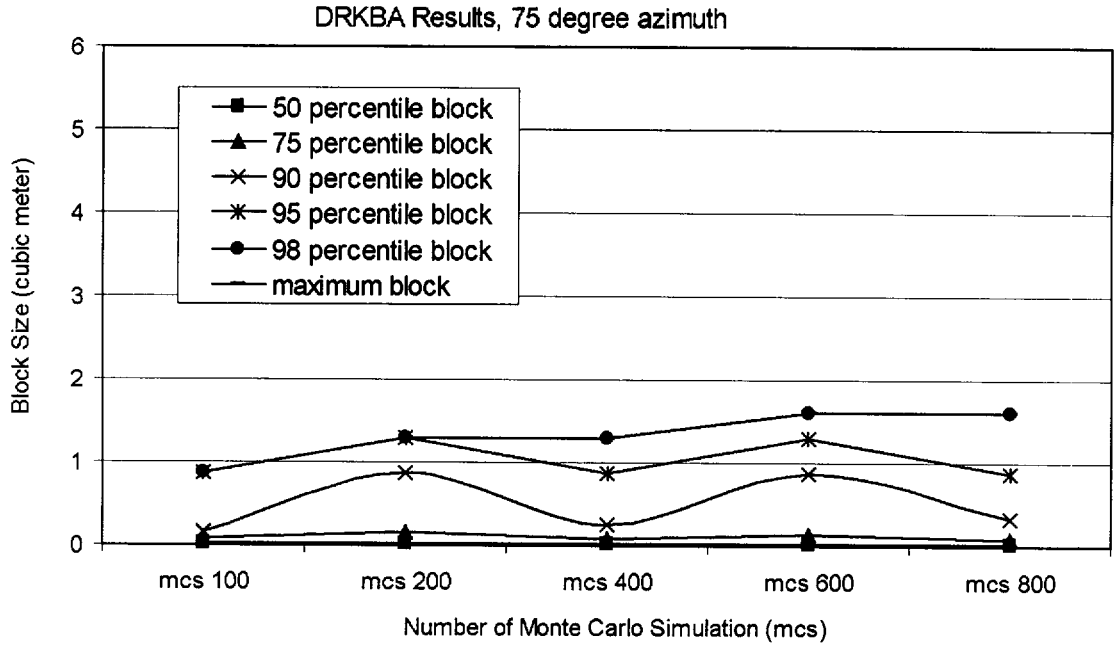

Note: The maximum block is the same as the 98 percentile block for each Monte Carlo simulation.

154_0442

154_0442

Source: BSC 2001 [DIRS 154537].

NOTE: Data for the Tptpll unit, 75° azimuth, using the discrete region key-block analysis (DRKBA) software.

Figure 6.3.4-8. Predicted Maximum Block Size for Various Monte Carlo Simulations in the Tptpll Unit

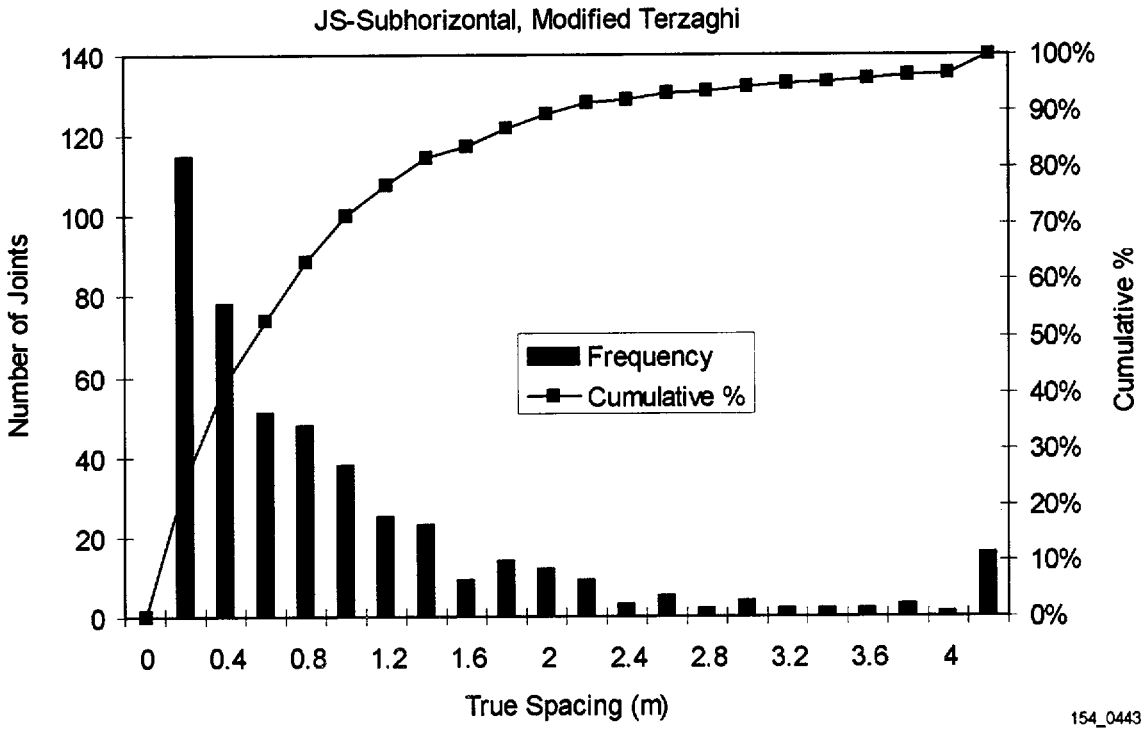

154_0443

Source: BSC 2001 [DIRS 154537].

NOTE: Data for the Tptpmn Unit Subhorizontal Joint Set, Original True Spacing.

Figure 6.3.4-9. Histogram and Cumulative Frequency Distribution of Fracture Spacing

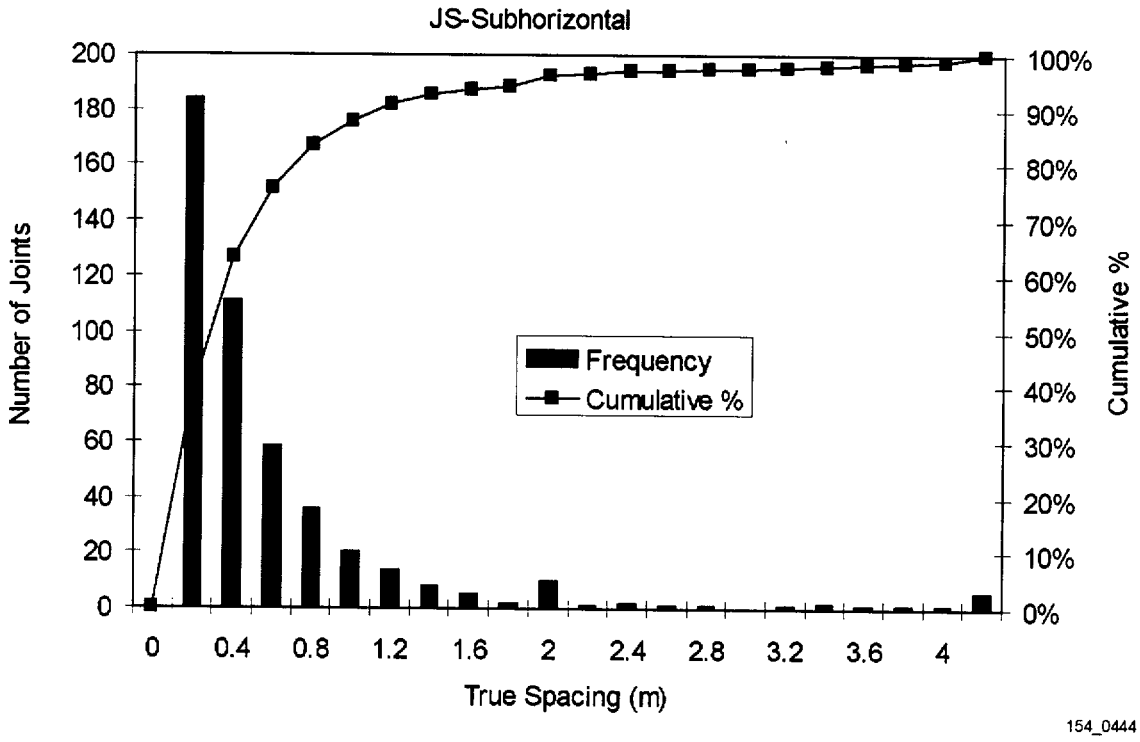

154_0444

Source: BSC 2001 [DIRS 154537].

NOTE: Data for the Tptpmn Unit Subhorizontal Joint Set, Modified True (Terzaghi) Spacing.

Figure 6.3.4-10. Histogram and Cumulative Frequency Distribution of Fracture Spacing

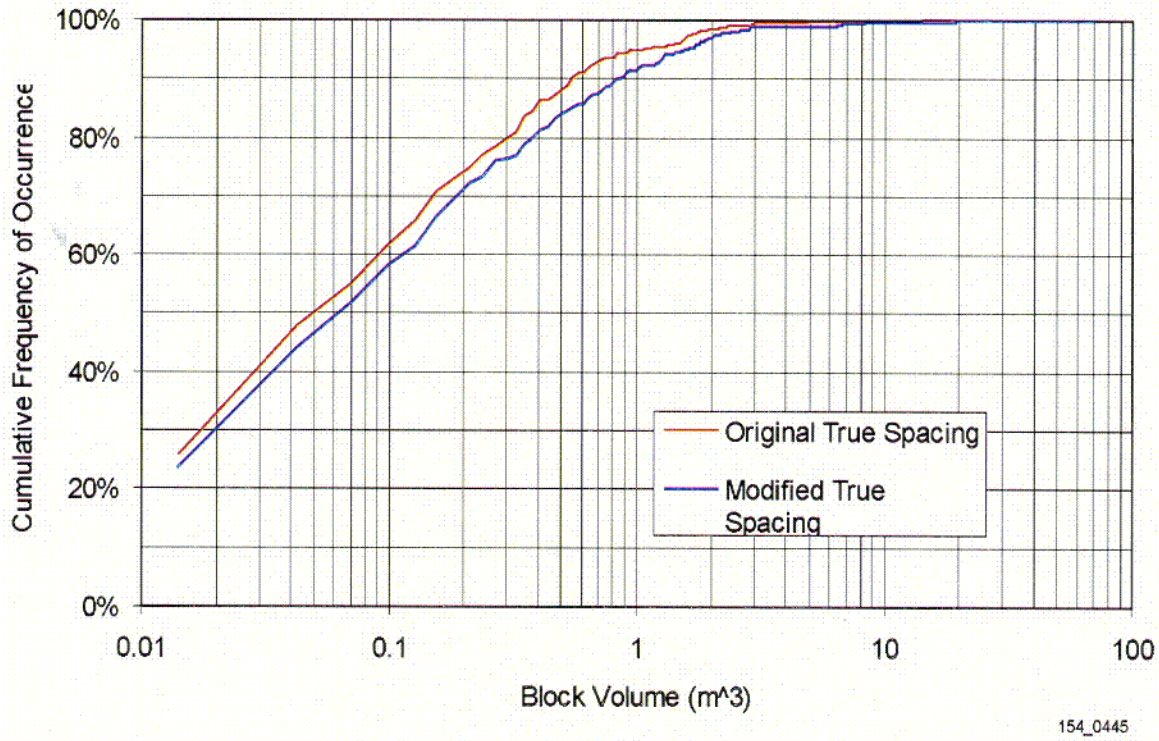

154_0445

Source: BSC 2001 [DIRS 154537].

NOTE: Data for the Tptpmn Unit, 75°-Azimuth, Subhorizontal Joint Set.

Figure 6.3.4-11. Cumulative Key-Block Size Distribution using Original and Modified Terzaghi Corrections

C23

INTENTIONALLY LEFT BLANK